TURUN
YLIOPISTO
UNIVERSITY
OF TURKU

TOWARDS SOLAR CHEMICALS: UNDERSTANDING AND REDESIGNING PHOTOSYNTHESIS

Michal Hubáček

TURUN YLIOPISTON JULKAISUJA – ANNALES UNIVERSITATIS TURKUENSIS
SARJA – SER. AI OSA – TOM. 742 | ASTRONOMICA – CHEMICA – PHYSICA – MATHEMATICA | TURKU 2025

TURUN
YLIOPISTO
UNIVERSITY
OF TURKU

TOWARDS SOLAR CHEMICALS: UNDERSTANDING AND REDESIGNING PHOTOSYNTHESIS

Michal Hubáček

TURUN YLIOPISTON JULKAISUJA – ANNALES UNIVERSITATIS TURKUENSIS
SARJA – SER. AI OSA – TOM. 742 | ASTRONOMICA – CHEMICA – PHYSICA – MATHEMATICA | TURKU 2025

University of Turku

Faculty of Technology
Department of Life Technologies
Molecular Plant Biology
Doctoral Programme in Technology

Supervised by

Professor, Yagut Allahverdiyeva-Rinne
University of Turku
Turku, Finland

Docent, Lauri Nikkanen
University of Turku
Turku, Finland

Reviewed by

Professor, Marc Nowaczyk
University of Rostock
Rostock, Germany

Associate Professor, Iftach Yacoby
Tel Aviv University
Tel Aviv, Israel

Opponent

Professor, Luning Liu
University of Liverpool
Liverpool, United Kingdom

ISBN 978-952-02-0261-3 (PRINT)
ISBN 978-952-02-0262-0 (PDF)
ISSN 0082-7002 (Print)
ISSN 2343-3175 (Online)
Painosalama, Turku, Finland 2025

There are no such things as applied sciences, only applications of science.

Louis Pasteur
September 1872

UNIVERSITY OF TURKU
Faculty of Technology
Department of Life Technologies
Molecular Plant Biology
MICHAL HUBÁČEK: Towards Solar Chemicals: Understanding and Redesigning Photosynthesis
Doctoral Dissertation, 260 pp.
Doctoral Programme in Technology
August 2025

ABSTRACT

Cyanobacteria are excellent model organisms for studying the regulation of photosynthesis. Furthermore, they serve as biocatalysts in light-driven whole-cell biotransformation applications, utilising solar energy for the production of chemicals. However, introducing additional electron sinks in the form of heterologous enzymes into a tightly regulated network of native pathways is challenging and requires a thorough understanding of photosynthesis and its regulation.

In this thesis, I focus on the Mehler-like reaction mediated by flavodiiron proteins, their electron donors, and activity modulation. I show that ferredoxin serves as their primary electron donor while their activity is dynamically controlled by changes in cytosolic pH. Furthermore, I demonstrate that a strong heterologous electron sink with high NAD(P)H consumption can outcompete flavodiiron proteins and other auxiliary electron transport pathways for electrons, thereby maintaining the photosynthetic electron transport chain in an oxidised state. Identifying and addressing the bioenergetic bottleneck is a crucial prerequisite for improving and deploying this technology on an industrial scale. If the bottleneck is cofactor availability, adding glucose at the start of the biotransformation reaction increases NAD(P)H production and enhances biotransformation. Similarly, a CO_2-rich atmosphere or a modified light spectrum can improve the biotransformation of enzymes where the bottleneck is their protein accumulation.

The results of my thesis expand our understanding of the regulation of flavodiiron proteins and the impact of biotransformation on the photosynthetic apparatus of *Synechocystis* sp. PCC 6803. Furthermore, they stress that the characterisation of each enzyme/strain combination is an essential step in engineering cyanobacteria as a future solar-to-chemical platform.

KEYWORDS: cyanobacteria, photosynthesis, biotransformation, flavodiiron protein, photosynthetic regulation, ene-reduction, oxyfunctionalisation

TURUN YLIOPISTO
Teknillinen tiedekunta
Bioteknologian laitos
Molekulaarinen kasvibiologia
MICHAL HUBÁČEK: Towards Solar Chemicals: Understanding and Redesigning Photosynthesis
Väitöskirja, 260 s.
Teknologian tohtoriohjelma
Elokuu 2025

TIIVISTELMÄ

Syanobakteerit ovat erinomaisia malliorganismeja fotosynteesin säätelyn tutkimukseen. Lisäksi ne voivat toimia biokatalyytteinä biotransformaatiosovelluksissa, hyödyntäen auringonvaloa kemikaalien tuotantoon. Uusien elektroninielujen, kuten heterologisten entsyymien, tuominen luonnollisten reaktioteiden tiukasti säädeltyyn verkostoon on kuitenkin haastavaa ja edellyttää perusteellista ymmärrystä fotosynteesistä ja sen säätelystä.

Tässä väitöskirjassa keskityn flavodiiron-proteiinien välittämään Mehler-tyyppisen reaktion elektroniluovuttajiin ja reaktion aktiivisuuden säätelyyn. Osoitan, että ferredoksiini toimii ensisijaisena elektroniluovuttajana flavodiiron-proteiineille, ja että sytosolin pH-muutokset säätelevät niiden aktiivisuutta dynaamisesti. Lisäksi osoitan, että heterologinen entsyymi, joka kuluttaa voimakkaasti NAD(P)H:ta, voi kilpailla tehokkaasti flavodiiron-proteiinien ja muiden vaihtoehtoisten elektroninsiirtoreittien kanssa. Tämä pitää fotosynteettisen elektroninsiirtoketjun hapettuneessa tilassa. Bioenergeettisen pullonkaulan tunnistaminen ja poistaminen on keskeinen edellytys tämän teknologian kehittämiselle ja teolliselle hyödyntämiselle. Mikäli pullonkaulana on kofaktorien saatavuus, glukoosin lisääminen biotransformaatioreaktion alkuvaiheessa lisää NAD(P)H:n tuotantoa ja parantaa biotransformaatiota. Vastaavasti korkea hiilidioksidipitoisuus tai muokattu valospektri voi tehostaa biotransformaatiota, kun pullonkaulana on itse entsyymin pitoisuus solussa.

Väitöskirjani tulokset laajentavat ymmärrystä flavodiiron-proteiinien säätelystä sekä biotransformaation vaikutuksista *Synechocystis* sp. PCC 6803:n fotosynteettisen koneiston toimintaan. Lisäksi ne korostavat sitä, että jokaisen entsyymi/solukanta-yhdistelmän karakterisointi on olennainen osa syanobakteerien kehittämistä tulevaisuuden auringonvaloon perustuvaksi kemikaalituotantoalustaksi.

ASIASANAT: syanobakteerit, fotosynteesi, biotransformaatio, flavodiiron-proteiinit, fotosynteesin säätely, kaksoissidosten pelkistys, oksidatiivinen funktionalisaatio

Table of Contents

Abbreviations

2-MM	2-methylmaleimide
2-MS	2-methylsuccinimide
2PG	2-phosphoglycolate
2PGA	2-phosphoglycerate
3PGA	3-phosphoglycerate
6PGA	6-phosphogluconate
6PGL	6-phosphogluconolactone
Ac-CoA	acetyl-coenzyme A
Acineto	Baeyer-Villiger monooxygenase from *Acinetobacter calcoaceticus*
ADH	alcohol dehydrogenase
AET	auxiliary electron transport pathways
AO	acridine orange
ATP	adenosine triphosphate
AY	acridine yellow
BiFC	Bimolecular Fluorescence Complementation
BPG	1,3-bisphosphoglycerate
BVMO	Baeyer-Villiger monooxygenases
CBB cycle	Calvin-Benson-Bassham cycle
CCCP	carbonyl cyanide m-chlorophenylhydrazone
CCM	carbon concentrating mechanism
CET	cyclic electron transport
Chl *a*	chlorophyll *a*
$Corr O_2$	corrected BVMO-specific O_2 uptake
COX	aa3-type cytochrome *c* oxidase
CRISPR	clustered regularly interspaced short palindromic repeats
Cyd	quinol oxidase
Cyt b_6f	cytochrome b_6f
Cyt c_6	cytochrome c_6
Cyt *f*	cytochrome *f*
DCMU	3-(3,4-dichlorophenyl)-1,1-dimethyl urea
DCW	dry cell weight

DHAP	dihydroxyacetone phosphate
DIRK	dark interval relaxation kinetics
DMSO	dimethyl sulfoxide
E4P	erythrose-4-phosphate
ED	Entner-Doudoroff pathway
EDTA	Ethylenediaminetetraacetic acid
EMP	Embden-Meyerhof-Parnas pathway
ETR(I)	electron transport rate through PSI
ETR(II)	electron transport rate through PSII
EU	European Union
F6P	fructose-6-phosphate
FAD	flavin adenine dinucleotide
FBP	fructose-1,6-bisphosphate
Fd	ferredoxin
FDP	flavodiiron proteins
FMN	flavin mononucleotide
FNR	ferredoxin-NAD(P)H oxidoreductase
G3P	glyceraldehyde-3-phosphate
G6P	glucose-6-phosphate
GC	gas chromatography
gH^+	thylakoid conductivity
HC	elevated CO_2 levels, 3%
HCO_3^-	bicarbonate ion
HOX	Ni-Fe hydrogenase
IPTG	isopropyl β-d-1-thiogalactopyranoside
LC	atmospheric CO_2 levels, 0.04%
LET	linear electron transport
MIMS	membrane inlet mass spectrometry
NADH	nicotinamide adenine dinucleotide
NADPH	nicotinamide adenine dinucleotide phosphate
NDH-1	NAD(P)H dehydrogenase-like complex 1
NPQ	non-photochemical quenching
$OD_{750(665)}$	optical density at 750 nm (665 nm)
OEC	oxygen-evolving complex
OEY	Old Yellow Enzyme
OPP	oxidative pentose phosphate pathway
P450	cytochrome P450 monooxygenase
Parvi	Baeyer-Villiger monooxygenase from *Parvibaculum lavamentivorans*
PBS	phycobilisome
Pc	plastocyanin

PCC	Pearson correlation coefficient
PEP	phosphoenolpyruvate
PETC	photosynthetic electron transport chain
PHB	polyhydroxybutyrate
pmf	proton motive force
PQ	plastoquinone
PQH_2	plastoquinol
PSI	photosystem I
PSII	photosystem II
R5P	ribose-5-phosphate
ROS	reactive oxygen species
RTO	respiratory terminal oxidase
Ru5P	ribulose-5-phosphate
RuBisCO	ribulose-1,5-bisphosphate carboxylase/oxygenase
RuBP	ribulose-1,5-bisphosphate
S7P	sedoheptulose-7-phosphate
SBP	sedoheptulose-1,7-bisphosphate
SDG	sustainable development goals
SDH	succinate dehydrogenase
TCA	tricarboxylic acid cycle
TRL	technology readiness level
Trx	thioredoxin
vH^+	proton flux
W+R/B	white light enriched with red and blue wavelengths
WLEs	wireless light emitters
WT	wild type
Xeno	Baeyer-Villiger monooxygenase from *Burkholderia xenovorans*
Xu5P	xylulose-5-phosphate
Y(I)	effective yield of PSI
Y(II)	effective yield of PSII
ΔpH	pH component of the proton motive force
ΔΨ	electric field component of the proton motive force

List of Original Publications

This dissertation is based on the following original publications, which are referred to in the text by their Roman numerals:

I Nikkanen, L., Vakal, S., Hubáček, M., Santana-Sánchez, A., Konert, G., Wang, Y., Boehm, M., Gutekunst, K., Salminen, T.A. and Allahverdiyeva, Y. Flavodiiron proteins associate pH-dependently with the thylakoid membrane for ferredoxin-1-powered O_2 photoreduction. *New Phytologist*, 2025; 246(5): 2048-2101.

II Hubáček, M., Wey, L.T., Kourist, R., Malihan-Yap, L., Nikkanen, L., Allahverdiyeva, Y. Strong heterologous electron sink outcompetes alternative electron transport pathways in photosynthesis. *The Plant Journal*, 2025; 119(5): 2500–2513.

III Barone, G.D., Hubáček, M., Malihan-Yap, L., Grimm, H.C., Nikkanen, L., Pacheco, C.C., Tamagnini, P., Allahverdiyeva, Y., Kourist, R. Towards the rate limit of heterologous biotechnological reactions in recombinant cyanobacteria. *Biotechnology for Biofuels and Bioproducts.*, 2023; 16(1): 4.

IV Hubáček, M., Nikkanen, L., Allahverdiyeva, Y. Optimising inorganic carbon level and light quality for enhanced whole-cell biotransformation reactions in *Synechocystis* sp. PCC 6803. *Manuscript.*

V Nikkanen, L., Hubáček, M., Allahverdiyeva, Y. 10 Photosynthetic microorganisms as biocatalysts. *In: Rögner, M. ed. Photosynthesis: Biotechnological Applications with Microalgae. Berlin, Boston: De Gruyter*, 2021; pp. 257-278.

1 Introduction

The global CO_2 concentration in our atmosphere reached ~425 ppm in December 2024 (Lan et al., 2025), a significant increase from the pre-industrial levels of ~280 ppm. This increase is driven by human activity, mainly by the fossil fuels combustion, but also by land use changes, agriculture, forestry, and other sectors of our society. The World Meteorological Organization has confirmed 2024 as the warmest year on record. It was also the first year with the average temperature higher by more than 1.5 °C compared to the pre-industrial level, a target outlined by the Paris Agreement (UNFCCC, 2015; "WMO confirms 2024 as warmest year on record," 2025).

The framework of planetary boundaries introduced in 2009 (Rockström et al., 2009) has recently received a new update with the evaluation of all nine boundaries (Richardson et al., 2023). This framework establishes areas and their tipping points, which, upon transgression, threaten to take Earth systems out of the Holocene-like interglacial state (Fig. 1). Six boundaries have already been transgressed globally according to Richardson et al. (2023). These are: Novel entities, Climate change, Biosphere integrity, Land system change, Freshwater change and Biogeochemical flows. However, the latest updates to the Ocean acidification boundary assesments indicate it has already been transgressed (Findlay et al., 2025). The only boundary with a positive development is Stratospheric ozone depletion, thanks to the adoption of the Montreal Protocol in 1987, which regulates the production and use of ozone-depleting substances. In 2015, the Sustainable Development Goals (SDGs) were introduced as part of the United Nations 2030 Agenda. They focus on several areas of human society, such as strengthening peace, eradicating poverty, improving human rights, protecting the environment and promoting a shift to a sustainable future. Goal 13: Climate action and Goal 9: Industry, innovation and infrastructure are two of the 17 SDGs related to this thesis (*Transforming our world: the 2030 Agenda for Sustainable Development*, 2015). Together, these concepts provide a framework and guidelines for sustainable development and innovations.

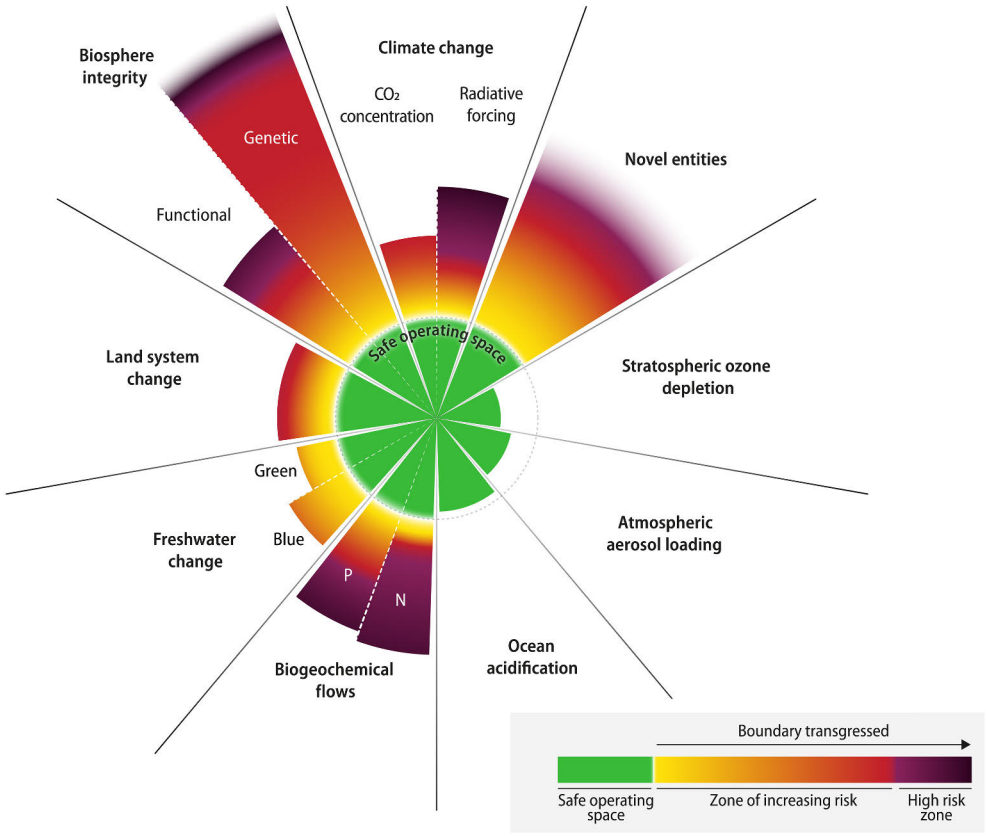

Figure 1. The current status of nine planetary boundaries with six boundaries being transgressed (ocean acidification is approaching the boundary). The green zone marks the safe operating space, while yellow to red represents the zone of increasing risk. Purple indicates the high-risk zone where interglacial Earth system conditions are transgressed with high confidence (Richardson et al., 2023).

1.1 Role of photosynthesis in future technologies

Photosynthesis is arguably the most important process on Earth. It converts solar energy and atmospheric CO_2 into the building blocks necessary for all living organisms. Photoautotrophic organisms, such as cyanobacteria, microalgae, and plants, are an essential part of primary production and form the basis of the food web. Fossil fuels are also the outcome of photosynthetic reactions performed by organisms millions of years ago. Continuous research efforts into understanding photosynthesis will lead to new paths exploiting this natural process in future technologies, which show promise in addressing the current climate emergency and the growing food and biomass demands.

On average, plant foods supply over 80% of the world's calorie intake (Food and Agriculture Organization of the United Nations, 2023), with rice, maize and wheat

forming the vast majority. In order to improve food security for regionally growing populations, improvements to crop yields are necessary. Furthermore, more resilient crop varieties that are able to adapt to the changing climate will be necessary (Croce et al., 2024). One prospective example is the transfer of the pyrenoid-based carbon concentrating mechanism (CCM) from the green alga *Chlamydomonas reinhardtii* (*Chlamydomonas*) into the chloroplast of C3 plants, such as rice or wheat, to improve yields (Adler et al., 2022; Mackinder, 2018). Another research direction is engineering C4 photosynthesis in C3 plants (Furbank et al., 2023; Smith et al., 2023; Talukder et al., 2024).

Cyanobacteria and eukaryotic microalgae already play an important role in biotechnological applications. Many strains are used in the pharmaceutical or health supplement industries and for the production of food, feed, bioactive compounds or pigments. Advances in synthetic biology toolkits, such as the CRISPR-Cas system for targeted DNA modification or suitable promoter availability, have opened the possibility of using recombinant organisms. This expands the microalgae potential into the production of oral vaccines, specific pharmaceutical proteins, modified lipid profiles for food and feed applications and many more (Barbosa et al., 2023; Borowitzka, 2015). Unfortunately, the regulation of genetically modified organisms in the European Union (EU) is strict and presents a hurdle to innovation.

Microalgae can serve as sustainable production platforms for carbon-based fuels and chemicals (Noreña-Caro and Benton, 2018). These applications rely on natively present pathways such as sucrose (Santos-Merino et al., 2023), ethylene (Vajravel et al., 2020; Zavřel et al., 2016), acetate (Roussou et al., 2025) or polyhydroxybutyrate (PHB) (Ilhami et al., 2025; Yashavanth et al., 2021). Alternatively, synthetic biology tools are used to steer metabolic flux towards novel pathways producing terpenes/terpenoids (Dienst et al., 2020; Rodrigues and Lindberg, 2021a, 2021b), ethanol (Dexter and Fu, 2009), butanol (Liu et al., 2022; Nilsson et al., 2020; Yeong et al., 2018), and many more (Matson and Atsumi, 2018). Both native and novel pathways require further strain optimisation. Among these are the introduction of exporters (Ducat et al., 2012; Niederholtmeyer et al., 2010), enhanced photosynthetic efficiency (Oliver and Atsumi, 2015; Santos-Merino et al., 2021), better extraction methods (Lo et al., 2024, 2023) or the deployment of natural or artificial biofilms (Bozan et al., 2025; Kosourov et al., 2025; Tóth et al., 2024).

Unfortunately, many of the abovementioned applications remain in the lower technology readiness levels (TRL), especially solar-to-fuels and solar-to-chemicals technologies (TRL3-6 – Reasearch/Development stage). Biomass productivity, scaling up and knowledge gaps remain as the major challenges to microalgal biotechnologies (Barbosa et al., 2023; Deprá et al., 2025).

1.1.1 Circular Bioeconomy

Our current economic model is based on the linear take-make-dispose approach. Considering that six planetary boundaries have been transgressed, a change to this approach is necessary. An alternative is the circular economy, defined as an "economic system that uses a systemic approach to maintain a circular flow of resources by recovering, retaining or adding to their value, while contributing to sustainable development" ("ISO 59004," 2024). Transitioning to a circular economy addresses several SDGs; however, the terminology surrounding circularity is susceptible to misuse, misinterpretation and greenwashing. Therefore, a careful assessment of the presented claims and implementation strategies is in order (Nobre and Tavares, 2021).

The circular bioeconomy is at the intersection of the circular economy and the bioeconomy. It generally encompasses the ideas of minimising the depletion of virgin materials, encouraging regenerative practices, protecting natural resources and stimulating the reuse and recycling whenever possible, thus ensuring we stay within the limits of planetary boundaries. Its implementation requires developing new technologies, a shift in consumer lifestyle and biomass valorisation in a cascade style (Muscat et al., 2021; Vogt and Weckhuysen, 2024). It will likely impact how we grow food, raise animals, fertilise fields or make packaging materials (Korhonen et al., 2020). Microalgae are expected to be an important player in the circular bioeconomy as the feedstock for novel materials, bioplastics or biofuels (Fernández et al., 2021; Majhi, 2024). Additionally, they can valorise wastewater or anaerobic digestate (Abdelfattah et al., 2023; Stiles et al., 2018).

As an example, the biogeochemical flow of nitrogen (N) and phosphorus (P), one of the planetary boundaries introduced above, has transgressed the tipping point mainly due to the excessive use of synthetic fertilisers in agriculture. While they are an important building element of living organisms, in excess, they cause the eutrophication of water bodies, which can lead to algal blooms. Various microalgal strains have been explored to recover these nutrients from hydroponic greenhouse wastewater (Abdelfattah et al., 2023; Salazar et al., 2023). This approach combines biomass production for further applications with nutrient recovery and safe water discharge according to the current EU regulations setting limits on N and P concentrations in urban wastewater from large settlements at 8 $mg \cdot L^{-1}$ and 0.5 $mg \cdot L^{-1}$, respectively (European Parliament, Council of the European Union, 2025). In addition to wastewater, microalgal cultivation can utilise flue gases or direct air capture technology to source CO_2. This can reduce CO_2 emissions for combustion plants (flue gas) and serve as a carbon sink, according to the final application of the biomass.

1.1.2 Policy Framework

The European Green Deal is the EU's response to the challenges of climate change and the need for sustainable development. It establishes a broad framework for all EU policies, ranging from clean energy production to preserving biodiversity and maintaining food security (Fig. 2). It requires the EU to aim at net-zero emissions by 2050, with economic growth decoupled from resource use (European Commission, Secretariat-General, 2019). In line with the European Green Deal, the EU passed "A new Circular Economy Action Plan: For a cleaner and more competitive Europe" to support its ambitions (European Commission, Directorate-General for Environment, 2020).

To support the proposed transition, the EU announced up to a trillion euros in funding, which is sourced from various sources, such as the EU budget, InvestEU or the Just Transition Mechanism. Horizon Europe allocates over €90 billion to support excellent research and innovations tackling climate change, the EU's competitiveness and the SDGs (European Parliament, Council of the European Union, 2021). Indeed, the latest synthesis report of the Intergovernmental Panel on Climate Change, published in 2023, underscores the urgency of taking ambitious actions to secure a liveable and sustainable future for all (Intergovernmental Panel on Climate Change, 2023). The development of Solar-to-X technologies is strongly supported by the European Innovation Council, which currently focuses on sustainable hydrogen and CO_2 and N_2 valorisation (European Commission: European Innovation Council and SMEs Executive Agency, 2024).

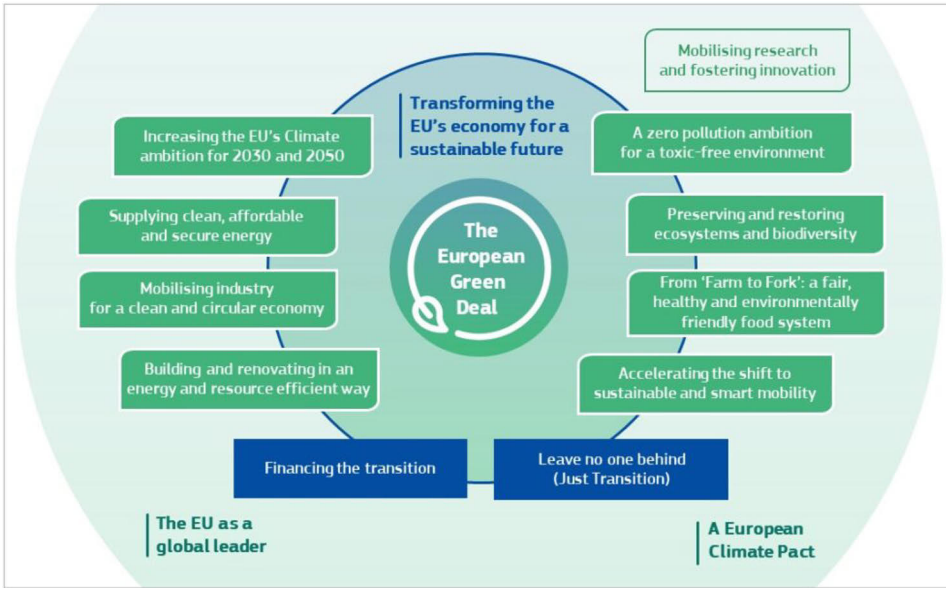

Figure 2. The various elements of the European Green Deal. (European Commission, Secretariat-General, 2019).

1.2 Cyanobacteria

Cyanobacteria, informally often called green-blue algae due to their pigmentation, are one of the most abundant taxa on Earth. These Gram-negative prokaryotes occupy a wide range of habitats. They have a significant presence in aquatic environments but can also be found in extreme conditions such as hot springs, polar regions or animal fur. Cyanobacteria likely evolved around three billion years ago, prior to the Great Oxygenation Event (2.4 billion years ago), during which the O_2 concentration in our atmosphere increased to less than 10% of the present atmospheric level and remained stable for the next 1.4 billion years. The current O_2 levels were reached following the Second Great Oxygenation Event (540–850 million years ago). However, the exact mechanisms and interplay between biological, geochemical, and geological factors remain up for debate (Ligrone, 2019; Olejarz et al., 2021; Ossa Ossa et al., 2022; Schirrmeister et al., 2015). Recently, dark O_2 production on the deep seafloor by seawater electrolysis was reported (Sweetman et al., 2024), adding to the complexity of our atmosphere's origin. Oxygenic photosynthesis evolved only once. Thus, all plants and algae share a common ancestor that absorbed a cyanobacterial cell. This event, known as endosymbiosis, occurred around 1.5 billion years ago and gave rise to the chloroplast (McFadden, 2001; Yoon et al., 2004).

Despite being classified as Gram-negative bacteria with only a thin peptidoglycan layer nestled between the cytoplasmic and outer membranes, cyanobacteria possess a more complex cell wall with varying thickness and cross-linking of the peptidoglycan layer (Hoiczyk and Hansel, 2000). The innermost layer, the thylakoid membrane, forms a shell-like structure at the cell's periphery, unlike in the chloroplast, where it is organised into grana stacks. Furthermore, in cyanobacteria, respiration and photosynthesis are situated in the thylakoid membrane, sharing several protein complexes and making up the cell's energy centre (Mullineaux, 2014).

In the biotechnological context, cyanobacteria are grouped with eukaryotic photosynthetic microorganisms under the term microalgae due to their similarities in cultivation and nutrient requirements. However, their cell structures and metabolic processes are different. Eukaryotes have a nucleus and specialised organelles for photosynthesis and respiration, while prokaryotes contain all cellular components in the cytoplasm. This thesis focuses on cyanobacteria, although references to eukaryotic organisms will be included where appropriate.

1.2.1 Environmental Significance

Cyanobacteria, along with eukaryotic microalgae and other protists, are the primary producers in aquatic environments and form the foundation of the aquatic food chain.

Although they represent only about 1% of total plant biomass, they account for half of the Earth's photosynthetic activity and O_2 production (Behrenfeld et al., 2001). They also contribute to the carbon cycle by fixing atmospheric CO_2 into organic compounds, which are then taken up by the food chain or become a part of the marine biological pump involved in long-term carbon storage deep on the ocean floor (Basu and Mackey, 2018; Passow and Carlson, 2012). In addition to the carbon cycle, some cyanobacteria are crucial components of the N cycle, fixing atmospheric N_2 into bioavailable compounds for other organisms in their surroundings (X. Zhang et al., 2020).

Despite their ecological importance, cyanobacteria can cause significant environmental and economic damage under certain conditions. When present in high abundance, they lead to algal blooms that can dye water bodies red, produce toxins harmful to fish and humans, and create anoxic conditions during eventual decay, effectively killing other vertebrates in the water column. While this is a natural process, it has become increasingly common due to nutrient runoff and eutrophication (Enevoldsen et al., 2003).

In addition to phytoplankton and benthic lifestyle (forming mats and biofilms), cyanobacteria can live in symbiosis with other organisms. Their symbiotic relationship with fungi evolved approximately 600 million years ago (Yuan et al., 2005), even before the first terrestrial lichens appeared. They can also be found in marine sponges (Charpy et al., 2012) or with higher plants (Álvarez et al., 2023). Eukaryotic microalgae from the *Simbiodinium* genus are commonly found in symbiosis with corals. The roles of cyanobacteria and microalgae in these relationships can vary from providing energy through photosynthesis and fixing atmospheric N_2 to producing UV-protective compounds or toxins serving as antibiotics or antifeedants (Usher et al., 2007).

1.2.2 *Synechocystis* sp. PCC 6803 - the model organism

Synechocystis sp. PCC 6803 (hereafter *Synechocystis*) is one of the most studied cyanobacteria. It was isolated from a lake in California, USA, in 1968 (Stanier et al., 1971), and its genome (3.6 Mbp) was fully sequenced (Kaneko et al., 1996). It is a unicellular, non-toxic freshwater β-cyanobacteria without N-fixing ability. Its versatility and natural transformability (Ikeuchi and Tabata, 2001) make *Synechocystis* the perfect model organism for fundamental studies of photosynthesis and biotechnological applications. While the originally isolated strain does not tolerate glucose, subsequent sub-strains developed glucose tolerance, enabling growth under various trophic conditions (Williams, 1988). These became the common “lab” strains used worldwide. However, it soon became evident that a large diversity had arisen between the wild-type (WT) strains, resulting in difficulties in

comparing results between different research groups and mutant strains not constructed in the same WT background (Koskinen et al., 2023).

1.3 Cyanobacterial photosynthetic electron transport chain

Photosynthetic reactions comprise the light reactions taking place in the thylakoid membrane, converting solar energy into chemical energy while producing O_2 as a by-product, and the dark reactions in which CO_2 is fixed into organic molecules in the Calvin-Benson-Bassham (CBB) cycle.

Four major protein complexes support the light reactions: photosystem II (PSII), cytochrome *b*$_6$*f* (Cyt *b*$_6$*f*), photosystem I (PSI), and adenosine triphosphate (ATP) synthase. Electrons released from H_2O at PSII pass through the photosynthetic electron transport chain (PETC) until they reach ferredoxin-NAD(P)H oxidoreductase (FNR), which then reduces nicotinamide adenine dinucleotide phosphate (NADPH). This flow of electrons, known as linear electron transport (LET), is supplemented by auxiliary electron transport (AET) pathways, which play an important regulatory and photoprotective role. Cyclic electron transport (CET) is essential for increasing the ATP/NADPH ratio required by the CBB cycle. The following sections describe the main protein complexes and soluble electron carriers of the PETC, LET, and AET, as well as the regulation of photosynthetic activity (Fig. 3).

1.3.1 Major membrane protein complexes

Based on the Z-scheme (Hill and Bendall, 1960), the first protein complex in the PETC is PSII, a transmembrane water-plastoquinone oxidoreductase. Its functional form is presumed to form a dimeric supercomplex with each monomer composed of two core subunits (D1 and D2), two core antenna proteins (CP43 and CP47) and other smaller subunits; however, a functional monomeric PSII *in vivo* has also been reported (Gisriel et al., 2022; Nickelsen and Rengstl, 2013; Takahashi et al., 2009; Yu et al., 2021). There are 35 chlorophylls bound in the PSII monomer, two of which constitute the reaction centre, P680. The oxygen-evolving complex (OEC), located on the lumenal side of the thylakoid membrane, harbours the Mn_4CaO_5 cluster, the catalytically active part of the OEC (Li et al., 2024; Umena et al., 2011).

The second protein complex is Cyt *b*$_6$*f*, a functional dimer with each monomer consisting of four major subunits: cytochrome *f* (Cyt *f*), cytochrome *b*$_6$, Rieske iron-sulphur protein and subunit IV; and four minor subunits. It plays an indispensable role in connecting PSII to PSI by transferring electrons from the plastoquinone (PQ) pool to plastocyanin (Pc) or cytochrome *c*$_6$ (Cyt *c*$_6$).

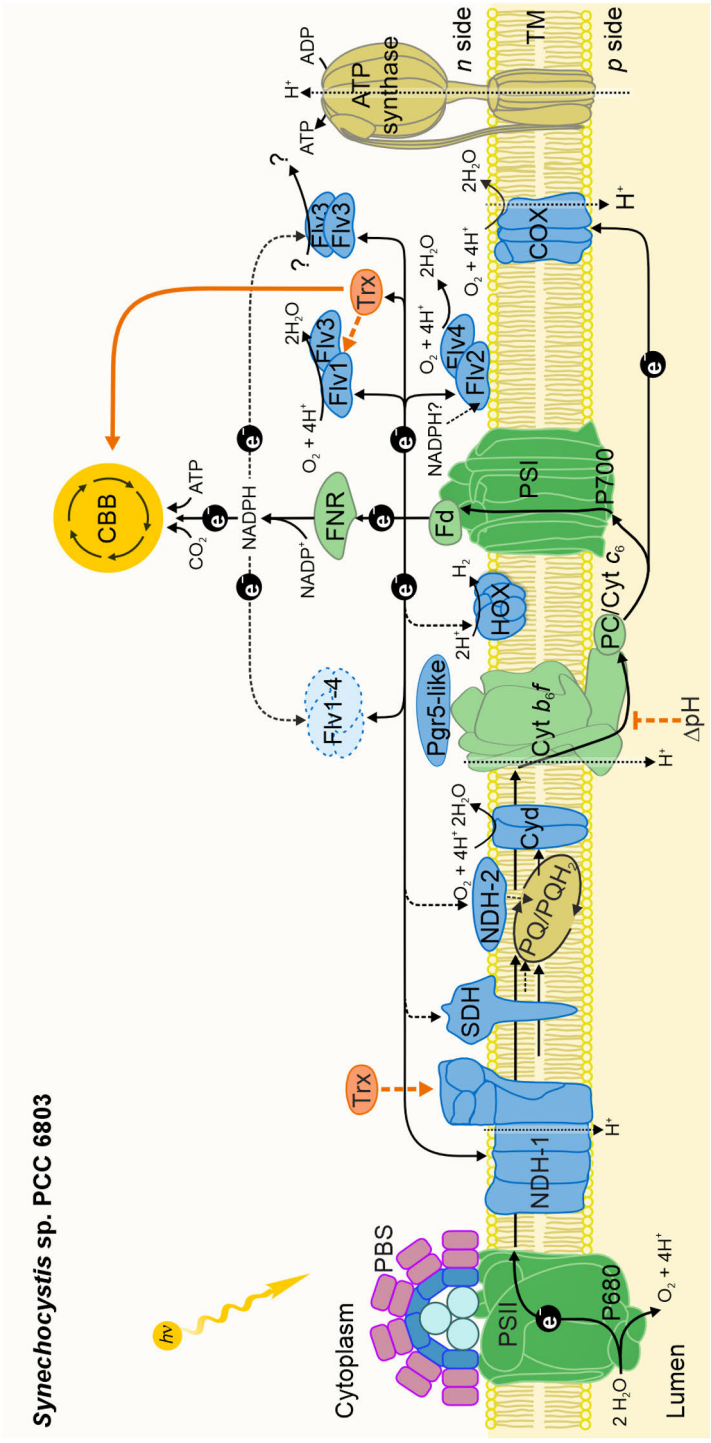

Figure 3. A schematic of the photosynthetic light reactions and auxiliary electron transport pathways nestled in the thylakoid membrane of *Synechocystis* sp. PCC 6803. The electron transport pathways branch into auxiliary routes, distributing excess electrons. The central electron distribution hub is ferredoxin (Fd), which supplies ferredoxin-$NADP^+$ reductase (FNR), flavodiiron proteins (FDPs, Flv1-4), Ni-Fe hydrogenase (HOX) or the NAD(P)H-like dehydrogenase (NDH-1) in the cyclic electron transport around photosystem I (PSI). The respiratory terminal oxidases (RTO) Cyd and COX remove excess electrons from Pc or PQ. The thioredoxin (Trx) system conveys redox signals from Fd to the CBB cycle, NDH-1, ATP synthase and possibly FDPs. The figure was adapted from Nikkanen et al. (2021).

PSI in cyanobacteria is generally organised as a trimer, although dimeric or tetrameric formations have also been isolated (Li et al., 2014). Tetrameric PSI is especially prevalent among heterocyst-forming species (Kato et al., 2019; Li et al., 2019). *Synechocystis* contains trimeric PSI, with each monomer consisting of eleven subunits (PsaA-F and PsaI-M), 95 chlorophylls, 24 carotenes, and 17 lipid molecules (Malavath et al., 2018). PsaA and PsaB form the reaction centre containing the chlorophyll dimer P700. The PSI complex further includes two phylloquinones and three iron-sulphur clusters (F_X, F_A, and F_B) involved in the electron transfer from P700 to Fd (Kanda et al., 2021). In *Thermosynechococcus elongatus*, Fd binds to PsaA, PsaC, and PsaE (Kubota-Kawai et al., 2018; Li et al., 2022), while in *Synechocystis*, PsaC, PsaD, and PsaE were proposed to bind Fd (Chitnis, 1996). However, a high-resolution crystal structure of PSI with bound Fd clearing out this discrepancy in *Synechocystis* is missing. Pc likely transfers electrons directly to PsaA and PsaB since cyanobacterial PsaF lacks the lysine-rich lumenal extension of eukaryotic PsaF, which carries the binding site (Sun et al., 1999; Viola et al., 2021).

Lastly, the ATP synthase consists of the membrane-peripheral F_1 portion and the membrane-embedded F_o portion, composed of five and three subunits, respectively. While F_1 contains the catalytic site for ATP production, F_o harbours the motor, which generates the rotational energy (Hahn et al., 2018). Fourteen protons are required for one rotation, producing three ATP molecules (Hisabori, 2020; Pogoryelov et al., 2007; Walker, 2013). However, tight regulation of its activity is needed as it can also perform an ATP hydrolysis reaction. While the structure and catalytic mechanism of ATP-synthase are generally well-conserved, the two F_o subunits, gamma and epsilon, show a high degree of diversity, likely due to their involvement in fine-tuning the ATP synthase activity (Imashimizu et al., 2011). The ATP synthase activity is redox-regulated via the interaction of the thioredoxin (Trx) system and the gamma subunit (Junesch and Gräber, 1987).

1.3.2 Mobile electron carriers

In addition to the above-mentioned protein complexes, several mobile electron carriers are an integral part of the PETC. PQ is a membrane-bound lipophilic electron carrier transferring electrons from PSII to Cyt b_6f. PQ also receives electrons from the NAD(P)H dehydrogenase-like complex 1 (NDH-1) complex in CET and respiration, and from succinate dehydrogenase (SDH) in respiration (Cooley et al., 2000). The reduced PQ (plastoquinol, PQH_2) then donates electrons to Cyt b_6f. Pc and Cyt c_6 transfer electrons from Cyt *f* to PSI. Their expression depends on copper availability in the medium. Pc is expressed in the presence of copper, while in copper-limiting conditions, Cyt c_6 expression is induced. This transition is gradual,

as both can be present at a copper concentration of 0.3 µM (Sétif et al., 2019; Zhang et al., 1992).

Fds are small iron-sulphur soluble proteins that shuttle electrons between reactions. They serve as the electron distribution hub downstream of PSI, donating electrons to various pathways (Lea-Smith et al., 2016). The main pathway of Fd is the reduction of $NADP^+$ by FNR, the final step of LET. However, a large proportion of reduced Fd can be used by NDH-1 complex in CET or transferred to O_2 by FDPs according to environmental conditions (see 1.3.5). Other pathways include the assimilation of nitrate and nitrite (Flores et al., 2005), sulphite (Kaneko et al., 1996), glutamate (Navarro et al., 2000) and biliverdin (Frankenberg et al., 2001). Furthermore, in N_2-fixing cyanobacteria, reduced Fd donates electrons to nitrogenase (Magnuson and Cardona, 2016). Lastly, the Trx system, which regulates multiple essential metabolic processes, also needs reduced Fd (Mallén-Ponce et al., 2022). There are eleven Fd isoforms in *Synechocystis*, with Fd1 being the main isoform and the remaining ten having a minor or unknown function (Artz et al., 2020; Cassier-Chauvat and Chauvat, 2014; Hanke et al., 2011; Mustila et al., 2014).

1.3.3 Light harvesting and Linear Electron Transport

In cyanobacteria, light harvesting is mediated by the phycobilisome (PBS) antennas. They are large protein supercomplexes composed of colourless linker proteins and phycobilin-binding phycobiliproteins such as phycocyanin, phycoerythrocyanin, phycoerythrin and allophycocyanin. Their absorption ranges from 490 nm to 650 nm, complementing chlorophyll *a* (Chl *a*) absorption maxima at ~440 and ~670 nm. Typically, PBS is organised into several rods extending from the core subcomplex. This arrangement allows a unidirectional transfer of excitation energy from anywhere in the antenna towards its core and, further, the photosystems (Watanabe and Ikeuchi, 2013). Different cyanobacterial strains possess morphologically distinct PBS. *Synechocystis* belongs to the hemi-discoidal PBS family with a tri-cylindrical core (Arteni et al., 2009; Domínguez-Martín et al., 2022).

The LET is initiated by charge separation at the reaction centre of PSII, P680, upon transferring the photon's energy from PBS. A positively charged $P680^+$ and a negatively charged pheophytin are created. The electron ejected by pheophytin is captured by the primary plastoquinone Q_A, which transfers the electron to the secondary plastoquinone Q_B. $P680^+$ regains the missing electron from the Mn_4CaO_5 cluster of the OEC via redox-active tyrosine Tyr Z. Upon the second excitation and charge separation at P680, the electron is passed to Q_B^-, creating a doubly reduced Q_B^{2-}, which gets protonated by cytosolic protons to Q_BH_2 (PQH_2) and released to the PQ pool. A free PQ then replaces this PQH_2 in the Q_B binding site. $P680^+$ again

regains an electron from the OEC. Four charge separations are needed to complete one oxidation cycle of OEC, also known as the Kok cycle (Kok et al., 1970), splitting two H_2O molecules, releasing one O_2 molecule and two PQH_2 molecules, each carrying two electrons (Rexroth et al., 2017).

PQH_2 donates the two electrons to Cyt b_6f at the Q_p binding site and releases two protons into the lumen. One electron is passed through the high-potential chain of Rieske iron-sulphur protein and Cyt *f*, ultimately reducing Pc or Cyt c_6. The other electron joins the low-potential chain in the Q-cycle, reducing first heme b_L, then heme b_H, and finally heme c_i at the Q_n binding site near the cytosol. A second PQH_2 molecule donates its electrons, with the low-potential chain electron reducing heme b_H and forming the highly reducing redox-coupled heme c_i/b_H pair. This leads to a quasi-concerted two-electron, two-proton reduction of PQ to PQH_2. This PQH_2 is released into the PQ pool and again oxidised by Cyt b_6f. Thus, two protons are translocated from the cytosol to the lumen for each electron passed through Cyt b_6f to Pc/Cyt c_6. The oxidised PQ returns to the PQ pool and eventually returns to the Q_B binding site in PSII (Malone et al., 2021).

Another charge separation takes place at the P700 reaction centre of PSI. The ejected electron is rapidly (picosecond scale) passed to the primary acceptor chlorophyll A_0 and then to phylloquinone A_1. The subsequent reduction of the iron-sulphur clusters is considerably slower (nanosecond to microsecond scale). Finally, the electron is transferred to Fd (millisecond scale). The missing electron at $P700^+$ is obtained from Pc/Cyt c_6 on the lumenal side of PSI. Reduced Fd donates an electron to FNR to reduce $NADP^+$ in the final step of LET, producing NADPH. Two electrons are needed per one NADPH molecule (Rexroth et al., 2017).

Proton motive force (*pmf*) builds up during the LET. It has two components: a difference in H^+ concentration (ΔpH) and an electric field (ΔΨ) between the lumenal and cytosolic sides of the thylakoid membrane. The ΔpH is formed by water-splitting at PSII and the proton translocation at Cyt b_6f, NDH-1 and the aa3-type cytochrome *c* oxidase (COX). Furthermore, H^+ consumption in the cytosol by respiratory terminal oxidases (RTO), FDPs, and the CBB cycle contributes to ΔpH. A significant fraction of *pmf* is stored as ΔΨ, which builds up as a result of ion flux across the thylakoid membrane, charge separation in the photosystems, and the electron transfer between b_L and b_H in the Q-cycle (Checchetto et al., 2012; Kramer et al., 2003; Nikkanen et al., 2021). The built-up *pmf* is mainly released by the activity of ATP synthase, which translocates protons to the cytosol while producing ATP.

1.3.4 Regulation and photoprotection of photosynthesis

Cyanobacteria are exposed to dynamic environmental conditions, such as inorganic carbon limitation or sudden fluctuations in light intensity. Under these conditions, the balance between harvested energy and cellular metabolism (source/sink ratio) can be disrupted, leading to electrons pooling in the PETC (PQ pool) and the Fd pool, which puts pressure on PSII or PSI, respectively (Kramer et al., 2004). This can trigger the generation of reactive oxygen species (ROS), which are toxic to the cell (Khorobrykh et al., 2020). To prevent oxidative damage, especially to PSI, which lacks the rapid repair cycle available to PSII, cyanobacteria have evolved several regulatory and photoprotective mechanisms.

In high-light intensity conditions, LET exceeds the electron demand of downstream processes. This leads to a build-up of electrons in the Fd pool, which increases CET and ΔpH generation. The decrease in lumenal pH slows down PQH_2 oxidation at the Q_p site of Cyt b_6f. This process, known as photosynthetic control, protects PSI from photodamage by limiting the LET rate (Malone et al., 2021). The excess absorbed energy can be redistributed between PSI and PSII by PBS associating with either photosystem via state transition. The latest proposed model suggests that the detachment of PBS from one or both photosystems, rather than their movements, is involved in the state transition, with the signal transduction pathway remaining uncertain (Calzadilla and Kirilovsky, 2020). Excess excitation energy can also be dissipated as heat through non-photochemical quenching (NPQ) induced by the orange carotenoid protein (Kerfeld et al., 2017; Liguori et al., 2024). Lastly, AET pathways relieve the pressure on PSI by circulating electrons around PSI or transferring electrons from the Fd pool, the PQ pool, or Pc.

1.3.5 Auxiliary Electron Transport

Several AET pathways exist in *Synechocystis* (Fig. 3): (i) CET mediated by the NDH-1 complex; (ii) Mehler-like reaction performed by FDPs; (iii) RTOs with relatively lower capacity (Ermakova et al., 2016); (iv) bidirectional Ni-Fe hydrogenase (HOX).

There are two RTOs located in the thylakoid membrane: COX takes electrons from Pc/Cyt c_6, and the quinol oxidase (Cyd) oxidises the PQ pool directly (Lea-Smith et al., 2013; Viola et al., 2021). They contribute to ΔpH generation by consuming H^+ in the reduction of O_2 to H_2O, releasing H^+ by oxidising PQH_2, or, in the case of COX, by translocating H^+ to the lumen (Brändén et al., 2006). HOX can divert electrons from Fd to produce H_2 or oxidise H_2 to reduce electron carriers (Appel et al., 2000; Gutekunst et al., 2014; Lettau et al., 2025).

1.3.5.1 Cyclic Electron Transport

Cyanobacterial NDH-1 is homologous to the respiratory complex I found in bacteria and mitochondria (Baradaran et al., 2013). However, it contains several oxygenic photosynthesis-specific subunits and lacks three NAD(P)H dehydrogenase subunits responsible for accepting electrons from NADPH; instead, Fd serves as the electron donor via the binding site in the K/I/S subunit region (Laughlin et al., 2019; Pan et al., 2020; Schuller et al., 2020, 2019; C. Zhang et al., 2020). Depending on which of the variable subunits are recruited to form the complex, there are four functional versions of NDH-1 in cyanobacteria. NDH-1_1 and NDH-1_2 (also referred to as NDH-1L and NDH-1L') contain D1 or D2 subunit, respectively, and are primarily involved in CET and respiration (Battchikova et al., 2011; Peltier et al., 2016). In addition, they both contain F1/O/P subunits. NDH-1_3 and NDH-1_4 (or NDH-1MS and NDH-1MS', respectively) are mainly involved in CCM converting CO_2 into bicarbonate ions (HCO_3^-). NDH-1_3 contains D3/F3/CupB/CupS subunits, while NDH-1_4 includes D4/F4/CupB subunits. All NDH-1 versions share the same core module, NDH-1M, formed by 14 subunits (A-C, E, G-O, and S) (Peltier et al., 2016).

CET mediated by the NDH-1 complex fulfils two roles: it alleviates excess electrons from Fd by transferring them back to the PQ pool, and contributes to the build-up of *pmf*, thus increasing ATP synthesis (Nikkanen et al., 2021; Zhang et al., 2023). NDH-1 also functions as a proton pump, translocating two protons for every electron (Strand et al., 2017), thus inducing the photosynthetic control by acidifying the lumen. Consequently, the ATP/NADPH ratio increases, which is essential to meet the CBB cycle requirement of 1.5 ATP/NADPH to fix one CO_2 molecule, given that the output of LET alone is only 1.3 ATP/NADPH. This ratio rises to 2–3 ATP/NADPH with CET involvement to support downstream metabolism (Kramer and Evans, 2011). Indeed, up to 40% of ΔpH generation was maintained by NDH-1 when PSII activity was blocked (Miller et al., 2021), demonstrating the significant contribution of CET in maintaining the ATP/NADPH ratio, and its regulatory role.

There are two isoforms of FNR in *Synechocystis*, both encoded by the *petH* gene, which contains two initiation methionines. The larger isoform, FNR_L, attaches to PBS and primarily functions in $NADP^+$ reduction. In contrast, the second, smaller isoform, FNR_S, is less abundant under standard conditions, soluble, and involved in NADPH oxidation, donating electrons to Fd, therefore supporting CEF via NDH-1 (Miller et al., 2022; Thomas et al., 2006).

1.3.5.2 Flavodiiron proteins

Four FDP proteins are present in *Synechocystis*, designated Flv1-Flv4 (Helman et al., 2003). The *flv4* and *flv2* genes are arranged in an operon containing an additional gene, *sll0218*, coding for a small protein involved in PSII stabilisation (Bersanini et

al., 2017). In contrast, *flv1* and *flv3* genes are located separately, although their protein accumulation is interlinked (Allahverdiyeva et al., 2015; Mustila et al., 2016), with Flv3 being significantly more abundant (Allahverdiyeva et al., 2013). Their minimal functional organisation is in a dimeric head-to-tail conformation, which brings together the diiron catalytic centre of one protein close to the C-terminal flavodoxin-like domain with a bound flavin mononucleotide (FMN) of the other. In *Synechocystis*, the hetero-oligomeric formations Flv1/3 and Flv2/4 are involved in the Mehler-like reaction, reducing O_2 to H_2O, while higher-order oligomers with additional functions cannot be excluded. The homodimer Flv3/3 has been detected *in vivo* (Mustila et al., 2016; Santana-Sanchez et al., 2019), but its role remains unknown.

The Mehler-like reaction, also known as the water-water cycle, performed by Flv1/3 and Flv2/4 hetero-oligomers alleviates excessive electrons downstream of PSI (Allahverdiyeva et al., 2011; Santana-Sanchez et al., 2019). Unlike the Mehler reaction, in which O_2 is reduced to superoxide radical mainly at the iron-sulphur clusters or phylloquinone at PSI (Kozuleva et al., 2021; Mehler, 1951), the Mehler-like reaction does not produce ROS. The presence of Flv1 and Flv3 is vital during sudden changes in light intensity, a common occurrence in cyanobacteria's natural environment. Their loss is lethal for *Synechocystis* when exposed to fluctuating light intensity (Allahverdiyeva et al., 2013). During the transition from dark to light or low to high light intensity, FDPs can redirect up to 60% (carbon-deplete conditions) or 20% (carbon-replete conditions) of electrons to O_2 (Allahverdiyeva et al., 2011; Helman et al., 2005), protecting PSI from over-reduction when downstream electron acceptors such as the CBB cycle are limited or inactive.

The electron donor to FDPs has remained elusive for a long time. Earlier *in vitro* studies and the presence of the C-terminal domain suggested NAD(P)H as the electron donor to Flv1, Flv3 and Flv4 (Brown et al., 2019; Shimakawa et al., 2015; Vicente et al., 2002). However, in these studies, FDPs were in a homo-oligomeric constitution, which is not responsible for the Mehler-like reaction (Mustila et al., 2016). The donor to FDP hetero- and homo-oligomers might be different. Alternatively, Fd or FNR could donate electrons to FDPs. Indeed, recent studies suggested Fd as the primary electron donor of the Flv1/3 heterodimer (Nikkanen et al., 2020; Sétif et al., 2020). However, *in vivo* electron donor to the Flv2/4 heterodimer remains uncertain. Furthermore, interactions of FDPs with putative electron donors or each other *in vivo* have not been fully reported.

In addition to their photoprotective role, FDPs contribute to *pmf* generation by consuming protons in the cytosol and allowing a higher rate of LET. Upon illumination, they are responsible for up to 75% of the generated *pmf* (Nikkanen et al., 2020). While Flv1/3 is mainly responsible for the O_2 photoreduction in the first 30s of illumination, Flv2/4 maintains its activity for longer (Nikkanen et al., 2020;

Santana-Sanchez et al., 2019). Thus, their activity must be tightly regulated. On the one hand, a large capacity to redirect excess electrons is needed, but on the other, competition with the CBB cycle would be undesirable. Redox regulation of their activity could be possible, as Flv1 and Flv3 demonstrated light-dependent redox modulation (Guo et al., 2014); therefore, they could respond to regulation by the Trx system, similarly to FDPs from the moss *Physcomitrium patens* (Beraldo et al., 2024). This mode of regulation could provide rapid and reversible modulation of their activity coordinated with the activation of the CBB cycle. Regulation by *pmf*, ionic concentration, or phosphorylation has also been proposed (Angeleri et al., 2016; Zhang et al., 2012). However, strong *in vivo* evidence is missing.

1.4 Carbon metabolism

The carbon metabolism of cyanobacteria evolved around CO_2 fixation and its incorporation into organic molecules using ATP and NADPH produced by photosynthesis. The CBB cycle represents a pathway with high energetic demand since fixing six CO_2 molecules to produce one glucose molecule requires 18 ATP and 12 NADPH molecules (1.5 ATP/NADPH ratio). Glyceraldehyde-3-phosphate (G3P), the end product of the CBB cycle, is a central intermediate in carbon metabolism.

There are several carbon metabolism pathways present in *Synechocystis* (Fig. 4). The Embden-Meyerhof-Parnas (EMP) pathway, also known as glycolysis, begins with glucose-6-phosphate (G6P) and ends with pyruvate, which is then dehydrogenated to acetyl-coenzyme A (Ac-CoA). Ac-CoA is metabolised in the tricarboxylic acid (TCA) cycle, which plays only a minor role in energy production in cyanobacteria (Wan et al., 2017) or is utilised to produce PHB as carbon/energy storage (Yashavanth et al., 2021) or other metabolites. The EMP pathway is bidirectional, producing G6P (through gluconeogenesis), the first metabolite of the oxidative pentose phosphate (OPP) pathway. The OPP pathway generates NADPH and ribulose-5-phosphate (Ru5P) in its oxidative phase. In the non-oxidative phase, Ru5P is converted into other pentoses and intermediates shared with the CBB cycle in the opposite direction, with the final products being G3P and fructose-6-phosphate (F6P). These then re-join the EMP pathway to regenerate G6P. The Entner-Doudoroff (ED) pathway was proposed to be present in cyanobacteria; however, its presence remained controversial (X. Chen et al., 2016; Makowka et al., 2020; Schulze et al., 2022). In *Synechococcus elongatus* PCC 7942, the ED pathway is incomplete, missing the 6-phosphogluconate dehydratase enzyme (Xie et al., 2025), similar to many other cyanobacteria, including *Synechocystis* (Evans et al., 2024).

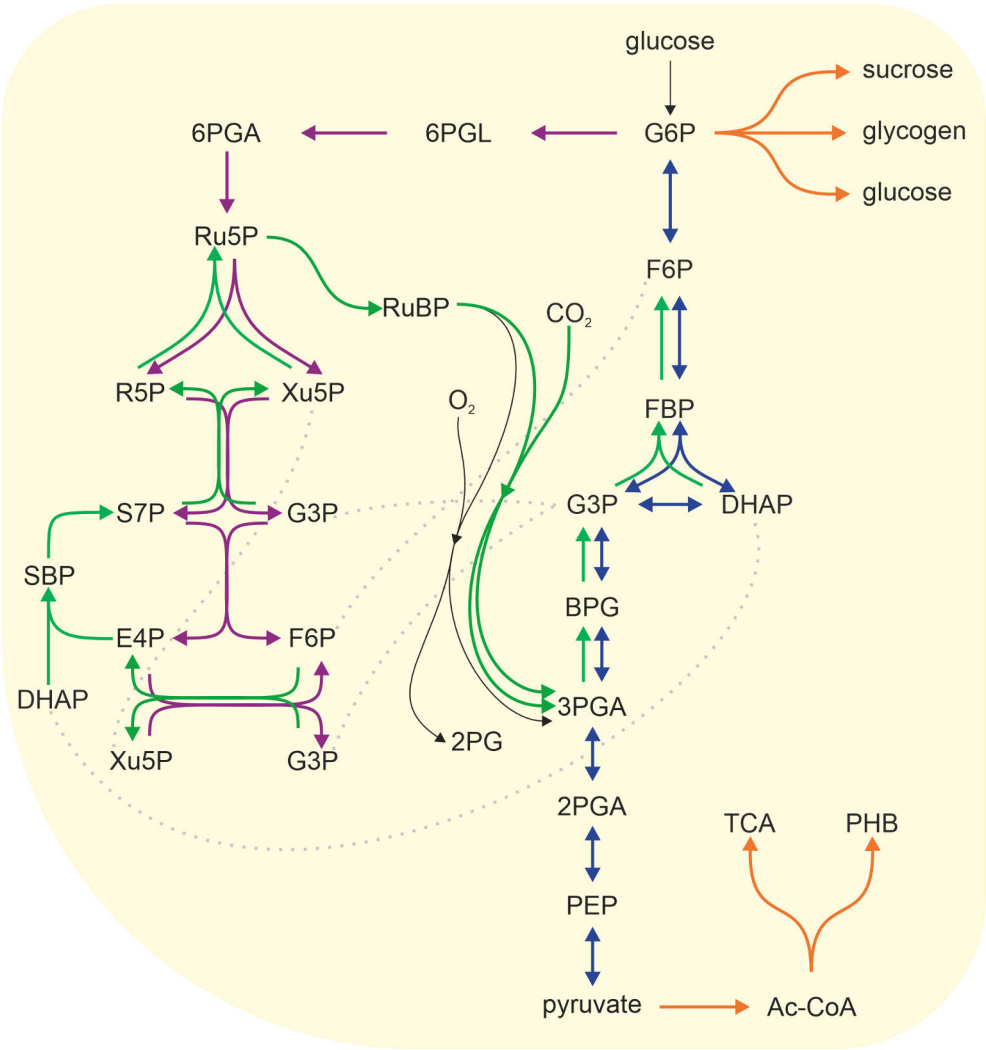

Figure 4. Schematic of carbon metabolism pathways in *Synechocystis*. The arrow colour signifies the pathway: green - CBB, blue - EMP, purple - OPP, black - photorespiration, orange - other pathways. Grey dotted lines connect shared metabolites between pathways. Glucose-6-phosphate (G6P), fructose-6-phosphate (F6P), fructose-1,6-bisphosphate (FBP), glyceraldehyde-3-phosphate (G3P), dihydroxyacetone phosphate (DHAP), 1,3-bisphosphoglycerate (BPG), 3-phosphoglycerate (3PGA), 2-phosphoglycerate (2PGA), 2-phosphoglycolate (2PG), phosphoenolpyruvate (PEP), acetyl-coenzyme A (Ac-CoA), tricarboxylic acid cycle (TCA), polyhydroxybutyrate (PHB), 6-phosphogluconolactone (6PGL), 6-phosphogluconate (6PGA), ribulose-5-phosphate (Ru5P), ribose-5-phosphate (R5P), xylulose-5-phosphate (Xu5P), sedoheptulose-7-phosphate (S7P), erythrose-4-phosphate (E4P), ribulose-1,5-bisphosphate (RuBP), sedoheptulose-1,7-bisphosphate (SBP).

During the light period, excess fixed carbon is stored as glycogen, a storage polysaccharide, giving the cell a high degree of plasticity. In carbon-replete conditions (or during N starvation), cells accumulate glycogen, which is later used during periods of carbon limitation. Furthermore, glycogen can be catalysed to supply G6P to the OPP and EMP pathways, producing NAD(P)H and ATP in the dark during respiration (Gründel et al., 2012). Glycogen thus plays a vital role in balancing the needs of cyanobacteria for carbon and electrons during different growth phases and environmental conditions (Ortega-Martínez et al., 2024). In *Synechocystis*, several PETC components (PQ pool, Cyt b_6f and Pc/Cyt c_6) are shared between photosynthetic and respiratory reactions as both are nestled in the thylakoid membrane. This arrangement complicates the regulatory network but provides energy during darkness, when electrons from catabolism are funnelled to the PQ pool, generating *pmf* for ATP production (Mullineaux, 2014).

1.4.1 CO_2 fixation

During photoautotrophic growth, the energy source is light, and the carbon source is CO_2. The ribulose-1,5-bisphosphate carboxylase/oxygenase (RuBisCO) is the enzyme responsible for the first step of the CBB cycle, which is the fixation of CO_2 into 3-phosphoglycerate (3PGA). However, RuBisCO has a low affinity for CO_2 and can also use O_2. Cyanobacteria, therefore, evolved CCM to increase the efficiency of RuBisCO's carboxylation and minimise its oxygenation activity. RuBisCO is enclosed in carboxysomes, protein shells permeable to HCO_3^-, containing carbonic anhydrase, which converts HCO_3^- to CO_2, increasing its concentration by approximately 1000-fold (Kaplan, 2017; Kerfeld and Melnicki, 2016). While CCM is indispensable in ambient air (0.04% CO_2), it is not necessary in conditions with high inorganic carbon availability (Kurkela and Tyystjärvi, 2024). In those, cyanobacteria exhibit significantly faster growth rates. However, in conditions with extremely high CO_2 concentrations (up to 30%), the growth becomes inhibited due to metabolic disbalance (Carrasquer-Alvarez et al., 2025).

CO_2 readily diffuses across cell membranes, while HCO_3^- is primarily transported through specific transporters. There are three transporters in *Synechocystis*: the two Na^+-dependent transporters SbtA (high affinity, low flux) and BicA (low affinity, high flux), and the ATP-dependent transporter BCT1 (high affinity). In addition, CO_2 is converted into HCO_3^- by NDH-1_3 and NDH-1_4 complexes, creating a pool of HCO_3^- while consuming NADPH (Kurkela and Tyystjärvi, 2024; Peltier et al., 2016; Price, 2011). This process prevents CO_2 from diffusing out of the cell and increases the cellular inorganic carbon concentration, which is conducive to carbon fixation.

Despite CCM, RuBisCO occasionally uses O_2 and oxygenates ribulose-1,5-bisphosphate (RuBP) in a process known as photorespiration. This reaction leads to one 3PGA and one 2-phosphoglycolate (2PG). 2PG is a toxic compound to the enzymes of the CBB cycle and must be converted back to 3PGA using additional ATP while releasing CO_2. Although often considered wasteful, photorespiration is essential for all photosynthetic organisms at ambient air CO_2 levels (Eisenhut et al., 2019, 2008; Moroney et al., 2013).

The CBB cycle consists of three phases. In the first phase (CO_2 fixation), RuBisCO incorporates CO_2 into RuBP, producing two 3PGA molecules. A fraction of 3PGA is used for biosynthesis, while the majority is phosphorylated and then reduced into G3P in the second phase (Reduction). In the third phase (Regeneration), Ru5P is regenerated via a cascade of intermediates in the opposite direction to the OPP pathway. Ru5P is then phosphorylated to RuBP, closing the cycle. In total, 9 ATP and 6 NADPH molecules are required to produce one 3PGA molecule, two of which are needed to make one glucose (Fig. 4).

Tight regulation of the CBB cycle is required due to its high energetic demand to ensure its activity occurs only under sufficient illumination. Several enzymes of the CBB cycle (phosphoribulokinase, sedoheptulose-bisphosphatase, fructose-1,6-bisphosphatase and glyceraldehyde-3-phosphate dehydrogenase) were shown to be redox-regulated by the Trx system (Guo et al., 2014). Furthermore, the conditionally disordered protein Cp12 binds to phosphoribulokinase and glyceraldehyde-3-phosphate dehydrogenase under dark, oxidised conditions, thus preventing their activity. Upon the transition to reducing conditions, Cp12 disassociates from these enzymes, activating the CBB cycle. The intracellular $NAD(P)^+$/NAD(P)H ratio is, therefore, a crucial aspect of the regulation of CO_2 fixation (Lucius et al., 2022; Lucius and Hagemann, 2024).

1.4.2 Photomixotrophy

In addition to photoautotrophic growth, some cyanobacteria can import and metabolise various carbohydrates from their environment, such as glucose, glycerol, sucrose, or acetate. This growth mode, in which organic molecules serve as an additional energy and carbon source alongside light and CO_2, is referred to as photomixotrophy. *Synechocystis* can grow in the presence of glucose; however, a low concentration of fructose is lethal (Flores and Schmetterer, 1986; Rippka, 1972; Rippka et al., 1979; Stebegg et al., 2023). To accommodate the shift in carbon source, *Synechocystis* undergoes significant metabolic changes, resulting in faster growth and optimisation of the metabolic pathways (X. Chen et al., 2016; Muth-Pawlak et al., 2022; Schulze et al., 2022).

The enhanced growth rate is of interest to biotechnological applications (Matson and Atsumi, 2018). However, metabolising the external carbohydrates releases CO_2, negatively impacting the CO_2 emissions of photomixotrophic applications (Patel et al., 2021). They would also compete with food production for arable land unless side and waste streams are used to source these carbohydrates. Engineering of strains capable of metabolising these streams is therefore important. Xylose, a wood derivative, could serve as the carbon source for an engineered *Synechocystis* (Ranade et al., 2015).

The effect of photomixotrophic growth on photosynthesis remains unclear, with contrasting results. Some studies report partial inhibition of O_2 evolution, while others indicate an increase in maximal photosynthetic activity (Haimovich-Dayan et al., 2011; Lee et al., 2007; Takahashi et al., 2008). Since photosynthesis is intertwined with respiration, the redox balance of the PETC and the NAD(P)H pool might be important regulatory factors. The pyridine nucleotide transhydrogenase PntAB localises to the thylakoid membrane and controls the $NADPH/NAD^+$ and $NADH/NADP^+$ ratios. Its expression is upregulated in photomixotrophy (Muth-Pawlak et al., 2022). Furthermore, glucose metabolism and CO_2 fixation are not separate in *Synechocystis*; thus, carbon metabolism must be rearranged under photomixotrophy (Nakajima et al., 2014; Yang et al., 2002). The flux through the CBB cycle decreases while the flux through the OPP shunt pathways increases (Takahashi et al., 2008), potentially replenishing the CBB cycle intermediates (Makowka et al., 2020). The activity of the CBB cycle is redox-regulated; furthermore, its activity affects the photosynthetic activity. It is, therefore, important to fully understand the carbon flux regulation in photomixotrophic cells before biotechnological application.

1.5 Light-driven whole-cell biotransformation

The advances in biocatalysis and photocatalysis have enabled the emergence of a combined approach - photo-biocatalysis - where light is utilised directly or indirectly to drive enzymatic reactions. Photosystems (PSI and PSII) are examples of photoenzymes, enzymes that directly require light for their catalytic activity. However, due to their structural complexity (see 1.3.1), the applications of PSII or PSI are mainly focused on semi-artificial photo-bioelectrochemical cells (Yehezkeli et al., 2013). In biocatalysis, the substrate transformation is performed by enzymes requiring a source of electrons in the form of a reduced cofactor. Two approaches exist: a purified enzyme and a sacrificial electron donor such as water or ethylenediaminetetraacetic acid (EDTA) in photo-chemocatalysis, or NAD(P)H/Fd provided by the cell's metabolism in whole-cell photo-biocatalysis. This is where cyanobacteria and other photosynthetic organisms offer a compelling platform for

photo-biocatalytic applications thanks to photosynthetic reactions (Madavi et al., 2022; Schmermund et al., 2019). Photosynthetic organisms provide a more environmentally friendly alternative to fossil-based feedstock in the chemical industry and traditional biocatalysis (Cheng et al., 2023a).

Photosynthesis is the source of reducing power and continuously replenishes the cofactor pool under illumination. Therefore, applications that combine photosynthesis and biocatalytic transformation are often referred to as light-driven whole-cell biotransformations (hereafter biotransformations). It is important to note that while photosynthesis provides reduced cofactors under light, in the dark, these cofactors are supplied by catabolic reactions of storage compounds. Consequently, the used enzymes remain active in the dark, albeit with lower activities, as long as the enzyme's substrates are also available. As a result, these applications are not strictly dependent on light but greatly benefit from it, achieving high conversion rates under illumination (Assil-Companioni et al., 2020; Spasic et al., 2022; Tüllinghoff et al., 2022).

WT cyanobacteria have been used in biotransformation applications that rely on native enzymes to convert supplied substrates into desired products (Balcerzak et al., 2014; Górak and Żymańczyk-Duda, 2015). For example, the reduction of cinnamaldehyde into cinnamyl alcohol, an important molecule for the pharmaceutical and food industries, was demonstrated using *Synechocystis* with high yield and strict chemoselectivity (Yamanaka et al., 2015). Additionally, new enzymes have been discovered by screening WT cyanobacteria for ketone reduction (Hölsch et al., 2008; Hölsch and Weuster-Botz, 2010). Moreover, advances in synthetic biology tools have enabled the creation and use of recombinant cyanobacteria in biotransformation applications. Proof-of-concept studies have demonstrated biotransformations employing ene-reductases, imine reductases, cytochrome P450 monooxygenases (P450), and other oxidoreductases (Fig. 5).

In addition to a single enzyme performing one conversion step, biotransformations can combine several enzymes into cascades, such as the engineering of an *in vivo* two-step cascade in *Synechocystis* to convert cyclohexanone into 6-hydroxyhexanoic acid, a polymer building block (Tüllinghoff et al., 2023). The substrates required by the enzymes can be native or delivered externally. In the case of the external addition, the enzymes should remain inactive before the substrate is added, posing limited effects on cell metabolism. On the other hand, enzymes with native substrates constitute a continuous consumption of cofactors, with a potential impact on the energy balance of the cells.

This thesis focuses on the applications where NAD(P)H is the donor to heterologous enzymes originating from different organisms expressed in *Synechocystis* (Papers II, III and IV). However, Fd-dependent systems and various other enzymes are included in this chapter to provide a wider overview of the current applications.

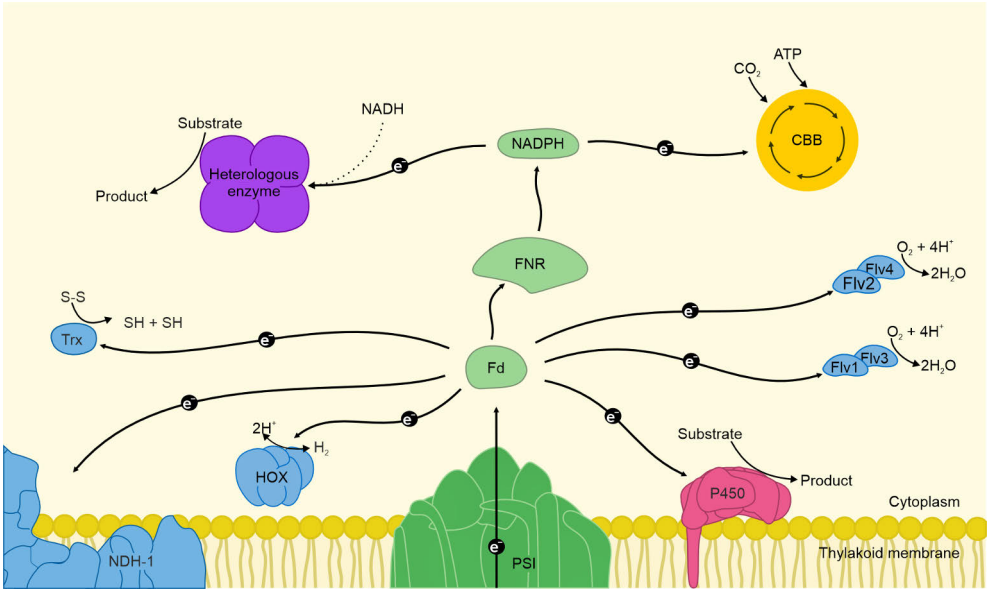

Figure 5. Examples of heterologous and native electron sinks in *Synechocystis*. CBB - Calvin-Benson-Bassham cycle, FNR - ferredoxin-NAD(P)H oxidoreductase, PSI - photosystem I, Fd - ferredoxin, P450 - cytochrome P450 monooxygenase, Trx - thioredoxin, NDH-1 - NADH dehydrogenase-like complex 1, HOX - Ni-Fe hydrogenase, NADPH - nicotinamide adenine dinucleotide phosphate, NADH - nicotinamide adenine dinucleotide, ATP - adenosine triphosphate, dotted line - alternative electron donor.

1.5.1 NAD(P)H-dependent systems

NAD(P)H is the central electron carrier used in cyanobacterial metabolism, produced by FNR in the last step of the LET (see 1.3.3) and in catabolic reactions within the OPP and EMP pathways (see 1.4). The primary sink for NADPH under illumination is the CBB cycle; however, some heterologous enzymes used in biotransformations also rely on the supply of NAD(P)H. This pits them against the CBB cycle and the rest of the cellular metabolic pathways reliant on NAD(P)H. Furthermore, these NAD(P)H-dependent enzymes create an additional electron sink, influencing the ATP/NAD(P)H ratio.

The source/sink ratio is tightly controlled. CO_2 fixation by RuBisCO is regarded as the main limiting factor for the electron flow from PSII to downstream carbon metabolism, and the excess electrons must be dissipated (see 1.3.4). This is especially true during sudden increases in light intensity or when inorganic carbon is limited. Therefore, increasing the overall electron sink capacity by adding a heterologous enzyme can improve photosynthetic efficiency. In addition to heterologous electron sinks, a similar enhancement of photosynthetic efficiency can be achieved through carbon sink engineering by targeting and increasing the carbon

flux to a desired metabolite (Ducat et al., 2012; Kugler and Stensjö, 2023; Oliver and Atsumi, 2015; Santos-Merino et al., 2021; Singh et al., 2022).

1.5.1.1 Ene-reduction

Asymmetric hydrogenation of alkenes is an important reaction in the chemical industry since it generates two stereogenic centres. Several enzyme families can reduce the carbon-carbon double bond (C=C), with ene-reductases from the Old Yellow Enzyme (OYE) oxidoreductase family being the most commonly applied. Other families include flavin-independent medium-chain dehydrogenase/reductases, clostridial enoate reductases, and short-chain dehydrogenase/reductases (Lonardi et al., 2023; Toogood and Scrutton, 2014). The OYE family is widespread in nature. The first enzymes were known already in the 1930s and cloned in the 1990s from *Saccharomyces cerevisiae* (Niino et al., 1995). Since then, enzymes native to cyanobacteria, microalgae, fungi, bacteria or plants have been tested for the hydrogenation of various compounds (Böhmer et al., 2020; G. Turrini et al., 2017; Hall et al., 2008; Meah and Massey, 2000; Robescu et al., 2022, 2020; Toogood and Scrutton, 2014). Furthermore, OYE showed substrate and function promiscuity. Through targeted protein engineering, an OYE from the thermophilic bacterium *Geobacillus kaustophilus* was modified to perform only its secondary function, the Morita-Baylis-Hillman reaction, a carbon-carbon bond-forming reaction whose products possess promising biological activity (Porto and Porto, 2023; Wang et al., 2024).

In papers II, III and IV, a representative of the OYE family from the soil bacterium *Bacillus subtilis*, YqjM, is used. It has been demonstrated to play a role in *B. subtilis* stress response to xenobiotics (Fitzpatrick et al., 2003) and its crystal structure was determined. Similarly to other OYEs, FMN is non-covalently bound to the C-terminus; however, in contrast to other OYEs, YqjM forms a homo-tetramer composed of two catalytically dependent dimers (Kitzing et al., 2005). The reaction mechanism is separated into two steps: the reductive half-reaction [electron transfer from NAD(P)H to YqjM] and the oxidative half-reaction (reduction of C=C) of various substrates (Kohli and Massey, 1998; Pesic et al., 2017). YqjM prefers NADPH as the electron donor. Furthermore, the oxidative half-reaction is approximately 50-fold faster when 2-methylmaleimide (2-MM) is used as the substrate, establishing the reductive half-reaction as the limiting step in YqjM's activity (Assil-Companioni et al., 2020).

The expression of heterologous enzymes suitable for biocatalytic application in cyanobacteria was established with esterase and decarboxylase, where the cell extract was used as the biocatalyst *in vitro* (Bartsch et al., 2015). The first proof-of-concept demonstration of *in vivo* biotransformation used the NAD(P)H-dependent

ene-reductase YqjM in *Synechocystis* (Köninger et al., 2016). It reached a specific activity of ~165 $U \cdot g_{DCW}^{-1}$ (OD_{750} = 2), the highest recorded to date with 2-MM as its substrate. Five additional substrates were tested, albeit reaching lower conversion (Assil-Companioni et al., 2020). A recent study compared YqjM with four more OYEs against six substrates and also evaluated their activity in larger volumes (Grimm et al., 2025). Nevertheless, YqjM represents a strong electron sink, establishing itself as a model for highly selective biotransformations. It can also serve as a tool in studies focusing on a fundamental understanding of photosynthetic electron flux.

1.5.1.2 Baeyer-Villiger oxidation

Another industrially relevant biotransformation reaction is the selective oxyfunctionalisation of cyclic ketones into their respective lactones. This reaction is known as the Baeyer-Villiger oxidation and is performed in the presence of peroxyacids or peroxides in the chemical industry. This process not only has a high environmental footprint but also leads to unwanted side-products (Sever and Root, 2003). In nature, this reaction is mediated by the Baeyer-Villiger monooxygenases (BVMOs). There are three types: type I, which contains bound flavin adenine dinucleotide (FAD) and requires NADPH; type II, which requires NADH and binds FMN (Kamerbeek et al., 2004); and an odd type O that interacts with FAD and NADPH but belonging to a different flavoprotein group (Fürst et al., 2019).

BVMOs present a diverse family, featuring examples from different organisms, various substrate specificities, and functional promiscuity. Furthermore, several crystal structures have been solved, allowing for rational protein engineering (Fürst et al., 2019). The availability of O_2 is a limiting factor for their activity in applications using heterotrophs (Baldwin and Woodley, 2006). Therefore, photosynthetic organisms offer a solution to this limitation thanks to photosynthesis. Several BVMO representatives have been commonly expressed in cyanobacteria. These BVMOs originate from *Acidovorax* sp. CHX100, *Parvibaculum lavamentivorans* (Parvi), *Burkholderia xenovorans* (Xeno), and *Acinetobacter calcoaceticus* (Acineto). An interesting cold-active BVMO was recently isolated from Arctic bacteria, showing good activity at low temperatures (Chánique et al., 2023).

ε-caprolactone is an important bulk chemical in the polymer industry. Currently, it is produced via a one-step reaction from cyclohexanone using acetic peracid or through a two-step enzymatic reaction from cyclohexanol by alcohol dehydrogenase (ADH) and BVMO, requiring molecular oxygen. However, BVMO is inhibited by its product at high concentrations (>60 mM) and, to a lesser extent, by cyclohexanone and cyclohexanol (Reimer et al., 2017). When expressed in *Synechocystis*, Acineto reached a specific activity of 2.3 $U \cdot g_{DCW}^{-1}$ (OD_{750} = 10) using

the light-inducible P_{psbA2} promoter (Böhmer et al., 2017) and 4 $U \cdot g_{DCW}^{-1}$ (OD_{750} = 10) using the P_{cpcB} promoter (Erdem et al., 2022). The specific activity of Parvi was ~5 $U \cdot g_{DCW}^{-1}$ (OD_{750} = 10), while Xeno reached ~20 $U \cdot g_{DCW}^{-1}$ (OD_{750} = 10), both using the P_{cpcB} promoter (Erdem et al., 2022). The expression of BVMO from *Acidovorax* sp. CHX100, under the control of a nickel-inducible promoter from the replicative plasmid, yielded ~60 $U \cdot g_{DCW}^{-1}$ (OD_{750} = ~2.5), while the same plasmid integrated into the chromosome resulted in only ~24 $U \cdot g_{DCW}^{-1}$ (OD_{750} = ~2.5). However, in a scale-up system (2L photobioreactor), the specific activity reached an initial maximum of 30 $U \cdot g_{DCW}^{-1}$. It gradually decreased over the course of the experiment, likely due to substrate, product or side-product inhibitory effects (Tüllinghoff et al., 2022). The inhibition by the product formation was circumvented by engineering an enzymatic cascade converting ε-caprolactone into 6-hydroxyhexanoic acid (Tüllinghoff et al., 2023).

1.5.1.3 Other enzymes

Cyanobacteria can harbour other NAD(P)H/O_2-dependent enzymes and supply them with reducing power through photosynthesis. Indeed, imine reductases have been expressed in *Synechocystis*, and their activity against eight cyclic imines was tested with promising results and high specific activities (Büchsenschütz et al., 2020). A wide variety of imine reductases was characterised through *Escherichia coli* (*E. coli*) biotransformation (Velikogne et al., 2018). Furthermore, amine dehydrogenases and imine reductases with biocatalytic potential have been recently reviewed (Yuan et al., 2024). Additionally, ω-hydroxylation of nonanoic acid methyl ester by recombinant *Synechocystis* expressing the alkane monooxygenase system resulted in a specific activity of ~3 $U \cdot g_{DCW}^{-1}$ in a 3L photobioreactor (Hoschek et al., 2017, 2019a).

1.5.2 Fd-dependent systems

Reduced Fd donates electrons to several pathways (see 1.3.2). A heterologous enzyme will thus compete with these native pathways for electrons. However, native pathways also show potential for biotechnological applications. Photobiological hydrogen production is one of the promising technologies in the solar fuels and chemicals field, aiding the transition towards a sustainable future. However, its widespread industrial application still remains in the future (Redding et al., 2022). Many cyanobacteria possess native hydrogenase, which produces H_2 in the dark during the catabolism of storage compounds (Kossalbayev et al., 2020). Additionally, the nitrogenase in N_2-fixing strains generates H_2 (Barney, 2020), as do some microalgal species (Kosourov et al., 2020). However, linking H_2 production to

photosynthetic electrons is challenging, mainly because hydrogenase and nitrogenase are O_2 sensitive (Khetkorn et al., 2017; Santana-Sánchez et al., 2023). The advances and strategies for improved productivity, such as introducing O_2-tolerant hydrogenase into *Synechocystis* (Lupacchini et al., 2021), were recently reviewed (Kosourov et al., 2021).

Enzymes from the P450 superfamily offer a wide range of interesting reactions for biocatalysis. There are over 300,000 enzymes across all living organisms (Nelson, 2018). While NADPH is commonly the energy source in native systems, when expressed in cyanobacteria, they depend on reduced Fd to supply the necessary reducing power (Agustinus and Gillam, 2023). The first use of P450s in cyanobacteria was the expression of *p*-coumarate-3-hydroxylase for caffeic acid production in *Synechocystis* (Xue et al., 2014). Two P450s were co-expressed in *Synechocystis* to reconstitute the dhurrin pathway, demonstrating the suitability of cyanobacteria for multi-enzyme cascades (Lassen et al., 2014; Wlodarczyk et al., 2016). Several P450s have been utilised since: mammalian P450 CYP1A1 in *Synechococcus* PCC 7002 (Berepiki et al., 2018, 2016; Torrado et al., 2022) or CYP450chx from *Acidovorax* sp. CHX100 (Hoschek et al., 2019b; Tüllinghoff et al., 2024), CYP110D1 from *Nostoc* sp. PCC 7120 (Mascia et al., 2022), and CYP79A1 from *Sorghum bicolor* (Sutardja et al., 2024) in *Synechocystis.*

1.5.3 Improvement strategies

Despite steady progress in cyanobacterial biotransformation applications, their large-scale deployment is still not feasible. Therefore, further improvements in activities and yields are necessary to make them competitive with currently used heterotrophic systems or traditional fossil-based catalysis. Every strain/enzyme/substrate/product combination might perform differently and have various limitations, making a uniform improvement strategy impossible. Thus, characterising each application regarding substrate or product toxicity on the selected strain, cofactor availability, enzyme expression, activity, and potential inhibition is essential (Köninger et al., 2016).

Genes encoding heterologous enzymes can be integrated into the genome or transcribed from replicative plasmids, which generally leads to higher protein accumulation (Y. Chen et al., 2016). Expression from a plasmid led to higher BVMO accumulation and specific activity compared to expression from a genomic integration site (Tüllinghoff et al., 2022). Similarly, selecting the appropriate promoter is crucial; however, the lack of a wide variety of promoters suitable for cyanobacteria complicates this selection. Commonly used native promoters originate from CO_2 fixation, PSI, or PSII components (Cheng et al., 2023b). The P_{cpcB} promoter of the C-phycocyanin β subunit has been shown to lead to the highest

accumulation and specific activity of BVMOs and YqjM compared to P_{psbA2} or P_{zia} (Assil-Companioni et al., 2020; Erdem et al., 2022). While high protein levels might be beneficial in some cases, a tuneable promoter might be required for other enzymes (Tüllinghoff et al., 2022). Recently, high-throughput screening of a large molecular toolbox (12 promoters, 20 ribosome-binding sites, a bicistronic domain, and a genetic insulator) yielded promising results and identified genetic elements leading to enhanced expression and biotransformation. However, it is important to note that selecting a universal combination of these elements suitable for all enzymes is likely impossible (Jodlbauer et al., 2024; Stensjö et al., 2018).

Deletion of native electron sinks that might compete with the heterologous enzyme is also a popular approach. Deleting Flv1/3 hetero-oligomer improved the specific activity of YqjM and BVMOs in *Synechocystis* (Assil-Companioni et al., 2020; Erdem et al., 2022). However, these enzymes are NAD(P)H-dependent, and Flv1/3 uses reduced Fd as the electron donor. They are thus not in direct competition for reducing power, suggesting that the improvements could have been caused indirectly. Indeed, the benefit was visible only under specific conditions. Similarly, the deletion of hydrogenase enhanced YqjM activity, but only under high culture density (Spasic et al., 2022). In combination with P450s (Fd-dependent enzymes), the deletion of COX significantly improved the activity of CYP1A1 (Torrado et al., 2022). Knocking out the NDH-1 complex, and thus the CET, was also beneficial for CYP1A1 (Berepiki et al., 2018). This suggests that deleting competing electron sinks is a viable option for Fd-dependent enzymes, but is more complex for NAD(P)H-dependent ones. Decreasing FNR's affinity for Fd can increase the availability of reduced Fd; however, it also presents a significant metabolic burden due to decreased availability of NADPH (Kannchen et al., 2020).

Localisation of heterologous enzymes is another interesting target for optimisation strategies. P450s are commonly bound to membranes in their original organisms, and anchoring them to the thylakoid membrane in *Synechocystis* via PetC1 protein (Rieske subunit of Cyt b_6f) has indeed proven beneficial to their activity (Hanamghar et al., 2025). Similar results were obtained by linking P450 to PSI in *Synechococcus* (Lassen et al., 2014) or hydrogenase to PSI in *Synechocystis* (Appel et al., 2020). Localising NAD(P)H-dependent enzyme to the thylakoid membrane can also prove advantageous, thanks to the proximity to FNR. However, this remains to be studied in cyanobacteria. Nevertheless, localising a BVMO to the chloroplast in *Chlamydomonas* increased the specific activity 1.6-fold (Siitonen et al., 2023). Linking P450 CYP79A1 directly to Fd has also led to improvements in *Nicotiana benthamiana* (Mellor et al., 2016), while a PSI/Fd/FNR fusion system enhanced NADPH regeneration in *Synechocystis* (Medipally et al., 2023). This can potentially enhance biotransformation using NADPH-dependent enzymes by fusing them to this complex.

Lastly, to overcome limitations in light availability, new types of photobioreactors need to be developed and optimised for use with cyanobacteria as biocatalysts. Promising results were achieved with an internal illumination system (Hobisch et al., 2021) or a thin coil bioreactor (Malihan-Yap et al., 2025).

2 Aims of the Study

Cyanobacteria hold promise for biotechnological applications, supporting the development of bio-based industries and the production of green chemicals. Light-driven whole-cell biotransformations are an emerging field harnessing solar energy to produce fine chemicals, replacing their fossil-based equivalents. However, a thorough understanding of the cell's physiological response to the presence of a strong electron sink in the form of heterologous enzymes is still lacking.

Understanding the regulation of photosynthesis and electron partitioning is of utmost importance for guiding the targeted approaches in engineering cyanobacteria as a viable chassis for sustainable green chemicals. Further development is needed to improve these applications' overall performance and economic competitiveness with the already established processes. This thesis aims to fill the knowledge gaps in understanding the regulatory mechanisms of native electron sinks and the interplay between native and heterologous electron sinks in the light-driven whole-cell biotransformation and to identify potential targets for improving strategies.

This thesis focuses on the following objectives:

I. Study the regulatory mechanisms controlling the activity of the strong inherent electron sink - flavodiiron proteins.

II. Investigate the effect of a strong heterologous electron sink (YqjM) on the photosynthetic apparatus of *Synechocystis* and elucidate the electron partitioning from ferredoxin, the central electron distribution hub downstream of PSI.

III. Address the bottleneck of ene-reduction using the strong heterologous enzyme YqjM.

IV. Identify and alleviate the limiting factors of the Baeyer-Villiger oxidation reaction in light-driven whole-cell biotransformation.

V. Review the role of photosynthetic microorganisms as biocatalysts.

3 Materials and Methods

3.1 Cyanobacterial strains and culturing conditions

3.1.1 Strains and cultivation conditions

Synechocystis sp. PCC 6803 was used in all studies included in this thesis. The complete list of strains used in this thesis and their brief descriptions are included in Table 1. *E. coli* Dh5α was used for cloning purposes and plasmid cryopreservation.

The dry cell weight (DCW) was previously determined using lyophilisation of the cell suspension at various ODs, with OD = 10 corresponding to 2.4 $g_{DCW} \cdot L^{-1}$ (Assil-Companioni et al., 2020).

Synechocystis strains were maintained as cryostocks (10% dimethyl sulfoxide, DMSO) at -80 °C for long-term storage or on 1.5 % agar BG-11 plates for short-term storage. Prior to experiments, strains were recovered in BG-11 medium (20 mM HEPES, pH = 7.5) at 30 °C and dim light. Subsequently, stock cultures were maintained using 100 mL Erlenmeyer flasks with a working volume of 30 mL of BG-11 at 30 °C, ambient CO_2 (0.04%), 50 $\mu mol_{photons} \cdot m^{-2} \cdot s^{-1}$ continuous broad white light illumination (fluorescent light) and orbital shaking at 115 rpm.

All experiments performed in Turku (Papers II, III and IV) followed the following cultivation procedure. Stock/recovery culture (3–5 days) - Preculture I (OD_{750} = 0.1, 2–3 days) - Preculture II (OD_{750} = 0.1, 2–3 days in experimental conditions) - Experimental culture (OD_{750} = 0.1, 4–5 days in experimental conditions). Antibiotics were used in all but experimental cultures. The precultures in Paper I were grown at 30 °C, 3% CO_2 (0.04%) and continuous 50 $\mu mol_{photons} \cdot m^{-2} \cdot s^{-1}$ broad white illumination. After harvesting, the cells were resuspended in fresh BG-11 with the starting OD_{750} = 0.2 for experimental cultures and grown at 30 °C, ambient CO_2 (0.04%) and 50 $\mu mol_{photons} \cdot m^{-2} \cdot s^{-1}$ broad white illumination.

Growth conditions in Paper II were 30 °C, ambient CO_2 (0.04%), 50 $\mu mol_{photons} \cdot m^{-2} \cdot s^{-1}$ of constant broad white illumination (fluorescent light), and orbital shaking at 115 rpm.

Table 1. List of strains used in this thesis.

Strain name	Genetic modification	Paper	Ref.
WT		Paper I-IV	Williams, 1988
ΔFlv1	Deletion of sll1521	Paper IV	Helman et al., 2003
ΔFlv2	Deletion of sll2019	Paper I	Zhang et al., 2012
ΔFlv3	Deletion of sll0550	Paper I	Helman et al., 2003
ΔFed2/Fed2	Deletion of sll1382	Paper I	Wang et al., 2022
ΔFed3	Deletion of slr1828	Paper I	
ΔFed4	Deletion of slr0150	Paper I	
ΔFed5/Fed5	Deletion of slr0148	Paper I	
ΔFed6	Deletion of ssl2559	Paper I	
ΔFed7/Fed8/Fed9	Deletion of sll0662, ssr3184, slr2059	Paper I	
ΔFed9	Deletion of slr2059	Paper I	
ΔFed10	Deletion of sll1584	Paper I	Paper I
ΔFed11	Deletion of ssl3044	Paper I	
ΔNdhD1NdhD2 (ΔD1D2)	Deletion of slr0331, slr1291	Paper I	Ohkawa et al., 2000
ΔFlv3 D1D2	Deletion of sll0550, slr0331, slr1291	Paper I	Nikkanen et al., 2020
ΔFNR_L (FS1)	Deficiency of the large FNR isoform	Paper I	Thomas et al., 2006
ΔFNR_S (MI6)	Deficiency of the small FNR isoform	Paper I	
Fed1-VC+Flv1-VN	IPTG-induced overexpression of proteins fused with N- or C-terminal fragment of Venus fluorescent protein variant I152L from pDF-lac2 plasmid (for BiFC)	Paper I	Paper I
Fed1-VC+Flv3-VN		Paper I	
Flv3-VC+Fed1-VN		Paper I	
Fed1-VC+Flv2-VN		Paper I	
Fed1-VC+Flv4-VN		Paper I	
Fed9-VC+Flv1-VN		Paper I	
Fed9-VC+Flv3-VN		Paper I	
Flv3-VC+Flv1-VN		Paper I	
Flv2-VC+Flv4-VN		Paper I	
Flv1-VC+Flv1-VN		Paper I	
Flv3-VC+Flv3-VN		Paper I	
Flv3-VC+Flv2-VN		Paper I	
Flv2-VC+VN		Paper I	
Fed1-VC+VN		Paper I	
FNR_L-VC+VN		Paper I	
Syn::YqjM	Expression of *yqjm* gene in WT background	Paper II-IV	Assil-Companioni et al., 2020
ΔFlv1::YqjM	Expression of *yqjm* gene in ΔFlv1 background	Paper II-IV	
Syn::Parvi	Expression of *parvi* gene in WT background	Paper IV	Erdem et al., 2022
ΔFlv1::Parvi	Expression of *parvi* gene in ΔFlv1 background	Paper IV	
Syn::Xeno	Expression of *xeno* gene in WT background	Paper IV	Paper IV
ΔFlv1::Xeno	Expression of *xeno* gene in ΔFlv1 background	Paper IV	Erdem et al., 2022

The experimental conditions in Paper III were set at 30 °C, ambient CO_2 (0.04%), 200 $\mu mol_{photons} \cdot m^{-2} \cdot s^{-1}$ constant broad white illumination in a growth chamber equipped with LED lights (AlgaeTron AG230, PSI, Czechia), and orbital shaking at 115 rpm. All experiments performed by the collaborators in Graz in Paper III used modified conditions. For low-light cultivation, a plant growth chamber (SWGC-1000, witeg Labortechnik, Germany) with white continuous illumination, 30 °C, 50% relative humidity, 40–60 $\mu mol_{photons} \cdot m^{-2} \cdot s^{-1}$ and 140 rpm was used. For high-light cultivation, a chamber from Thermo Electro Corporation at 30 °C was combined with tuneable red and blue LED illumination set to 200 $\mu mol_{photons} \cdot m^{-2} \cdot s^{-1}$. The orbital shaker was set to 160 rpm. Furthermore, cells were grown photoautotrophically or photomixotrophically with 5 mM D-glucose added during inoculation.

Photoautotrophic cultivation in Paper IV was performed under 30 °C, ambient CO_2 (0.04%, LC) or 3% CO_2 (HC), 150 $\mu mol_{photons} \cdot m^{-2} \cdot s^{-1}$ continuous broad white or white light enriched with red and blue wavelengths (W+R/B) and orbital shaking at 115 rpm. Precultures II and experimental cultures were kept in a growth chamber with LED lights (AlgaeTron AG230, PSI, Czechia) equipped with custom red and blue LED strips.

3.1.2 Spectra measurements

The light spectra were measured using SpectraPen (PSI, Czech Republic). For Paper I, the spectra of the light source in membrane inlet mass spectrometry (MIMS) and DUAL-KLAS-NIR, set to 500 $\mu mol_{photons} \cdot m^{-2} \cdot s^{-1}$ (Paper II - Fig. S1), were measured. For Paper IV, the white and W+R/B light spectra were measured at 150 $\mu mol_{photons} \cdot m^{-2} \cdot s^{-1}$and 300 $\mu mol_{photons} \cdot m^{-2} \cdot s^{-1}$ (Paper IV - Fig. S2).

3.1.3 Construction of mutant strains

Strains for the Bimolecular Fluorescence Complementation (BiFC) test were created using a modular cloning approach (details in Paper I - Supplementary text). Briefly, proteins of interest were fused with either the N- or C-terminus of the Venus fragment through a short linker and co-expressed under an isopropyl β-d-1-thiogalactopyranoside (IPTG)-inducible lac2 promoter and S3 ribosome binding site of the *cpcB* gene on the pDF-lac2 plasmid (Thiel et al., 2018).

To create the two ferredoxin mutants in Paper I, the respective genome fragments were amplified by PCR and the final plasmids were constructed using the Gibson assembly technique (Gibson et al., 2009). Plasmids were sequenced to verify the assembly and transformed into *Synechocystis* (Williams, 1988). Our collaborators from Graz kindly provided the plasmid for Syn::Xeno creation in Paper IV, and the

standard transformation protocol was followed. In both papers, colony PCR was performed to confirm the full segregation of mutant strains.

3.2 Light-driven whole-cell biotransformation

3.2.1 Biotransformation conditions

Before the biotransformation reaction, cells were harvested in the logarithmic growth phase (OD_{750} = ~0.8 in LC or OD_{750} = ~1.8 in HC in Papers II and IV) by centrifugation (5000 g, 8 min, 21 °C). The pellet was resuspended in fresh BG-11 and adjusted to the desired OD. Samples were left in the growth conditions for 30 min before continuing with experimental procedures.

To measure the biotransformation rate over time, samples were set to OD_{750} = 2.5 (Paper I) or OD_{750} = 10 (Paper IV). The reaction was initiated by adding 10 mM of 2-MM for YqjM or 5 mM of cyclohexanone for BVMOs. The final volume of the reaction was 5 mL. Samples (300 µL) were taken at specified intervals, quickly frozen in liquid N_2 and stored at -20 °C until liquid-liquid extraction and gas chromatography (GC) analysis. The reaction conditions were 30 °C, 200 $\mu mol_{photons} \cdot m^{-2} \cdot s^{-1}$ white light, ambient CO_2 (Paper II) or 30 °C, 300 $\mu mol_{photons} \cdot m^{-2} \cdot s^{-1}$ white or W+R/B light and ambient or 3 % CO_2 (Paper IV).

To calculate the dark biotransformation rates, samples were placed in Falcon tubes covered in aluminium foil in the incubator for 60 min (Paper II).

Samples for biophysical and gas exchange measurements were set to OD_{750} = 2.5 (Papers II and III) or Chl *a* = 10 $\mu g \cdot mL^{-1}$ (OD_{750} = ~2.5, Paper IV). The reaction time was 5 min (Paper II) or 30 min (Paper III), after which samples were taken for specific measurements. When applicable, 2.5 mM D-glucose was added to the samples (Paper III). In Paper IV, the cyclohexanone concentration was 1.25 mM, and the reaction time was 50 min. The remaining conditions for the biotransformation rate experiment were as described above.

Further experiments in Paper III were performed in Graz under the following conditions. The cells were harvested after 4–5 days of growth (OD_{750} = 1–2). The pellet was resuspended in fresh BG-11 and set to a specific OD. The reaction was set up in a vial with a final volume of 1.2 mL and initiated by adding 10 mM substrate. Samples (250 µL) were taken at specified time points, quickly frozen in liquid N_2, and stored for analysis. To study the effect of external carbon sources, various concentrations of selected carbohydrates (D-fructose, D-galactose, D-glucose, D-saccharose or D-sorbitol) were added simultaneously with the substrate (Paper III).

3.2.2 Large-scale application using a bubble column reactor

Cells were grown until OD_{750} = 1–1.5. They were then centrifuged (3220 g, 20 min, 24 °C), and the pellet was resuspended in fresh BG-11 to reach OD_{750} = 10. The biotransformation reaction was run using the bubble column reactor (φi = 5 cm, h = 50 cm, V = 200 mL) fitted with emitting coils. 40 Wireless Light Emitters (WLEs) were suspended in the reactor to provide internal illumination. The WLEs consist of a white LED and a receiving coil inside a polycarbonate shell, as described previously (Hobisch et al., 2021). The air was supplied via an electric pump (Boyu S-4000B) at a rate of 0.6 $L \cdot min^{-1}$. A fan was used to maintain the temperature at 30 °C. The reaction was initiated by adding 10 mM 2-MM alongside 5 mM D-glucose. At predetermined time points, 100 µL aliquots were taken, quickly frozen in liquid N_2 and stored until liquid-liquid extraction and GC analysis (Paper III).

3.2.3 Liquid-liquid extraction and gas chromatography

For the detection of 2-MM and 2-methylsuccinimide (2-MS) in Paper II and cyclohexanone, cyclohexanol and ε-caprolactone in Paper IV, samples were thawed out at room temperature and extracted using a 3-step liquid-liquid extraction with ethyl acetate. The organic phase was dried with anhydrous $MgSO_4$ and analysed on GC-2010 Pro gas chromatograph (Shimadzu, Japan) equipped with an HP-5MS 30 m × 0.25 mm (5%-Phenyl)-methylpolysiloxane column (19091S-133, Agilent) with nitrogen as the carrier gas in splitless injection mode. Compounds were separated at 35 °C (hold 3 min), 200 °C (hold 3 min, 10 $°C \cdot min^{-1}$) and 300 °C (hold 3 min, 25 $°C \cdot min^{-1}$). The linear velocity was 11 $cm \cdot sec^{-1}$. Acetophenone (2 mM) was used as the internal standard. Samples containing known amounts of 2-MM and 2-MS (Papers II and IV) or cyclohexanone, ε-caprolactone and cyclohexanol (Paper IV) were used to obtain calibration curves.

The quantification of substrates (2-MM, N-methylmaleimide and 2-methyl-N-methylmaleimide) and their respective products in Paper III was performed at the facilities of our collaborators in Graz according to the following description. Samples were extracted by adding 300 µL ethyl acetate with 2 mM n-decanol as the internal standard. The organic phase was dried using anhydrous $MgSO_4$, centrifuged and analysed using a Gas Chromatography Flame Ionization Detector (GC-FID) GC-2010 Pro gas chromatograph (Shimadzu, Japan) equipped with a ZB-5 column (Macherey-Nagel, Düren, Germany). For the substrate 2-cyclohexen-1-one and its product, dichloromethane was used instead of ethyl acetate. See Paper III and Assil-Companioni et al. (2020) for detailed information.

3.3 Biophysical methods to study photosynthesis

3.3.1 Fluorescence and absorbance measurements

Chl *a* fluorescence was followed with a DUAL-PAM 100 spectrophotometer (Walz, Effeltrich, Germany) equipped with red actinic light. In Paper II, biotransformation samples were dark-adapted for two minutes before exposure to 100 $\mu mol_{photons} \cdot m^{-2} \cdot s^{-1}$ for 240 s, followed by 240 s of 170 $\mu mol_{photons} \cdot m^{-2} \cdot s^{-1}$. An additional 60 s were recorded in the dark to observe the dark relaxation of the fluorescence signal and the F_0 rise. A saturating pulse (5000 $\mu mol_{photons} \cdot m^{-2} \cdot s^{-1}$, 500 ms) was distributed every 20 s to calculate the effective yields of PSI and PSII [Y(I) and Y(II), respectively]. Their values were taken from the DUAL-PAM software (Papers II and III). For simultaneous quantification of the electron transport rates through PSII and PSI (ETR(II) and ETR(I), respectively) in Paper II, Chl *a* fluorescence and P700 absorbance changes were followed. Samples were dark-adapted for ten minutes before exposure to 200 $\mu mol_{photons} \cdot m^{-2} \cdot s^{-1}$ for 120 s. The following equations were used to calculate ETR(II) and ETR(I): ETR(II) = Y(II) x PAR x 0.5 x 0.84 and ETR(I) = Y(I) x PAR x 0.5 x 0.84, PAR is the photosynthetically active radiation (in $\mu mol_{photons} \cdot m^{-2} \cdot s^{-1}$), 0.84 is the proportion of photons absorbed by the cells, and 0.5 is a correction factor assuming that photons are absorbed equally by PSII and PSI (Baker et al., 2007).

To examine the redox changes of Pc, P700, and Fd, I used the DUAL-KLAS-NIR spectrophotometer (Walz, Effeltrich, Germany) as described previously (Nikkanen et al., 2020). In brief, absorbance changes between 780–820, 820–870, 840–965 and 870–965 nm were used to deconvolute the redox changes using differential model plots. These were prepared by measuring a set of *Synechocystis* mutants with scripts provided by the manufacturer and modified according to (Theune et al., 2021). The Chl *a* concentration of the samples was adjusted to 10 $\mu g \cdot mL^{-1}$ (Paper II) or 20 $\mu g \cdot mL^{-1}$ (Paper I), and the samples were dark-adapted for ten (Paper II) or fifteen minutes (Paper I). The NIRMAX script (3400 $\mu mol_{photons} \cdot m^{-2} \cdot s^{-1}$ red actinic light for 3 s, dark for 4 s, and far-red light for 10 s) was used to follow the redox changes. A saturating pulse to achieve complete Fd pool reduction was given after 200 ms of red actinic light illumination. BG-11 used in these experiments was copper-replete; therefore, Pc was the dominant electron carrier between Cyt b_6f and PSI. The presence of Cyt c_6 could have a minor effect on the Pc signal (Sétif et al., 2019).

NAD(P)H fluorescence was followed using the NADPH/9-AA module (Schreiber and Klughammer, 2009) for DUAL-PAM (Walz, Effeltrich, Germany). Samples with Chl *a* set to 5 $\mu g \cdot mL^{-1}$ (Papers I, II and IV) or 2.5 $\mu g \cdot mL^{-1}$ (Paper III) were dark-adapted for ten (Papers II, III and IV) or fifteen minutes (Paper I). The

fluorescence was monitored for 10 s of darkness followed by 180 s of 200 $\mu mol_{photons} \cdot m^{-2} \cdot s^{-1}$ (Papers II and III) or 300 $\mu mol_{photons} \cdot m^{-2} \cdot s^{-1}$ (Paper IV) of red actinic light and 60 s of a dark period. In Paper I, fluorescence was followed for 40 s under 500 $\mu mol_{photons} \cdot m^{-2} \cdot s^{-}1$ and 40 s in the dark. The light-induced NADPH accumulation was calculated as the difference between fluorescence shortly after the onset of illumination and the initial dark period.

3.3.2 Redox changes of cytochrome *b*$_6$*f* complex

The redox changes of Cyt *f* and *b* hemes of the Cyt b_6f protein complex were deconvoluted from the absorbance changes at 546, 554, 563 and 573 nm, measured by JTS-10 spectrophotometer (BioLogic, Seyssinet-Pariset, France). Appropriate 10 nm full width at half-maximal interference filters (EdmundOptics, Barrington, NJ, USA) and BG39 filters (Schott, Mainz, Germany) were used to protect the light detectors from scattering effects. The Chl *a* concentration was adjusted to 5 $\mu g \cdot mL^{-1}$. Samples were dark-adapted for three minutes before exposure to 500 $\mu mol_{photons} \cdot m^{-2} \cdot s^{-1}$ green actinic light for 5 s with white detection flashes administered during 200 µs dark intervals.

3.3.3 Electrochromic shift as the means to calculate *pmf*

Electrochromic shift (ECS) was measured as established previously (Nikkanen et al., 2020) using a JTS-10 spectrophotometer (BioLogic, Seyssinet-Pariset, France) with appropriate filters (Edmund Optics). In brief, the Chl *a* concentration was set to 7.5 $\mu g \cdot mL^{-1}$. Samples were dark-adapted before exposure to 500 $\mu mol_{photons} \cdot m^{-2} \cdot s^{-1}$ green actinic light interrupted with dark intervals. *pmf* was calculated as the extent of the ECS decrease at the dark intervals. Proton flux (vH^+) was calculated as *pmf* × gH^+, where gH^+ represents thylakoid conductivity calculated as the inverse of the time constant of a first-order fit to ECS relaxation kinetics during a dark interval (Cruz et al., 2005). In Paper I, low- and high-cation BG-11 variants were used in addition to standard BG-11.

3.3.4 Cyclic electron transport rate assessment

To quantify linear and cyclic electron transport rates, I measured the dark interval relaxation kinetics (DIRK) of the P700 and Pc signals using DUAL-KLAS-NIR (Walz, Effeltrich, Germany), as established previously (Theune et al., 2021). The Chl *a* concentration was adjusted to 15 $\mu g \cdot mL^{-1}$. Briefly, the sample was pre-illuminated for two minutes with 500 $\mu mol_{photons} \cdot m^{-2} \cdot s^{-1}$, after which the light was repeatedly turned off for 20 ms (100x). The P700 and Pc signals were averaged, and

the electron flow through PSI was calculated using a script in Origin developed by Lauri Nikkanen based on the equations in Theune et al. (2021). Samples were measured with or without 20 µM DCMU.

3.3.5 Acridine orange and acridine yellow fluorescence measurements

The acridine orange (AO) and acridine yellow (AY) fluorescence changes were monitored to assess the light-induced alkalisation of the cytosol (Teuber et al., 2001). The AO/AY module for DUAL-PAM 100 was used (Schreiber and Klughammer, 2009). The Chl *a* concentration was set to 5 $\mu g \cdot mL^{-1}$, and 5 µM of AO or AY were added before ten minutes of dark adaptation. The fluorescence was measured under 216 or 500 $\mu mol_{photons} \cdot m^{-2} \cdot s^{-1}$ as specified in Paper I.

3.4 Biochemical approaches

3.4.1 Chlorophyll concentration

Chl *a* concentration was quantified by extraction with 90% methanol. Briefly, 100 µL of samples were mixed with 900 µL of pure methanol (≥99.9%, Sigma-Aldrich), incubated at 65 °C for 15 min and centrifuged down. The extract was measured at OD_{665} and multiplied by 12.7 to obtain the final Chl *a* concentration in $\mu g \cdot mL^{-1}$.

3.4.2 Protein extraction and immunoblotting

Total protein extracts were isolated as previously described (Zhang et al., 2009), separated by sodium dodecyl sulphate-polyacrylamide gel electrophoresis on BioRad Mini-PROTEAN TGX 4-15% precast gels and blotted on polyvinylidene fluoride membranes. Membranes were probed with commercial Anti-polyHistidine-Peroxidase antibody (Sigma-Aldrich) recognising His-tagged heterologous enzymes in Paper IV, followed by detection using Amersham ECL (GE Healthcare, Chicago, IL, USA). In Paper II, the membranes were probed with custom polyclonal antibodies raised against Flv1, Flv2, Flv3 and Flv4 (GenScript, USA). Horseradish peroxidase-conjugated secondary antibody (GE Healthcare, Chicago, IL, USA) and Amersham ECL (GE Healthcare) were used for detection. In Paper I, the samples were taken from light, dark-adapted for 20 minutes, light-supplemented with 30 µM CCCP, and frozen in liquid N_2. They were then treated as above with membranes probed with antibodies against the N-terminal fragment of YFP (Origene), Flv1 and Flv4 (Genscript), Flv2 and Flv3 (Antiprot), and PetH (kindly shared by H. Matthijs).

3.5 Gas exchange monitoring

3.5.1 Membrane Inlet Mass Spectrometry

The *in vivo* fluxes of $^{16}O_2$ (m/z = 32), $^{18}O_2$ (m/z = 36), and CO_2 (m/z = 44) were followed by an in-house built MIMS as described (Mustila et al., 2016). The final Chl *a* concentration was ~10 $\mu g \cdot mL^{-1}$ (Papers I and IV) or ~6 $\mu g \cdot mL^{-1}$ (Paper II). When necessary, the total dissolved inorganic carbon concentration was adjusted to 1.5 mM by adding $NaHCO_3$. Samples were briefly flushed with N_2 to partially remove O_2, enriched with $^{18}O_2$ and measured. Samples with no substrate (control samples) were handled in the same way as biotransformation samples.

In Papers I and II, the illumination period was set to 5-5-5 minutes of dark-light-dark with the light intensity adjusted to 500 $\mu mol_{photons} \cdot m^{-2} \cdot s^{-1}$. A broad white light was used, or a filter (LEE Filter, 106 Primary Red) set in front of the light source provided red illumination.

In Paper IV, the illumination period was 2-5-3 minutes of dark-light-dark, and the broad white light intensity was 300 $\mu mol_{photons} \cdot m^{-2} \cdot s^{-1}$.

Gas exchange rates were calculated as reported previously (Beckmann et al., 2009). The rates are calculated from a sliding window; thus, they appear to increase before the onset of illumination and decrease before the end of the illumination period.

The sample was set in the MIMS chamber with minor modifications to couple the gas exchange measurements with a biotransformation reaction. The Chl *a* concentration was 11 ± 1 $\mu g \cdot mL^{-1}$, and the volume was 1 mL. The samples were set as described above; 10 mM of 2-MM was added, and the measurement was started with five minutes of darkness followed by ten minutes of illumination (200 $\mu mol_{photons} \cdot m^{-2} \cdot s^{-1}$) and five minutes of darkness. After that, samples were frozen in liquid N_2 and stored at -20 °C before GC analysis.

The electron flux towards active YqjM was calculated from the light-dependent product concentration (total product concentration - dark rate in 20 minutes) and the amount of evolved O_2 during the illumination period. The ratio of electrons released at PSII per one molecule of O_2 and the production of one molecule of NADPH is 2:1. YqjM requires one molecule of NADPH to reduce one molecule of 2-MM.

The corrected BVMO-specific O_2 uptake was calculated to account for the substrate effect on each strain's respective background. See Paper IV - Equation 1 and the adjacent section for detailed information.

3.6 Bimolecular fluorescence complementation

Strains were grown in the presence of antibiotics at 30 °C, 3% CO_2 and continuous 50 $\mu mol_{photons} \cdot m^{-2} \cdot s^{-1}$ white light illumination until OD_{750} = 0.5. Then, cultures were set to OD_{750} = 0.25 in standard BG-11, BG-11 without Mg^{2+} or Ca^{2+}, or BG-11 with 25 mM $MgCl_2$ and 30 mM $CaCl_2$. 1 mM IPTG was added to induce the expression of BiFC proteins. Cells were grown, harvested and resuspended in 2 mL of fresh BG-11 and taken for imaging with a Zeiss LSM880 confocal microscope. Venus fluorescence and Chl *a* autofluorescence were measured with excitation at 488 and 543 nm and detection at 517–597 nm (for Venus) and 651–758 nm (for Chl *a*). When specified, 30 µM CCCP, 20 µM Nigericin, 20 µM DCMU, or 40 µM Valinomycin were added to the sample. The fluorescence co-localisation was analysed using Fiji software with the EzColocalization plugin and Pearson correlation coefficient (Stauffer et al., 2018).

3.7 *In silico* modelling

The detailed description can be found in the Materials & Methods section of Paper I. Briefly, sequences for Flv1, Flv2, Flv3 and Flv4 were retrieved from the UniProt database. The crystal structures were obtained via BLAST from PDB using these sequences. The 3D models were built using MODELLER v.10.4 (Webb and Sali, 2016).

3.8 Statistical analysis

Analysis and visualisation were conducted using R statistical software (R Core Team, 2020) and Origin, version 2016 or 2024 (“Origin,” 2024; “Origin,” 2016). Two-way ANOVA or unpaired t-tests were used to test for significance. Tukey’s test was used to compare the means of different groups with one another, with $p<0.05$ as the significance cut-off.

4 Results

4.1 Regulation of the activity of flavodiiron proteins is dependent on cytosolic pH changes

4.1.1 Ferredoxin is likely the primary electron donor of FDPs

To investigate whether FDPs use FNR or NADPH as their electron donors, I monitored the NAD(P)H fluorescence changes and O_2 photoreduction of the FNR mutants deficient in the large (ΔFNR_L) or the small (ΔFNR_S) FNR isoform (Thomas et al., 2006). In ΔFNR_L, the light-dependent reduction of $NADP^+$ decreased compared to WT and ΔFNR_S, which showed no difference between each other (Paper I - Fig. 1a-b). However, O_2 photoreduction in ΔFNR_L was not significantly impacted, contrary to what would be expected should NADPH serve as the electron donor to FDPs (Paper I - Fig. 1c-d). The slight decrease in O_2 photoreduction could be attributed to lower Flv2 and Flv4 accumulation under air CO_2 levels (Paper I - Fig. 1e). When grown under 3% CO_2, where Flv2 and Flv4 are not expressed (Zhang et al., 2009), no difference in O_2 photoreduction was observed between ΔFNR_L and WT (Paper I - Fig. S4f). However, $NADP^+$ reduction remained impaired in ΔFNR_L even under 3% CO_2 (Paper I - Fig. S5a-b). Deleting Flv1/3 prevents the re-oxidation of Fd, P700 and Pc during the first seconds of illumination (Nikkanen et al., 2020; Sétif et al., 2020). Indeed, ΔFlv3 demonstrated a sustained reduction of Fd, P700 and Pc, while ΔFNR_L and ΔFNR_S showed kinetics similar to WT (Paper I - Fig. 1g). Furthermore, Fd reduction was faster in ΔFNR_L than in WT, but the standard re-oxidation kinetics resumed once FDPs were activated after ~500 ms (Nikkanen et al., 2020).

There are 11 Fd isoforms in *Synechocystis* (Wang et al., 2022). I assessed how the absence of one or multiple of them affects the Mehler-like reaction. No significant changes were observed in Mehler-like activity, which was calculated as the ratio of maximal O_2 photoreduction to gross O_2 evolution, or in Fd, P700, and Pc redox kinetics in Fd2-11 (Paper I - Fig. 3; Fig. S2; Fig. S9). Therefore, low-abundance Fds likely do not constitute a major contributor to the Mehler-like reaction.

Potential protein-protein interactions were investigated using the Bimolecular Fluorescence Complementation (BiFC) system. Due to the nature of the *Synechocystis* cell structure and the localisation of the thylakoid membrane at the periphery, Chl *a* fluorescence forms an M-shaped pattern across the cell's cross-section. The Pearson correlation coefficient (PCC) was calculated to assess the co-localisation of Chl *a* and Venus fluorescence, indicating the protein-protein interaction. The interaction of Flv3 with FNR_L localised to the thylakoid membranes (Paper I - Fig. 2). No interaction was detected for Flv1 with FNR_L or Flv2 with FNR_L or FNR_S (Paper I - Fig. 2; Fig. S7). Furthermore, the possible interactions of Fd1 with FDPs were also tested. The Fd1-Flv1 interaction co-localised to thylakoid membranes, while the Fd1-Flv3 interaction showed cytosolic localisation (Paper I - Fig. 4a-b). Similarly, Fd1-Flv2 showed cytosolic localisation, while Fd1-Flv4 showed no interaction. This suggests that the Flv2/4 hetero-oligomer might receive electrons from Fd1 via Flv2. Interestingly, Fd9 showed the same interaction pattern with Flv1 and Flv3 as Fd1 (Paper I - Fig. S11), suggesting a possible minor role of Fd9 as the electron donor to the Flv1/3 hetero-oligomer or their respective homo-oligomers.

The self-interaction between FDPs was also tested. The Flv1-Flv1 interaction was detected mainly at the thylakoid membrane (Paper I - Fig. S26a), while the Flv3-Flv3 interaction varied, with one subpopulation of cells showing cytosolic localisation and another showing thylakoidal localisation (Paper I - Fig. S26b). No interaction was detected for Flv2-Flv3, which supports the inability of these two FDPs to form a hetero-oligomeric complex (Mustila et al., 2016).

4.1.2 Regulation of FDP localisation through cytosolic pH changes

The reversible association of FDPs with the thylakoid membrane has previously been hypothesised to depend on cytosolic pH changes, *pmf* generation, or cation concentrations (Nikkanen et al., 2021; Zhang et al., 2012). Under standard conditions during the BiFC test, the interaction between Flv1-Flv3 and Flv2-Flv4 showed predominantly cytosolic localisation, with a small subpopulation showing an association with the thylakoid (Fig. 6a-b). Thus, the interactions were tested in the presence of several chemical effectors to evaluate the hypothesis of reversible regulation. These effectors included the proton gradient uncoupler carbonyl cyanide m-chlorophenyl hydrazone (CCCP), H^+/K^+ exchanger nigericin, K-specific ionophore valinomycin, and PSII electron transport inhibitor 3-(3,4-dichlorophenyl)-1,1-dimethyl urea (DCMU).

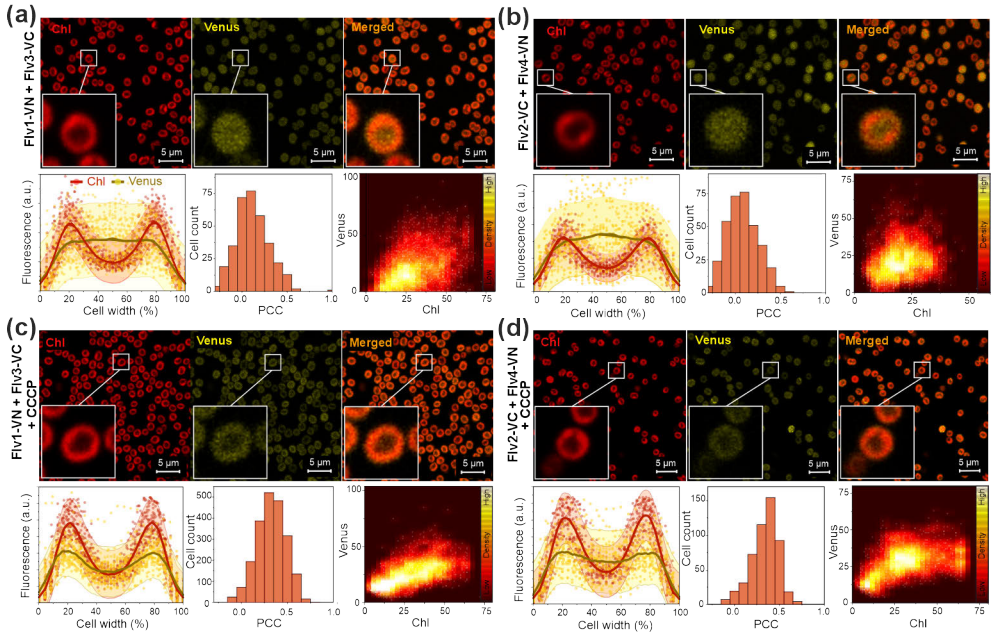

Figure 6. Subcellular localisations of Flv1/3 and Flv2/4 interactions. BiFC tests between (a) Flv1-VN and Flv3-VC. (b) Flv2-VC and Flv4-VN. (c) Flv1-VN and Flv3-VC with 30 µM CCCP added in the medium. (d) Flv2-VC and Flv4-VN with 30 µM CCCP added in the medium. The upper panels show representative confocal micrographs from the Chl *a* and Venus fluorescence channels. Fluorescence intensity across the cell's cross-section demonstrates localisation. The histogram shows the distribution of the Pearson correlation coefficient (PCC) for Chl and Venus fluorescence co-localisation (Adapted from Paper I - Fig. 4).

The addition of 30 µM of CCCP effectively diminished *pmf* generation (Paper I - Fig. S13). As a result, the thylakoid localisation of Flv1-Flv3 and Flv2-Flv4 interactions increased significantly (Fig. 6c-d). A similar effect was also observed after adding 20 µM nigericin (Paper I - Fig. 5e-f; Fig. S16). Nigericin, in combination with valinomycin, further increased the thylakoid localisation of Flv2-Flv4 (Paper I - Fig. 5f). DCMU also increased the thylakoid association of Flv1-Flv3 and Flv2-Flv4 interactions, although this change was visually less evident (Paper I - Fig. S17). Immunoblotting analysis of samples with and without CCCP showed a lower accumulation of Flv1, Flv2, and Flv3 in the soluble fraction, while Flv4 was consistently detected only in the membrane fraction (Paper I - Fig. S18).

Reliance on ΔpH would benefit the rapid activation of the Mehler-like reaction needed upon strong illumination. In the dark, when cytosolic pH is close to neutral, FDP hetero-oligomers associate with the membrane, while upon illumination and the subsequent cytosol alkalisation, they disassociate. Indeed, in the presence of CCCP, the maximal O_2 photoreduction to gross O_2 evolution ratio increases significantly. A similar effect was also observed with nigericin, which, unlike CCCP, does not

negatively affect O_2 evolution (Paper I - Fig. S19-20). Fluorescence measurements of Acridine Orange (AO) and Acridine Yellow (AY) showed delayed cytosol alkalisation, suggesting that FDPs remain associated with the thylakoid membrane (Paper I - Fig. S21). Contrastingly, changes in cation concentrations or the thiol redox state (by adding dithiothreitol or $CuCl_2$) did not significantly alter the Flv1-Flv3 or Flv2-Flv4 localisation. $CuCl_2$ caused a slight elevation of *pmf* while decreasing the thylakoid association (Paper I - Fig. S22-25).

4.1.3 Surface charge modelling supports pH-dependency

The natural range of cytosolic pH is between 7 in the dark and 8.5 during strong illumination, depending on extracellular pH (Coleman and Colman, 1981; Mangan et al., 2016). Low pH may protonate acidic protein residues, making their surface charge more positive, thereby enhancing electrostatic interactions with negatively charged membranes (Johnson and Cornell, 1999; Mulgrew-Nesbitt et al., 2006). Therefore, the surface charge of FDP monomers and oligomers was modelled at the relevant pH. Flv1 and Flv3 monomers have a negative surface charge at neutral pH, which becomes more negative at alkaline pH. Flv1/3 hetero-oligomers carry a net negative charge at neutral pH with positive patches, allowing them to interact with the negatively charged membrane. At alkaline pH, their charge is strongly negative, increasing repulsion from the membrane. In contrast, Flv2 has a strong negative charge at both pH levels, while Flv4 has a positive charge at neutral pH and only a slightly negative one at alkaline pH with large positive patches. The Flv2/4 hetero-oligomers have a negative surface charge at neutral pH and a highly negative surface charge at alkaline pH, hindering their membrane interaction (Paper I - Fig. 7). However, the positive patches on Flv4 might allow the Flv2/4 to associate with the membrane for longer compared to Flv1/3.

4.2 Cell's response to light-driven whole-cell biotransformation

Despite various recent attempts to engineer and improve the biotransformation yield of several enzymatic applications by altering the PETC, a thorough understanding of the effects of employing cyanobacterial cells as a chassis for biotransformation on the cell's bioenergetics has been missing. The strong electron sink - NAD(P)H-dependent ene-reductase YqjM from *B. subtilis* - serves as an appropriate tool to address this knowledge gap.

2-methylmaleimide (2-MM), the substrate of YqjM, is a thiol-active organic compound that has previously shown toxic effects on the viability of *Synechocystis*, as observed by growth on agar plates after exposure. The reaction's product,

2-methylsuccinimide (2-MS), did not affect the cell's viability (Assil-Companioni et al., 2020). However, the specific effects of 2-MM on the photosynthetic apparatus have remained unknown. I added 2-MM to WT cells (background of Syn::YqjM) and assessed the response of the photosynthetic apparatus by biophysical measurements (Paper II - Fig. S3-4; Fig. S6-9; Fig. S12). 2-MM inhibits CO_2 fixation, likely due to its thiol-binding activity affecting the redox regulation of the CBB cycle. O_2 evolution was also inhibited. As a result, the ratio of O_2 photoreduction to gross O_2 evolution increased, as did the CET:LET ratio. However, in the strain expressing YqjM (Syn::YqjM), O_2 evolution remained unchanged in the presence of 2-MM (Paper II - Fig. 2), demonstrating that 2-MM did not directly affect PSII. Furthermore, 2-MM caused an increase in the proton conductivity of the thylakoid membrane, dissipating the *pmf*, thus preventing the induction of photosynthetic control. The expression of YqjM with no substrate present did not cause any detectable effects on the photosynthetic apparatus (Paper II - Fig. S2).

4.2.1 Ferredoxin, the electron distribution hub downstream of PSI

Fd is the electron distribution hub downstream of PSI, with several metabolic pathways dependent on reduced Fd as their electron donor. The main pathway for reduced Fd is the production of NADPH by FNR. YqjM has a strong affinity for NADPH, and the decay of NAD(P)H fluorescence in Syn::YqjM in the presence of 2-MM is significantly faster (Assil-Companioni et al., 2020). Therefore, it creates a strong electron sink. Indeed, I did not detect light-induced NADPH accumulation in Syn::YqjM with 2-MM added (Fig 7c; Paper II - Fig. S9). As a result, the Fd pool remained oxidised upon illumination and demonstrated even stronger oxidation after 2 s of strong illumination (Fig. 7d).

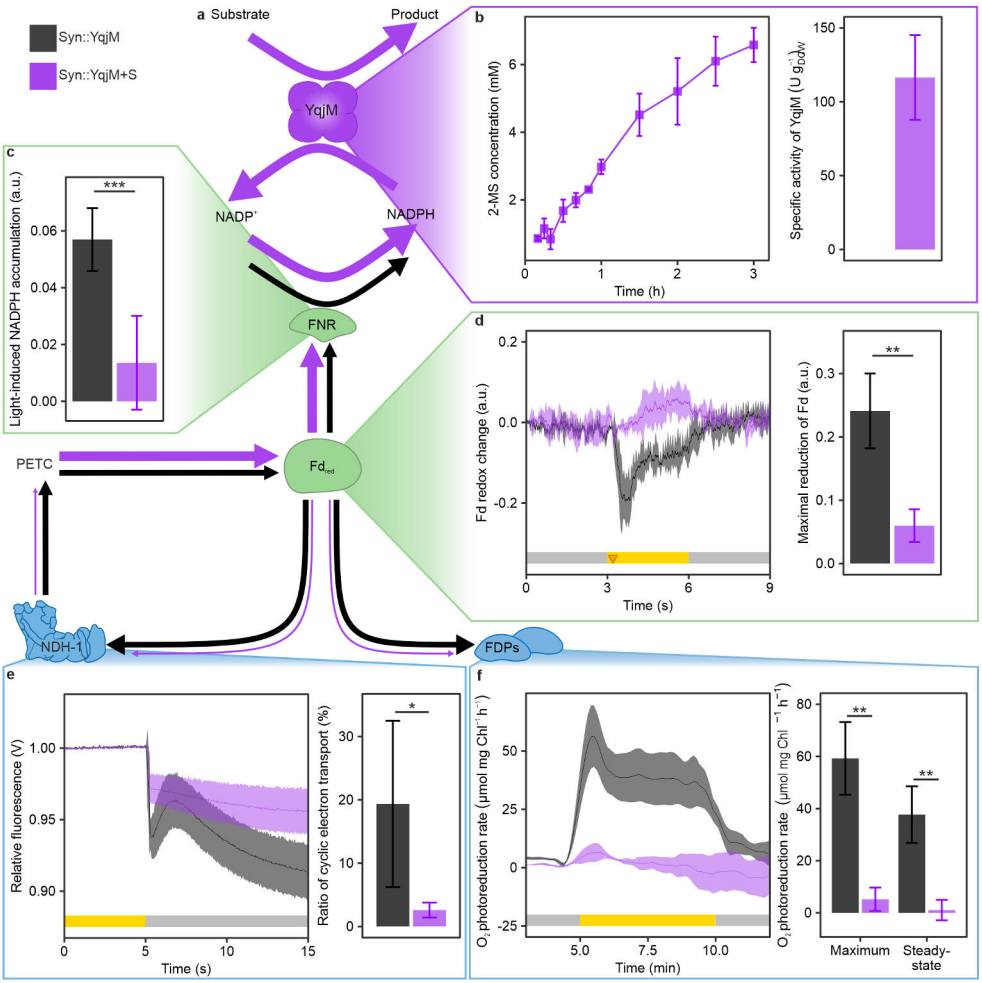

Figure 7. The electron distribution downstream of PSI in Syn::YqjM ± S. (a) Schematic of electron flux. The black arrows signify Syn::YqjM - S, while the purple arrows signify Syn::YqjM + S. The arrows' thickness indicates the electron flow. (b) The product concentration (2-MS) and the initial specific activity of YqjM. (c) Light-induced accumulation of NADPH. (d) The Fd redox kinetics and the maximal reduction of Fd upon illumination relative to the dark level. (e) The post-illumination F_0 rise, and CET ratio as assessed by dark-interval relaxation kinetics of P700 and Pc during illumination. (f) The kinetics of the O_2 photoreduction rate upon illumination and the maximal and steady-state O_2 photoreduction rate as a proxy for the activity of FDPs. (Paper II - Fig. 3).

The AET pathways are also dependent on reduced Fd. Since no reduced Fd was observed, I assessed the activity of the FDPs and CET mediated by the NDH-1 complex. The post-illumination rise in fluorescence was eliminated, and the CET:LET ratio decreased from 19 ± 13% to 3 ± 1% (Fig. 7e). The activity of FDPs was monitored by measuring the O_2 photoreduction upon strong illumination. When

2-MM was added to Syn::YqjM, no O_2 photoreduction was detected (Fig. 7f). No changes in the abundance of individual FDPs were observed (Paper II - Fig. S10). Thus, the active YqjM, which maintains the NADPH/$NADP^+$ pool oxidised, drives up the activity of FNR, which in turn outcompetes AET for electrons.

4.2.2 The photosynthetic electron transport chain is strongly oxidised

The high FNR activity keeps the Fd pool oxidised during illumination. I, therefore, examined the redox state of PSI and Cyt b_6f complexes and the soluble electron carrier Pc. The P700 reaction centre of PSI lacked the standard transient reduction upon illumination, which coincides with the transient Fd reduction observed under control conditions (Fig. 7d - black trace; Fig. 8f). Similarly, Pc showed no reduction and was strongly oxidised during illumination with an incomplete re-reduction in the dark (Fig. 8e). Cyt *f* and *b* hemes, the integral components of Cyt b_6f, lacked the standard kinetics and the transient reduction peak shortly after illumination. Furthermore, both components demonstrated strong oxidation in the dark after the lights were turned off (Fig. 8c-d). Despite the low CET contribution, the total PSI electron transport rate increased (Fig. 8b; Paper II - Fig. S4; Fig. S7).

4.2.3 Coupling light-driven whole-cell biotransformation with real-time gas exchange measurements

To perform an electron flux analysis of the YqjM biotransformation, I coupled real-time gas exchange measurements using MIMS with biotransformation. I followed the O_2 evolution and analysed substrate and product concentrations (2-MM and 2-MS, respectively) of YqjM's activity by liquid-liquid extraction and GC. The samples were illuminated in the MIMS sample chamber for ten minutes, and 0.69 ± 0.07 mM of 2-MS was detected. By subtracting the dark rate (0.01 mM·min^{-1}), I determined that the light-dependent production yielded 0.45 ± 0.07 mM of 2-MS (Paper II - Fig. 5; Fig. S13). After including the 0.41 ± 0.03 mM of total evolved O_2 in the calculations, it was concluded that YqjM used $54 \pm 5\%$ of electrons released from PSII to reduce 2-MM into 2-MS. Thus, active YqjM consumes a significant fraction of the chemical energy downstream of PSI.

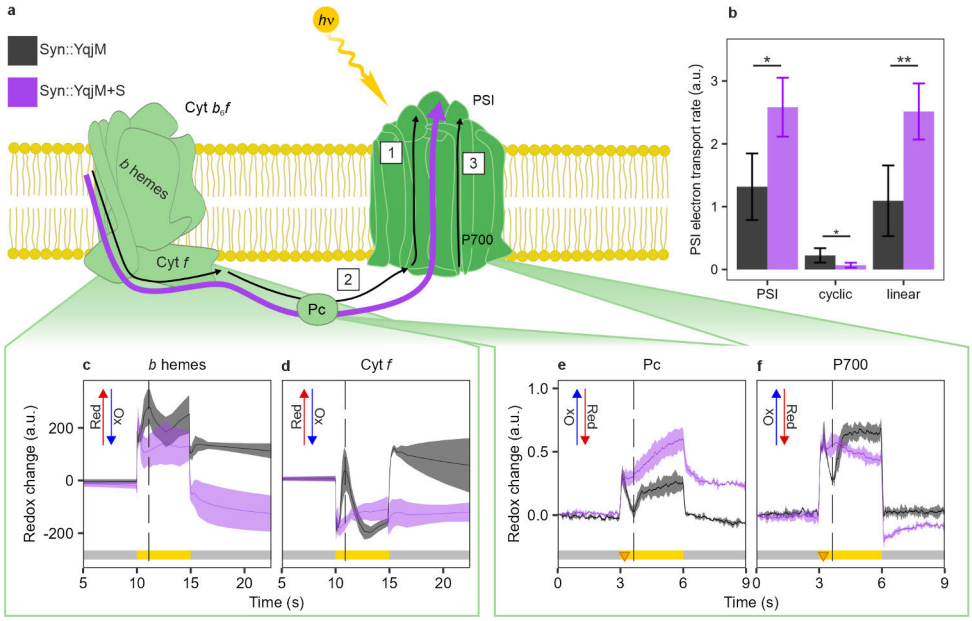

Figure 8. The redox state of the PETC and the electron transport through PSI in Syn::YqjM ± S. (a) Schematic of the oxidation/reduction steps of the PETC upon illumination in Syn::YqjM - S (black) and Syn::YqjM + S (purple). (b) Total electron transport through PSI and the individual cyclic and linear electron transport during steady-state illumination. Redox signatures of Cyt b_6f components (c) *b* hemes and (d) Cyt *f*. The redox signature of (e) the electron carrier Pc and (f) PSI reaction centre chlorophylls P700. The triangle represents a saturating pulse distribution. The dashed vertical line points at the transient reduction of P700, Pc, *b* hemes and Cyt *f* (Paper II - Fig. 4).

4.3 YqjM is NADPH-limited under standard conditions

Based on theoretical calculations of NADPH production (Kauny and Sétif, 2014) and the results of Paper II, ene-reduction mediated by YqjM is presumed to be NADPH-limited. In addition to photosynthesis, NADPH is produced through glucose metabolism via the OPP pathway. YqjM can also utilise NADH, although YqjM's affinity for NADH is significantly lower than that for NADPH (Assil-Companioni et al., 2020). Therefore, the addition of D-glucose and other carbohydrates to the biotransformation reaction was studied to determine whether it leads to an improved specific activity of YqjM.

4.3.1 The addition of D-glucose transiently enhances light-driven whole-cell biotransformation

The biotransformation reaction was performed at various cell densities, light regimes, and with or without the addition of D-glucose to observe the contribution

of glycolytic pathways under different conditions. As expected, the specific activity was highest at low cell densities and decreased with increasing culture density. However, the specific activity in the dark did not change with increasing culture density. This is a common occurrence in biotransformation reactions using heterotrophic organisms, where the specific activity remains stable in relation to cell density until a limitation in substrate or energy is reached. Concerning the different light intensities tested, the highest specific activity was reached when the biotransformation reaction was performed under high light intensity with cultures grown in high light, although the differences between different illuminations were less pronounced at higher cell densities (Fig. 9).

The addition of 2.5 mM D-glucose enhanced the production of 2-MS in several conditions, with the most significant improvement observed in OD_{750} = 2.5, while dense cultures showed mostly insignificant change (Paper III - Fig. 2a-b). However, a consistent improvement was reached in biotransformation reactions performed in the dark (Fig. 9). This improvement was also universal for other tested substrates of YqjM (Paper III - Fig. 3), suggesting NADPH limitation as the universal bottleneck for YqjM with all substrates, despite their different specific activities. Interestingly, increasing the concentration of D-glucose did not result in further improvements in the biotransformation activity (Paper III - Fig. S2a). Furthermore, other saccharides (D-fructose, D-galactose, D-saccharose, or D-sorbitol) had negligible effects (Paper III - Fig S2b). Thus, this improvement was specific only to 2.5 mM D-glucose.

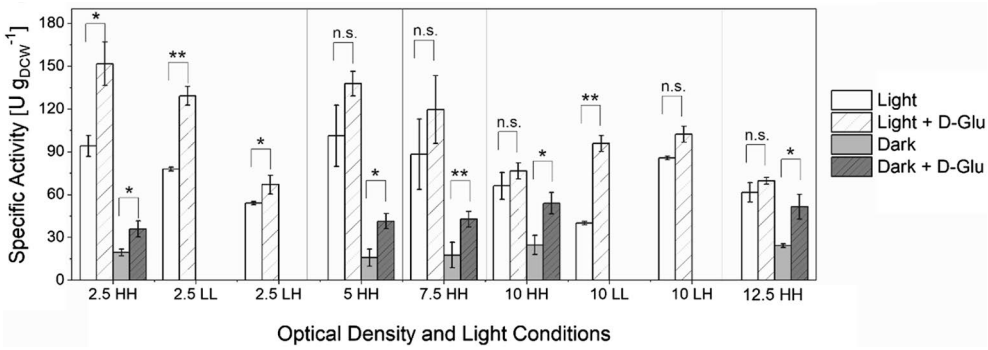

Figure 9. Specific activity of YqjM at different optical densities ± D-glucose. HL = high light cultivation and low light reaction; LL = low light cultivation and reaction; HH = high light cultivation and reaction; LH = low light cultivation and high light reaction (Adapted from Paper III - Fig. 2).

I assessed the effect of 2.5 mM D-glucose addition during biotransformation on the photosynthetic apparatus by measuring the effective yield of PSI and PSII [Y(I) and Y(II), respectively]. No significant changes in Y(II) or Y(I) were observed when D-glucose was added on top of 2-MM (Paper III - Fig. 4). I also measured the light-

induced NAD(P)H kinetics in samples with or without D-glucose. As in Paper II, no light-induced reduction of NADPH was observed in samples with 2-MM. Furthermore, in samples with D-glucose added, the NAD(P)H fluorescence continued to increase steadily (Paper III - Fig. 5). This suggests an increase in the overall NAD(P)H pool size, supporting higher biotransformation activity.

4.3.2 Mixotrophic growth is detrimental to light-driven whole-cell biotransformation activity

To verify whether the addition of D-glucose during the growth phase could benefit biotransformation, the cultures were grown under photomixotrophy for two days. However, the specific activity decreased significantly compared to cells grown photoautotrophically, except for the reaction run in the dark (Fig. 10). The intracellular *in vitro* activity of YqjM also decreased in mixotrophically grown cells (Paper III - Fig. S3). Interestingly, addition of D-glucose at the start of the biotransformation reaction improved the activity; however, it remained lower than in autotrophically grown cells (Fig. 10).

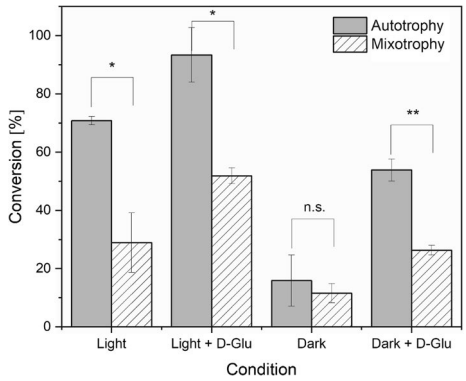

Figure 10. Conversion of 2-MM by Syn::YqjM grown in photoautotrophy or photomixotrophy. The yield was obtained after 30 minutes of the reaction (Adapted from Paper III - Fig. 6).

4.3.3 Upscaling with bubble column reactor

The use of internal illumination in a bubble column reactor to overcome self-shading in high-density biotransformation has been previously reported (Hobisch et al., 2021). To test whether the addition of D-glucose provides the same benefit in a small-scale-up system, the experiment was performed using the 200 mL bubble column reactor. Indeed, the volumetric productivity of 2-MS increased by 2.4-fold, and complete conversion was reached within an hour, which is twice as fast as without D-glucose (Paper III - Fig. 7).

4.4 Baeyer-Villiger oxidation for lactone production in cyanobacteria

Caprolactone is an important bulk chemical in the polymer industry. Engineered cyanobacteria expressing BVMOs can replace the traditional production method using acids. I characterised two BVMOs, Parvi and Xeno, under standard conditions: ambient air CO_2 (0.04%, LC) and white light illumination. In line with previous research (Erdem et al., 2022), Xeno exhibited higher specific activity than Parvi. However, the previously reported benefit of deleting Flv1 was replicated for Parvi but not for Xeno (Paper IV - Fig. 1; Fig. S4). This suggests a more nuanced cause behind the improvement from Flv1 deletion.

4.4.1 Identifying the limiting factor of BVMO activity

BVMOs require O_2 and NADPH for their activity. Therefore, I focused on establishing whether their availability could be the limiting factor. The light-induced accumulation of NADPH was assessed by measuring the changes in NAD(P)H fluorescence upon illumination. No difference was observed in samples with or without cyclohexanone (Fig. 11a).

The dynamics of O_2 consumption were monitored by MIMS under biotransformation conditions with and without cyclohexanone. A significant increase in total O_2 uptake in all BVMO-expressing strains was observed in the presence of cyclohexanone. Interestingly, the background strains responded differently; total O_2 uptake increased in WT but did not change in ΔFlv1 (Paper III - Fig. 1b, c). To normalise each BVMO-expressing strain to its background and the respective cyclohexanone effect, I calculated the "corrected BVMO-specific O_2 uptake" ($CorrO_2$). Syn::Xeno showed significantly higher $CorrO_2$ than Syn::Parvi, while ΔFlv1::Xeno and ΔFlv1::Parvi were comparable (Fig. 11b). Interestingly, the $CorrO_2$ of ΔFlv1::Xeno is (though insignificantly) lower than that of Syn::Xeno, despite their specific activities being the same (Paper IV - Fig. 1e). $CorrO_2$ correlates with the biotransformation rate, where after five hours, Syn::Xeno showed a higher ε-caprolactone concentration than ΔFlv1::Xeno, while Syn::Parvi reached a slightly lower concentration than ΔFlv1::Parvi (Paper IV - Fig. S4).

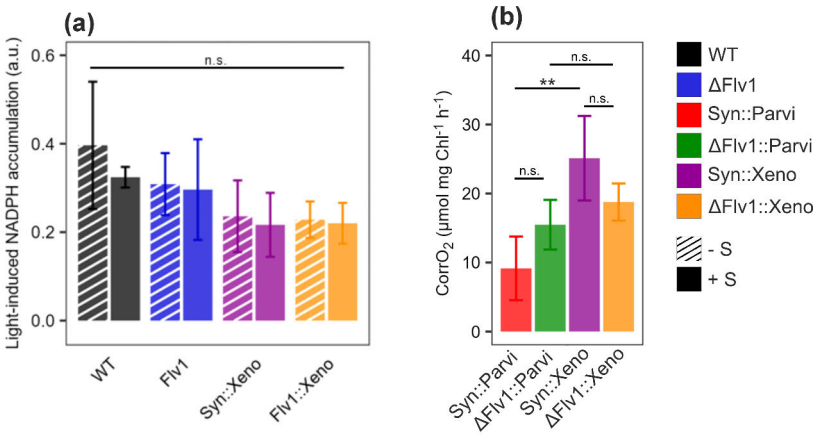

Figure 11. Characterisation of WT, ΔFlv1 and strains expressing BVMO under standard conditions - white light illumination and ambient air. (a) The light-induced NADPH level determined as the difference between NAD(P)H fluorescence shortly after and before the onset of illumination. (b) $CorrO_2$ of BVMO-expressing strains. The column bars represent Mean ± SD. Black - WT, blue - ΔFlv1, red - Syn::Parvi, green - ΔFlv1::Parvi, magenta - Syn::Xeno, orange - ΔFlv1::Xeno, striped - - S, full - + S, (Adapted from Paper IV - Fig. 1).

4.4.2 Growth under elevated CO_2 enhances light-driven whole-cell biotransformation

I decided to optimise growth and biotransformation conditions to enhance BVMOs' activity. Cells were grown, and biotransformation was performed under a CO_2-rich atmosphere (3%, HC). Syn::Xeno reached a 4-fold higher specific activity, while Syn::Parvi demonstrated a 3-fold increase. In line with the higher specific activity, Syn::Xeno fully converted the supplied 5 mM cyclohexanone in under two hours (Fig. 12a). The immunodetection of the N-terminal His-tag revealed an increased abundance of BVMOs in cells grown under HC conditions compared to LC (Fig. 12c). Furthermore, a significant difference was detected between WT and ΔFlv1 background strains, with ΔFlv1::Parvi showing a significantly higher abundance of Parvi compared to Syn::Parvi. ΔFlv1::Xeno also demonstrated a higher abundance of Xeno than Syn::Xeno, although this difference was smaller (Paper IV - Fig. S5).

The light-induced accumulation of NADPH showed no differences between samples with and without cyclohexanone, consistent with observations under LC conditions. However, strains expressing Xeno showed a decrease in light-induced NADPH accumulation, particularly ΔFlv1::Xeno compared to its background ΔFlv1. This suggests that the strong expression of Xeno might affect light-induced NADPH accumulation even in the absence of the enzyme's substrate (Fig. 12b). The $CorrO_2$ of Xeno-expressing strains was 5-fold higher than that of those expressing Parvi (Fig.

12e). Interestingly, the ΔFlv1 background displayed a higher $CorrO_2$ for both enzymes, while the specific activity was higher only with Parvi. ΔFlv1::Xeno showed lower specific activity than Syn::Xeno (Fig. 12a,e).

The improvements achieved with BVMOs were promising; therefore, I decided to test whether the same approach would also benefit other enzymes. To do this, I grew two strains expressing the ene-reductase YqjM (also used in Papers II and III) under LC and HC conditions. However, no changes were observed in the specific activity or the biotransformation rate. No difference was further observed between Syn::YqjM and ΔFlv1::YqjM under LC or HC conditions. YqjM accumulation remained constant in the WT background and slightly decreased in the ΔFlv1 background under HC (Paper IV - Fig. 4).

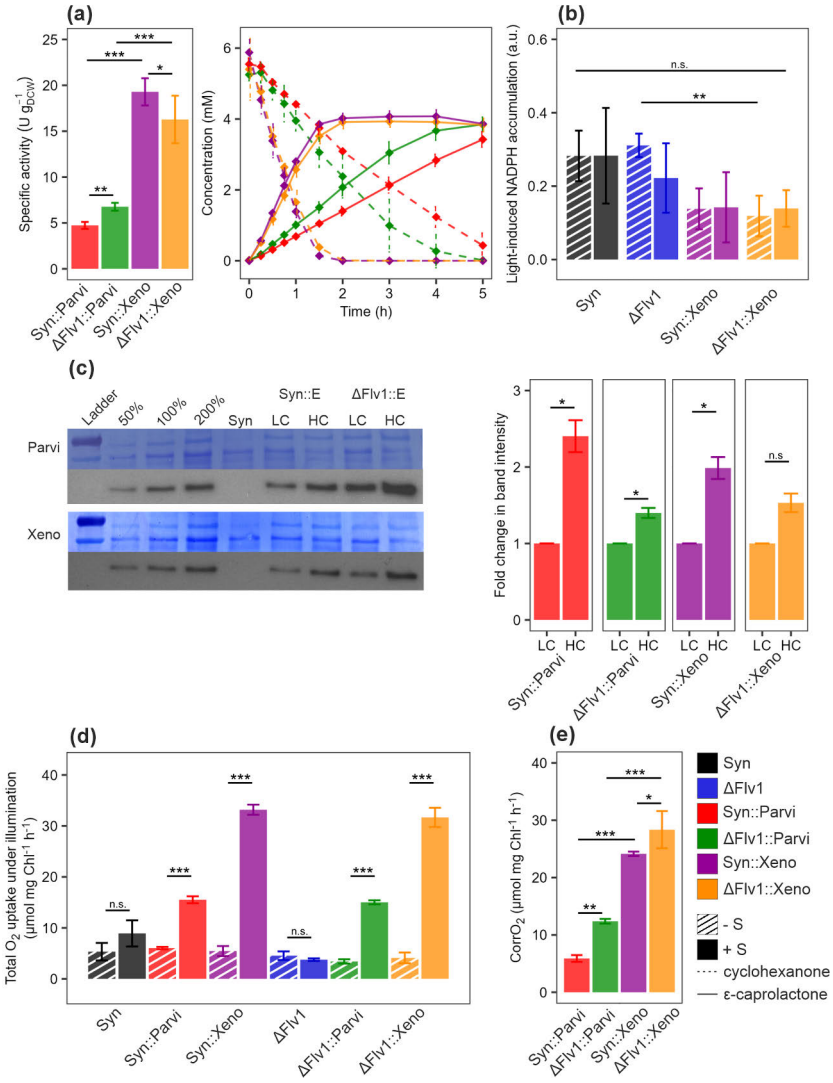

Figure 12. Characterisation of strains expressing BVMO under HC conditions and white light illumination. (a) Specific activity calculated from the 45-min time point of the biotransformation reaction and the concentration of ε-caprolactone during the biotransformation reaction. (b) The light-induced NADPH accumulation calculated as the difference between NAD(P)H fluorescence shortly after and before the onset of illumination. (c) Immunodetection of BVMO enzymes with an anti-His antibody and relative protein abundance change in relation to the LC sample. Syn::E - *Synechocystis* expressing Parvi or Xeno, ΔFlv1::E - ΔFlv1 strain expressing Parvi or Xeno. (d) The total O_2 uptake under illumination with and without substrate in the media. (e) CorrO_2 of BVMO-expressing strains. The column bars represent Mean ± SD [SEM in (c)]. Black - WT, blue - ΔFlv1, red - Syn::Parvi, green - ΔFlv1::Parvi, magenta - Syn::Xeno, orange - ΔFlv1::Xeno, striped - -S, full - +S, (Adapted from Paper IV - Fig. 2).

4.4.3 Light quality strongly influences light-driven whole-cell biotransformation

In addition to CO_2 availability, the effect of modified light quality during growth and biotransformation reaction was tested with Xeno-expressing strains. I used broad white light enriched with red and blue wavelengths (W+R/B, Paper IV - Fig. S2). Under LC conditions, the cells grown under W+R/B lights showed a 2-fold increase in specific activity compared to those under white light (Fig. 13a; Paper IV - Fig. 1e). However, when W+R/B lights were combined with HC conditions, no further benefit to biotransformation was observed, and the specific activity was comparable to that under white light and HC conditions (Fig. 13a; Fig. 12a). The results of immunodetection showed a nonsignificant increase in protein accumulation in W+R/B light compared to white light samples in both LC and HC conditions (Fig. 13b). This suggests that the effects of light quality and CO_2 availability might differ, with each enhancing the biotransformation through different mechanisms.

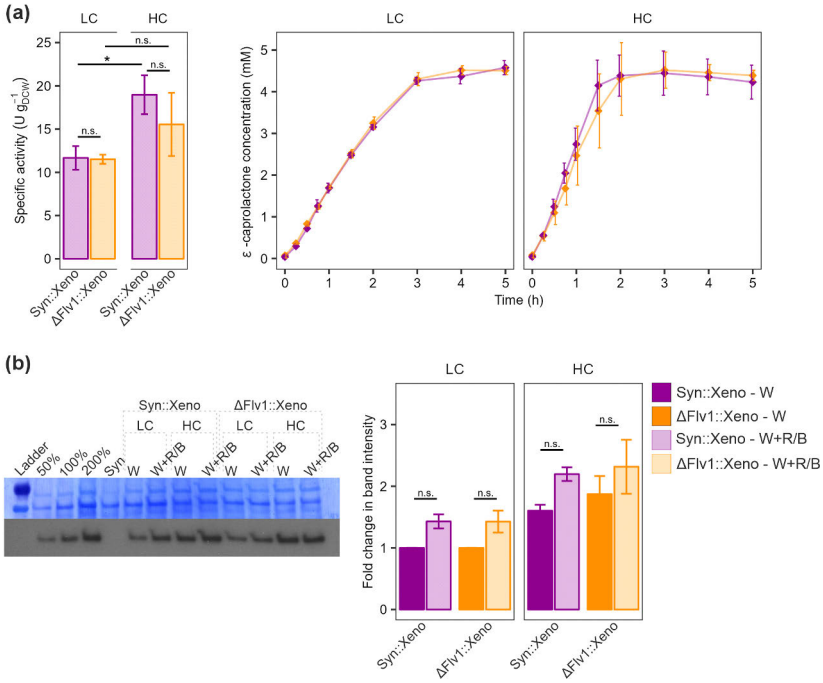

Figure 13. Effects of W+R/B illumination under LC or HC conditions on Xeno-expressing strains. (a) Specific activity calculated from the 45-min time point of the biotransformation reaction and the concentration of ε-caprolactone during the biotransformation reaction. The column bars represent Mean ± SD. (b) Immunodetection of BVMO enzymes with anti-His antibody and relative protein abundance change in relation to the LC sample. The column bars represent Mean ± SEM. W - white light, W+R/B - white light enriched with red and blue wavelengths, magenta - Syn::Xeno, orange - ΔFlv1::Xeno, full colour - W, light colour - W+R/B, (Paper IV - Fig. 4).

5 Discussion

Cyanobacteria are excellent model organisms for studying the regulation of photosynthesis, the process responsible for life on Earth. Moreover, they are poised to play a significant role in the green transition. This thesis focuses on deciphering the regulation of FDP-mediated Mehler-like reaction (Paper I), the physiological response of *Synechocystis* to light-driven whole-cell biotransformation (Paper II), enhancing the activity of ene-reductase YqjM by boosting NADPH production (Paper III), characterising and enhancing the Baeyer-Villiger oxidation in *Synechocystis* (Paper IV), and reviewing the role of microalgae in future technologies as biocatalysts (Paper V).

5.1 Self-regulatory feedback mechanism controls the activity of the FDP-mediated Mehler-like reaction

FDPs, in their hetero-oligomeric composition, constitute one of the main safety outlets of the LET by dissipating excess electrons from Fd to O_2. The activity of the Flv1/3 hetero-oligomer is indispensable under fluctuating light intensity and during the transition from dark to high light, whereas the Flv2/4 hetero-oligomer is rather involved in steady-state O_2 photoreduction. The rapid changes in light intensity necessitate quick activation and flexible regulation of FDPs' activity. Several aspects of their activity, localisation, and regulation remain unclear, and contrasting results have been reported. Paper I exploited the BiFC technique to study *in vivo* protein-protein interactions and the localisation of FDPs and Fd isoforms.

Although previous *in vitro* studies demonstrated FDP activity using NAD(P)H as their electron donor (Brown et al., 2019; Shimakawa et al., 2015; Vicente et al., 2002), the reported rates were several-fold lower than the O_2 photoreduction rates observed in *in vivo* studies (Santana-Sanchez et al., 2019). Furthermore, these *in vitro* studies used FDPs in their monomeric or homo-oligomeric composition; however, Flv1 or Flv3 monomers and homo-oligomers do not contribute to the Mehler-like reaction *in vivo* (Mustila et al., 2016). Our results showed that no significant impairment of O_2 photoreduction could be observed in the ΔFNR_L mutant lacking the large FNR isoform responsible for $NADP^+$ reduction. Should NADPH

be donating electrons to the Mehler-like reaction, a decrease would be expected. No differences were also observed in P700 or Fd redox kinetics (Paper I - Fig. 1). The increased abundance of Flv1 and Flv3 in ΔFNR_S (an insignificant increase was also observed in ΔFNR_L) could be related to the increased pressure on the Fd pool due to a missing electron sink (ΔFNR_L) or disrupted CET (ΔFNR_S), as both Flv1/3 hetero-oligomer and CET contribute to the oxidation of Fd (Nikkanen et al., 2020; Storti et al., 2020). Based on the results in Paper I and previous studies (Nikkanen et al., 2020; Sétif et al., 2020), it is unlikely that FNR or NADPH could serve as the main electron donors to Flv1/3 and Flv2/4 hetero-oligomers performing the Mehler-like reaction. However, NADPH could still play a role as the electron donor in the unknown physiological role of FDP homo-oligomers. Accordingly, FNR_L can interact with Flv3 homo-oligomers in BiFC tests (Paper I - Fig. 2), and their additional physiological role has been suggested (Mustila et al., 2016).

Out of the ten low-abundant Fd isoforms (Fd2-11), only Fd2, which is involved in a low-iron response (Schorsch et al., 2018), is essential for photoautotrophic growth (Cassier-Chauvat and Chauvat, 2014). Fd9 is involved in photomixotrophic growth (Wang et al., 2022), and its interaction with Flv3 in a two-hybrid system was reported (Cassier-Chauvat and Chauvat, 2014). Furthermore, Fd1 interacted with Flv1, Flv2, and Flv3 (Paper I - Fig. 4) and Fd9 with Flv1 and Flv3 (Paper I - Fig. S9). The contribution of the low-abundant Fd isoforms to the Mehler-like reaction is likely rather insignificant, as demonstrated by WT-like O_2 photoreduction in strains lacking one or multiple Fd isoforms (Paper I - Fig. 3). This confirms Fd1 as the likely main electron donor to Flv1/3 and Flv2/4 hetero-oligomers *in vivo*; though, a minor role of Fd9 cannot be excluded.

The protein-protein interactions of Fd1 with Flv1 were primarily localised to the thylakoid, whereas interactions with Flv3 occurred in the cytosol (Paper I - Fig. 4). However, the localisation might be further controlled by the physiological state of the cell. Upon the addition of the *pmf*-uncoupler CCCP or nigericin, the Flv1/3 interaction showed stronger thylakoid localisation, while Flv2/4 presented a smaller change (Fig. 6). In agreement, the ΔD1D2 mutant, deficient in the D1 and D2 subunits of NDH-1, which has disrupted CET and *pmf* generation, maintains high O_2 photoreduction (Nikkanen et al., 2020). The loss of the ΔpH component of *pmf* strongly influences Flv1/3 hetero-oligomers, while the localisation of Flv2/4 hetero-oligomers might be further influenced by ionic balance across the membrane since it responded more strongly to the potassium-specific ionophore valinomycin (Paper I - Fig. 5).

Thus, the results of Paper I suggest that FDP activity is regulated by cytosolic pH changes (Paper I - Fig. 8). In dark or low light, the cytosol is near-neutral, promoting the localisation of FDP hetero-oligomers on the thylakoid membrane. Upon the shift to high light, FDPs catalyse rapid O_2 photoreduction. It takes 3–4

minutes to reach full alkalisation of the cytosol (Paper I - Fig. S21b). FDPs then disassociate from the thylakoid membrane, lowering the O_2 photoreduction rate (Santana-Sanchez et al., 2019).

The results of in silico modelling are in agreement with this proposed mechanism. The net surface charge changes with the physiological range of cytosolic pH. At near-neutral pH, Flv1/3 and Flv2/4 hetero-oligomers showed low negative charge with positive patches, allowing for association with the negatively charged thylakoid membrane. Upon the alkalisation of the cytosol, the surface charge became more negative, repelling FDP hetero-oligomers from the membrane. Interestingly, the Flv2/4 hetero-oligomer retained positive patches on Flv4, which could enable it to remain associated with the membrane for longer and potentially explain the distinct kinetics of Flv1/3 and Flv2/4.

5.2 Strong heterologous sink outcompetes alternative electron pathways for electrons

Fd is not only the donor to FDP hetero-oligomers (Paper I) but also serves as an important electron distribution hub downstream of PSI. The CET, hydrogenase, nitrogen assimilation, or the Trx regulation system use Fd as their electron donor. Furthermore, it plays a central role in electron sink engineering applications that directly utilise photosynthetic reducing power. Thus, Paper II explores the orchestration of the electron distribution from Fd using a strong heterologous electron sink, NAD(P)H-dependent ene-reductase YqjM from *B. subtilis*.

I showed that the substrate of YqjM, 2-MM, blocked carbon fixation via the CBB cycle and dissipated *pmf*, affecting ATP synthesis. It is important to note, that its effects on the Trx system can have broader physiological impact (Paper II - Appendix S1). As a result of *pmf* dissipation, the photosynthetic control at Cyt b_6f at acidic lumenal pH (Malone et al., 2021) was not induced. Once YqjM was activated by adding 2-MM, it efficiently consumed available NAD(P)H, keeping the $NADP^+$/NADPH pool oxidised (Fig. 7). This, in turn, caused the FNR to readily oxidise any available reduced Fd, preventing the accumulation of reduced Fd upon illumination (Fig. 7). The lack of reduced Fd potentially disrupts other metabolic and regulatory pathways, which can have detrimental effects on the long-term efficiency of biotransformation by lowering the cell's fitness. The longevity of YqjM ene-reduction remains to be explored.

The lack of reduced Fd eliminated the O_2 photoreduction and decreased the CET mediated by the NDH-1 complex (Fig. 7). The energetic demand of YqjM is high enough to outcompete FDPs for electrons despite the *pmf* dissipation, which promotes their activity (Paper I). Furthermore, the ETR(I) increased, but the contribution of CET was strongly diminished. This finding is counterintuitive since

O_2 evolution at the OEC at PSII and ETR(II) did not change significantly. A simultaneous measurement by DUAL-PAM showed a higher ETR(I)/ETR(II) ratio, removing the uncertainty introduced by measurements performed with different instruments (DKN and MIMS for separate assessments of PSI and PSII, respectively). It is important to note that discrepancies between increases in ETR(I) and ETR(II) have been previously reported (Ermakova et al., 2016; Torrado et al., 2022; Viola et al., 2021), and the simultaneous quantification of electron transport is challenging (Fan et al., 2016; Kauny and Sétif, 2014).

The strong electron consumption of YqjM was also observed in the PETC components. The transient reduction upon illumination observed in standard conditions was completely missing from Fd, P700, Pc, and both components of Cyt *b*$_6$*f* (Fig. 7; Fig. 8). During the transition from dark to light, when downstream processes such as CO_2 fixation are not yet active, electrons pool at Fd and further upstream in the PETC. However, active YqjM prevented this pooling, maintaining the PETC in an oxidised state up until the *b* hemes of Cyt *b*$_6$*f*, which remained reduced during illumination (Fig. 8). This demonstrates that a highly catalytically active NADPH-dependent heterologous enzyme can "empty" the PETC by driving up the activity of FNR.

In conclusion, the availability of $NADP^+$ limits the activity of FNR under standard conditions. However, when a strong NADPH sink is introduced, and $NADP^+$ is no longer a limiting factor for FNR's activity, it will outcompete other electron acceptors that rely on reduced Fd. It is important to note that the substrate's broad effects make the physiological assessment complex. Nevertheless, the results of Paper II shed light on the electron distribution between Fd-dependent pathways.

5.3 Identification of bottlenecks is a crucial prerequisite to successful engineering

To design targeted modifications for biotransformation improvements, it is important to thoroughly characterise the selected enzymatic system and assess its potential bottlenecks. The cofactors required by each enzyme can differ; thus, an improvement strategy that is effective for one might not benefit another. YqjM (Papers II and III) requires NAD(P)H as the electron donor, and while it has a stronger affinity for NADPH, it can also oxidise NADH (Assil-Companioni et al., 2020). On the other hand, BVMOs used in Paper IV are type I (Kamerbeek et al., 2004; Malito et al., 2004) and require NADPH and O_2. It is necessary to determine whether the availability of the cofactor or O_2 might be the limiting factor. Therefore, bottlenecks must be assessed separately for each enzyme and setup.

Based on the results of Paper II and previous studies (Assil-Companioni et al., 2020), NADPH availability was pinpointed as the limiting factor for YqjM.

Therefore, an approach to increase the rate of $NADP^+$ reduction could be beneficial. Indeed, this direction was explored in Paper III with promising results. In contrast, neither NADPH nor O_2 availability appeared to limit the activity of BVMOs under the studied conditions (Paper IV). BVMOs also showed lower specific activity than YqjM, indicating that their limitation lies within the inherent enzymatic activity, expression levels or other characteristics. Indeed, targeting their protein levels in Paper IV proved beneficial.

Deleting competing electron sinks has become a popular approach to improving biotransformation yields. The deletion of FDPs increased the specific activity of YqjM or BVMOs (Assil-Companioni et al., 2020; Erdem et al., 2022; Spasic et al., 2022); however, the results of Paper II suggest that this improvement was likely caused indirectly rather than by removing the competition for electrons. It is important to note that NADPH-dependent enzymes are not in direct competition with Fd-dependent pathways. Paper II demonstrates that FNR can fully oxidise the Fd pool when the $NADP^+$/NADPH pool is also oxidised. Instead, other NADPH-consuming pathways, such as the CBB cycle, could be considered direct competitors. It is important to note that every modification of the PETC or wider metabolism carries a risk of unexpected side effects and necessitates careful characterisation. Cells will attempt to acclimate and rebalance themselves after these modifications. Additionally, the role of FDPs is complex, with the function of their homo-oligomeric organisation unknown and their involvement in other metabolic pathways uncertain. Therefore, each deletion or modification of the PETC should be carefully considered.

For Fd-dependent enzymes, however, deleting FDPs or other AET pathways can still be beneficial (Appel et al., 2020; Berepiki et al., 2018; Lassen et al., 2014; Mellor et al., 2016; Torrado et al., 2022). Alternatively, attaching heterologous enzymes directly to PSI, Fd, or FNR showed positive results (Medipally et al., 2023).

5.4 Glucose addition can temporarily alleviate NADPH limitation in light-driven whole-cell biotransformation using ene-reductase YqjM

Stopped-flow kinetics measurements revealed that the turnover rate of the oxidative half-reaction (the reduction of the substrate) of YqjM is over 50 times higher than that of the reductive half-reaction [oxidation of NAD(P)H]. Therefore, YqjM will maintain an oxidised state in the presence of its substrate (Assil-Companioni et al., 2020). The reported intracellular concentration of NADPH in photoautotrophically grown *Synechocystis* is 87.4 nM OD_{730}^{-1} (Tanaka et al., 2021), which is well below the saturation point for YqjM at 500 µM. As also demonstrated in Paper II, the availability of NAD(P)H is thus limiting YqjM's activity. The production of

NAD(P)H by glycolytic pathways contributes to the heterologous activity as the biotransformation proceeds in the dark (Papers II and III) or in the presence of DCMU (Nakamura and Yamanaka, 2002). Therefore, the addition of D-glucose to boost this contribution was tested in both lab-scale and larger-scale setups in Paper III.

The addition of D-glucose improved biotransformation performance mainly at low cell densities (0.6 $g_{DCW} \cdot L^{-1}$), while the improvement was generally low in high cell densities (up to 3.0 $g_{DCW} \cdot L^{-1}$). However, the effect in the dark was consistent across all cell densities (Fig. 3). This suggests that the observed improvement also depends on light availability and the physiological state of the cells. Interestingly, at high cell densities, the addition of D-glucose showed a significant improvement only in cultures grown under low light intensities, with the reaction also performed under low light (Fig. 3). Cultures grown under high light intensity or when the reaction was performed under high light intensity showed no benefit.

Synechocystis can readily switch to mixotrophic growth with a fast growth rate upon the addition of D-glucose into the media. Interestingly, mixotrophy was detrimental to YqjM's conversion rate (Fig. 4), but adding D-glucose at the start of the biotransformation reaction remained beneficial. This could be attributed to the downregulation of several OPP pathway enzymes or the broader metabolic changes occurring during mixotrophic growth (Muth-Pawlak et al., 2022). It has also been reported that photosynthesis is downregulated in mixotrophy (Solymosi et al., 2020). However, this might depend on the particular *Synechocystis* strain, as different WT strains can respond differently to the same conditions or modifications (Koskinen et al., 2023). Nonetheless, the lower contribution of photosynthetic NADPH could partially explain the poor performance under mixotrophy.

Targeting the bottleneck of biotransformation is a successful strategy, as demonstrated in Paper III. Other strategies aiming at increasing the $NADP^+$/NADPH pool size or the $NADP^+$ reduction rate could be combined to achieve higher biotransformation rates. The pyridine nucleotide transhydrogenase PntAB could be another target as it converts NADH into NADPH (Kämäräinen et al., 2017). Optimising the D-glucose concentration or the timing of addition also has the potential to yield new results. It would be interesting to test different concentrations of D-glucose with varying culture densities, where the glucose per cell ratio changes or is kept constant. However, using organic carbon sources lowers the sustainability potential of photosynthetic organisms in biotechnological applications unless a waste stream is available as the source of these carbohydrates.

5.5 Carbon availability and light quality enhance the Baeyer-Villiger oxidation reaction

BVMOs require O_2 in addition to NADPH to mediate the Baeyer-Villiger oxidation, while YqjM requires only NAD(P)H for ene-reduction. Furthermore, they generally reach lower specific activities than YqjM, with values ranging from 5 to 50 $U \cdot g_{DCW}^{-1}$ (Erdem et al., 2022; Tüllinghoff et al., 2024, 2022). Considering that *Synechocystis* can support activities of ~150 $U \cdot g_{DCW}^{-1}$ with YqjM, the availability of NADPH is unlikely to be the limiting factor for BVMO's activity. The theoretical maximal rate of O_2 evolution of the cyanobacterial OEC at PSII is 850 $U \cdot g_{DCW}^{-1}$ based on assumptions of the turnover rate and its abundance per cell. However, experiments with intact WT cells typically reach significantly lower values (Hoschek et al., 2018). Our values reach ~50 $U \cdot g_{DCW}^{-1}$ using WT *Synechocystis*. Under conditions with ample illumination, O_2 availability will be sufficient. However, at high cell densities with significant self-shading, O_2 evolution might decrease, causing the BVMO activity to become limited by O_2 availability.

Heterologous enzymes can be introduced into cells either on a replicative plasmid or as a cassette integrated into the genome via homologous recombination at a neutral site. Genomic integration under the control of the P_{cpcB} promoter of the C-phycocyanin β subunit was used for all enzymes in this thesis. It demonstrated stronger expression compared to the P_{psbA} promoter (Assil-Companioni et al., 2020). Nickel and copper-inducible promoters have also been explored to improve enzyme levels. Furthermore, expression from a plasmid proved to be advantageous compared to genomic integration (Tüllinghoff et al., 2022). In addition to promoters, other genomic elements, such as ribosome binding sites, bicistronic domain and genetic insulators, play an important role in heterologous enzyme expression and biotransformation performance (Jodlbauer et al., 2024; Stensjö et al., 2018).

The expression of *cpcB* is upregulated in HC conditions (Muth-Pawlak et al., 2022); thus, I grew the cultures in HC to observe its effect on protein accumulation and biotransformation activity. Indeed, the accumulation of BVMOs significantly increased along with their specific activities (Fig. 11; Fig. 12). This suggests that, at ambient CO_2 concentration, the limitation for BVMOs was likely its protein accumulation. However, YqjM accumulation did not respond to growth in HC despite sharing the same promoter. This was surprising, and the exact reason behind YqjM's response remains unknown. Interestingly, BVMO protein accumulation was significantly higher in the ΔFlv1 background, especially with Parvi. The WT background used to create these mutant strains is different, suggesting that the selected background strain might significantly affect the expression of heterologous enzymes for yet unknown reasons.

Different light spectra have been previously used (Assil-Companioni et al., 2020). However, a comparison of different light spectra under otherwise equal

conditions was missing. I employed broad white and W+R/B illumination under LC and HC conditions and compared the biotransformation performance of Syn::Xeno and ΔFlv1::Xeno. Under LC conditions, the specific activity increased 2-fold, but under HC conditions, no differences between white and W+R/B were observed (Fig. 13). The effects of single-wavelength illumination on cyanobacterial physiology and photosynthesis have been reported (Zavřel et al., 2024). However, especially blue light has been shown to impact photosynthesis negatively (Bernát et al., 2021; Luimstra et al., 2020), while I observed a benefit for biotransformation. These studies commonly used only a single or narrow wavelength, while Paper IV used a broad white spectrum enriched with red and blue wavelengths simultaneously. A thorough characterisation of the physiological response to different types of spectra would provide valuable insights into the regulation of photosynthesis and potential improvements in biotechnological applications.

The results of Paper IV highlight the importance of characterising strains selected for biotechnological applications. Each heterologous enzyme has different cofactor and substrate requirements and might respond differently to identical environmental conditions. Furthermore, growth conditions have wide impacts on cell physiology. Different CO_2 availability, light quality, or intensity will likely influence biotransformation in distinct ways. The selection of an appropriate WT background strain can also impact biotransformation activity, as demonstrated by the protein accumulation in Syn::Parvi.

6 Conclusion and Future Perspective

This thesis set out to address a knowledge gap in understanding the electron partitioning between native and heterologous electron sinks downstream of PSI. Firstly, reduced Fd was established as the primary electron donor to FDPs, and the regulation of their activity via changes in cytosolic pH was elucidated (Paper I). The competition between the heterologous ene-reductase YqjM and the native AET pathways, and the PETC demonstrated that a strong electron sink can "empty" out the PETC, keeping it in an oxidised state and outcompeting the AET pathways (Paper II). However, each system has its bottleneck. For YqjM, this is cofactor availability. Enhancing NAD(P)H production by combining photosynthesis with glucose supply transiently boosted biotransformation productivity; however, the transition to photomixotrophic growth mode proved detrimental (Paper III). Lastly, the production of ε-caprolactone by *Synechocystis* was increased by optimising growth and reaction conditions. A CO_2-rich atmosphere and white light enriched with red and blue wavelengths improved BVMO's specific activity independently; however, when combined, no further improvement was observed (Paper IV).

Microalgae play a vital role in the transition to green circular bioeconomy, whether through nutrient recovery from wastewater streams, the production of pigments and fatty acids, or by serving as biocatalysts for the production of fine chemicals (Paper V). However, they are complex organisms with a long evolutionary history and intricate physiology. Their response to being used as biocatalysts or other production platforms must be carefully considered. Future studies characterising other heterologous enzymes with various activities and turnover rates would provide additional insight into the tight regulation of photosynthesis and the balance between native and heterologous electron pathways. Furthermore, there is a strong need for interdisciplinary collaboration with inputs from enzymologists providing new or engineered enzymes; biologists understanding the complex microalgal physiology; and process engineers designing novel photobioreactors suitable for upscaling.

To conclude, microalgal biotechnology has immense potential; however, it needs to be supported by fundamental understanding of their biology.

Acknowledgements

After nearly five years, my PhD studies are coming to their end. It is, therefore, time to sum up the journey and acknowledge everyone who has made a difference.

This thesis is based on the results of work conducted at the Molecular Plant Biology unit at the University of Turku. However, it would not be complete without the contributions of collaborators from Åbo Akademi University, Graz University of Technology, University of Kassel, University of Kiel and University of Porto.

My studies would also not be possible without the financial contribution from the European Union (projects "FuturoLEAF" and "SUNER-C CSA"), Research Council of Finland (projects "Revisiting Photosynthesis" and "AlgaeLEAF"), University of Turku Graduate School, Jane and Aatos Erkko Foundation (project "PhotoFactory") and Novo Nordisk Foundation (project "PhotoCat"), which is greatly appreciated.

Firstly, I would like to thank Professor **Marc Nowaczyk** and Assistant Professor **Iftach Yacoby** for critically reviewing my thesis and providing valuable feedback and suggestions. I also want to thank Professor **Luning Liu** for agreeing to serve as my opponent and dedicating his time to read my thesis.

Yagut, I will forever be deeply grateful for the opportunity to join your group and embark on the journey of photosynthetic research. While not always easy, it has been an enriching experience, and I have learnt a lot from you. Your openness to discussing more serious topics of mental health and burnout meant a lot, and the support you provided in those moments ensured that I am now writing these words. Thank you for allowing me to carve my own, perhaps less traditional, path through the PhD. The involvement in SUNER-C CSA has been formative in shaping my future career direction beyond academia.

Lauri, I received an email from you at 10:58 CEST on the 5th of August 2020, inviting me to an interview. Everything happened rather quickly, and within a month, I was already in Turku, albeit in a mandatory two-week-long quarantine (pandemic times, yay!). Your help in the first weeks, but especially your deep expertise in the biophysics of photosynthesis and your continuous support, were integral to my PhD studies. Thank you also for translating the various grant application summaries and abstracts, including the abstract of this thesis, into Finnish.

Taina and **Eva-Mari**, thank you for being part of my Advisory Committee and providing valuable feedback, words of encouragement, and support during our annual meetings. I have always left with a new dose of motivation for the next steps in my research plans.

Laura W, your arrival to the group brought a gust of fresh air and a different perspective. Our scientific, linguistic and life chats, troubleshooting R scripts, occasional "beveraginos" or burgers at Woolshed (R.I.P.) were great additions to otherwise mundane days. Your ambition, determination and enthusiasm for science are truly inspiring. I also want to thank you for your invaluable contribution to my first first-author paper, whether it be the colour scheme, figure layout, or wording.

To my office mates, **Marjatta**, **Martina**, **Gábor**, **Eba**, and **Han**, thank you for a very peaceful working environment and the occasional informal chats. Thank you, **Martina**, for providing input on the plethora of things I asked you about. Unfortunately (but fortunately for me), you sat just behind me and were always willing to help. Also, thank you for the apple cake recipe! **Jatta**, it has been a privilege to share the window desk with you. Your stories and lifelong dedication to science are exceptional.

To my students, **Asuka**, **Ville**, and **Joonas**, I want to thank you for your patience and the work you have done while working with me, whether it was for five weeks or eight months. I wish you all the best in your future careers. It was a pleasure working with you.

The research included in this thesis would not have been possible without the support of **Tapio R**, **Mika**, **Eve**, **Vipu**, **Anniina**, and **Laura K**, who kept the labs and instruments functional and the chemical storage stocked. **Vilja**, **Henna**, and **Tuomas**, thank you for all the help with western blots, liquid-liquid extractions and gas chromatography. Without you, my life would have been much more complicated.

Laura L, thank you for being up for co-organising the afterparty of the PhD seminar this year and tackling the box wines the year before. I'm grateful for the lab-related chats as well as the informal ones during various events and on our trip to Venice, Padova and Desenzano del Garda.

Tapio L, your assistance in troubleshooting with DUAL-PAM and DKN was incredibly helpful. Thank you for listening to my rants about the lab, chatting about life, and being my swimming buddy.

To the Stitch & B*tch club, **Pulmu**, **Iia**, and **Darius**, thank you for all those evenings over pastries, spilling the tea, and finally teaching me how to knit a proper pair of woollen socks, thus making me feel a bit more Finnish.

Pablo, you came to our group for a three-month research stay. We quickly became friends as we were using the same instruments and struggling with R scripts. All those long evenings at MIMS, museum visits, and trips around Finland and

Estonia helped brighten up the autumn blues. Thank you for your continuous friendship and the fond memories made here in the Nordics and Spain.

To the newest batch of PhDs, **Samuele**, **Filippo**, **Elia**, **Radin**, and **Kayla**, thank you for your company during lunch and coffee breaks, weekends, and fun nights out in Dynamo. **Filippo**, I will miss watching funny TikToks and your "mean" jokes, which I thoroughly enjoy. **Samuele**, your sense of humour can be sometimes concerning, but the point is that, it's also very funny and makes me laugh. **Kayla**, thank you for being such a caring person and the Irish gin! And, thank you all for keeping the last months of writing my thesis packed with fun and good luck in your own projects. I hope our paths shall cross again.

There are many more people not yet mentioned that have contributed to my PhD in one way or another. My current and former fellow PhDs (**Daniel**, **Anita**, **Olli**, **João**, **Elisa**, **Emren**, **Otso**, and **Khadijatul**), the Photosynthetic Microbes group (**Sergey**, **Mai**, and **Sema**) and the whole Molecular Plant Biology unit, thank you for being part of my PhD journey.

Molli, we met back in Brno during your Erasmus+ exchange and reconnected when I moved to Turku. You made me feel at home, despite the challenging times of 2020, introduced me to your circle of friends, and invited me to your family home for Christmas when I couldn't travel home. Thank you for that! Our Juhannus weekends were exceptionally marvelous. It is always a pleasure to catch up, even if we won't live in the same country or even on the same continent.

Andělka a **Keisy**, naše cesty se protly díky ESNku v Brníčku. Ač se zase rozešly do jiných měst a následně i zemí, zůstali jsme pořád v kontaktu. Díky za naše callindy, oslavu v dobrých a podporu v těžších momentech. Díkičko!

Lastly, to my family, děkuji za ty roky neutuchající podpory při studiu a za volnost jít si za svým cílem s vědomím Vaší podpory.

That's all.

Miranda Priestly

Turku, June 2025

Michal

List of References

Abdelfattah, A., Ali, S.S., Ramadan, H., El-Aswar, E.I., Eltawab, R., Ho, S.-H., Elsamahy, T., Li, S., El-Sheekh, M.M., Schagerl, M., Kornaros, M., Sun, J., 2023. Microalgae-based wastewater treatment: Mechanisms, challenges, recent advances, and future prospects. Environ. Sci. Ecotechnology 13, 100205. https://doi.org/10.1016/j.ese.2022.100205

Adler, L., Díaz-Ramos, A., Mao, Y., Pukacz, K.R., Fei, C., McCormick, A.J., 2022. New horizons for building pyrenoid-based CO2-concentrating mechanisms in plants to improve yields. Plant Physiol. 190, 1609–1627. https://doi.org/10.1093/plphys/kiac373

Agustinus, B., Gillam, E.M.J., 2023. Solar-powered P450 catalysis: Engineering electron transfer pathways from photosynthesis to P450s. J. Inorg. Biochem. 245, 112242. https://doi.org/10.1016/j.jinorgbio.2023.112242

Allahverdiyeva, Y., Ermakova, M., Eisenhut, M., Zhang, P., Richaud, P., Hagemann, M., Cournac, L., Aro, E.-M., 2011. Interplay between flavodiiron proteins and photorespiration in Synechocystis sp. PCC 6803. J. Biol. Chem. 286, 24007–24014. https://doi.org/10.1074/jbc.M111.223289

Allahverdiyeva, Y., Isojärvi, J., Zhang, P., Aro, E.-M., 2015. Cyanobacterial Oxygenic Photosynthesis is Protected by Flavodiiron Proteins. Life 5, 716–743. https://doi.org/10.3390/life5010716

Allahverdiyeva, Y., Mustila, H., Ermakova, M., Bersanini, L., Richaud, P., Ajlani, G., Battchikova, N., Cournac, L., Aro, E.-M., 2013. Flavodiiron proteins Flv1 and Flv3 enable cyanobacterial growth and photosynthesis under fluctuating light. Proc. Natl. Acad. Sci. 110, 4111–4116. https://doi.org/10.1073/pnas.1221194110

Álvarez, C., Jiménez-Ríos, L., Iniesta-Pallarés, M., Jurado-Flores, A., Molina-Heredia, F.P., Ng, C.K.Y., Mariscal, V., 2023. Symbiosis between cyanobacteria and plants: from molecular studies to agronomic applications. J. Exp. Bot. 74, 6145–6157. https://doi.org/10.1093/jxb/erad261

Angeleri, M., Muth-Pawlak, D., Aro, E.-M., Battchikova, N., 2016. Study of O-Phosphorylation Sites in Proteins Involved in Photosynthesis-Related Processes in Synechocystis sp. Strain PCC 6803: Application of the SRM Approach. J. Proteome Res. 15, 4638–4652. https://doi.org/10.1021/acs.jproteome.6b00732

Appel, J., Hueren, V., Boehm, M., Gutekunst, K., 2020. Cyanobacterial in vivo solar hydrogen production using a photosystem I–hydrogenase (PsaD-HoxYH) fusion complex. Nat. Energy 5, 458–467. https://doi.org/10.1038/s41560-020-0609-6

Appel, J., Phunpruch, S., Steinmüller, K., Schulz, R., 2000. The bidirectional hydrogenase of Synechocystis sp. PCC 6803 works as an electron valve during photosynthesis. Arch. Microbiol. 173, 333–338. https://doi.org/10.1007/s002030000139

Arteni, A.A., Ajlani, G., Boekema, E.J., 2009. Structural organisation of phycobilisomes from *Synechocystis* sp. strain PCC6803 and their interaction with the membrane. Biochim. Biophys. Acta BBA - Bioenerg. 1787, 272–279. https://doi.org/10.1016/j.bbabio.2009.01.009

Artz, J.H., Tokmina-Lukaszewska, M., Mulder, D.W., Lubner, C.E., Gutekunst, K., Appel, J., Bothner, B., Boehm, M., King, P.W., 2020. The structure and reactivity of the HoxEFU complex from the cyanobacterium Synechocystis sp. PCC 6803. J. Biol. Chem. 295, 9445–9454. https://doi.org/10.1074/jbc.RA120.013136

Assil-Companioni, L., Büchsenschütz, H.C., Solymosi, D., Dyczmons-Nowaczyk, N.G., Bauer, K.K.F., Wallner, S., Macheroux, P., Allahverdiyeva, Y., Nowaczyk, M.M., Kourist, R., 2020. Engineering of NADPH Supply Boosts Photosynthesis-Driven Biotransformations. ACS Catal. 10, 11864–11877. https://doi.org/10.1021/acscatal.0c02601

Baker, N.R., Harbinson, J., Kramer, D.M., 2007. Determining the limitations and regulation of photosynthetic energy transduction in leaves. Plant Cell Environ. 30, 1107–1125. https://doi.org/10.1111/j.1365-3040.2007.01680.x

Balcerzak, L., Lipok, J., Strub, D., Lochyński, S., 2014. Biotransformations of monoterpenes by photoautotrophic micro-organisms. J. Appl. Microbiol. 117, 1523–1536. https://doi.org/10.1111/jam.12632

Baldwin, C.V.F., Woodley, J.M., 2006. On oxygen limitation in a whole cell biocatalytic Baeyer–Villiger oxidation process. Biotechnol. Bioeng. 95, 362–369. https://doi.org/10.1002/bit.20869

Baradaran, R., Berrisford, J.M., Minhas, G.S., Sazanov, L.A., 2013. Crystal structure of the entire respiratory complex I. Nature 494, 443–448. https://doi.org/10.1038/nature11871

Barbosa, M.J., Janssen, M., Südfeld, C., D'Adamo, S., Wijffels, R.H., 2023. Hypes, hopes, and the way forward for microalgal biotechnology. Trends Biotechnol. 41, 452–471. https://doi.org/10.1016/j.tibtech.2022.12.017

Barney, B.M., 2020. Aerobic nitrogen-fixing bacteria for hydrogen and ammonium production: current state and perspectives. Appl. Microbiol. Biotechnol. 104, 1383–1399. https://doi.org/10.1007/s00253-019-10210-9

Bartsch, M., Gassmeyer, S.K., Köninger, K., Igarashi, K., Liauw, P., Dyczmons-Nowaczyk, N., Miyamoto, K., Nowaczyk, M.M., Kourist, R., 2015. Photosynthetic production of enantioselective biocatalysts. Microb. Cell Factories 14, 53. https://doi.org/10.1186/s12934-015-0233-5

Basu, S., Mackey, K.R.M., 2018. Phytoplankton as Key Mediators of the Biological Carbon Pump: Their Responses to a Changing Climate. Sustainability 10, 869. https://doi.org/10.3390/su10030869

Battchikova, N., Eisenhut, M., Aro, E.-M., 2011. Cyanobacterial NDH-1 complexes: Novel insights and remaining puzzles. Biochim. Biophys. Acta BBA - Bioenerg., Regulation of Electron Transport in Chloroplasts 1807, 935–944. https://doi.org/10.1016/j.bbabio.2010.10.017

Beckmann, K., Messinger, J., Badger, M.R., Wydrzynski, T., Hillier, W., 2009. On-line mass spectrometry: membrane inlet sampling. Photosynth. Res. 102, 511–522. https://doi.org/10.1007/s11120-009-9474-7

Behrenfeld, M.J., Randerson, J.T., McClain, C.R., Feldman, G.C., Los, S.O., Tucker, C.J., Falkowski, P.G., Field, C.B., Frouin, R., Esaias, W.E., Kolber, D.D., Pollack, N.H., 2001. Biospheric Primary Production During an ENSO Transition. Science 291, 2594–2597. https://doi.org/10.1126/science.1055071

Beraldo, C., Traverso, E., Boschin, M., Cendron, L., Morosinotto, T., Alboresi, A., 2024. Physcomitrium patens flavodiiron proteins form heterotetrametric complexes. J. Biol. Chem. 300, 107643. https://doi.org/10.1016/j.jbc.2024.107643

Berepiki, A., Gittins, J.R., Moore, C.M., Bibby, T.S., 2018. Rational engineering of photosynthetic electron flux enhances light-powered cytochrome P450 activity. Synth. Biol. 3, ysy009. https://doi.org/10.1093/synbio/ysy009

Berepiki, A., Hitchcock, A., Moore, C.M., Bibby, T.S., 2016. Tapping the Unused Potential of Photosynthesis with a Heterologous Electron Sink. ACS Synth. Biol. 5, 1369–1375. https://doi.org/10.1021/acssynbio.6b00100

Bernát, G., Zavřel, T., Kotabová, E., Kovács, L., Steinbach, G., Vörös, L., Prášil, O., Somogyi, B., Tóth, V.R., 2021. Photomorphogenesis in the Picocyanobacterium Cyanobium gracile Includes Increased Phycobilisome Abundance Under Blue Light, Phycobilisome Decoupling Under Near Far-Red Light, and Wavelength-Specific Photoprotective Strategies. Front. Plant Sci. 12. https://doi.org/10.3389/fpls.2021.612302

Bersanini, L., Allahverdiyeva, Y., Battchikova, N., Heinz, S., Lespinasse, M., Ruohisto, E., Mustila, H., Nickelsen, J., Vass, I., Aro, E.-M., 2017. Dissecting the Photoprotective Mechanism Encoded by the flv4-2 Operon: a Distinct Contribution of Sll0218 in Photosystem II Stabilization. Plant Cell Environ. 40, 378–389. https://doi.org/10.1111/pce.12872

Böhmer, S., Köninger, K., Gómez-Baraibar, Á., Bojarra, S., Mügge, C., Schmidt, S., Nowaczyk, M.M., Kourist, R., 2017. Enzymatic Oxyfunctionalization Driven by Photosynthetic Water-Splitting in the Cyanobacterium Synechocystis sp. PCC 6803. Catalysts 7, 240. https://doi.org/10.3390/catal7080240

Böhmer, S., Marx, C., Gómez-Baraibar, Á., Nowaczyk, M.M., Tischler, D., Hemschemeier, A., Happe, T., 2020. Evolutionary diverse *Chlamydomonas reinhardtii* Old Yellow Enzymes reveal distinctive catalytic properties and potential for whole-cell biotransformations. Algal Res. 50, 101970. https://doi.org/10.1016/j.algal.2020.101970

Borowitzka, M.A., 2015. Algal Biotechnology, in: Sahoo, D., Seckbach, J. (Eds.), The Algae World. Springer Netherlands, Dordrecht, pp. 319–338. https://doi.org/10.1007/978-94-017-7321-8_11

Bozan, M., Berreth, H., Lindberg, P., Bühler, K., 2025. Cyanobacterial biofilms: from natural systems to applications. Trends Biotechnol. 43, 318–332. https://doi.org/10.1016/j.tibtech.2024.08.005

Brändén, G., Gennis, R.B., Brzezinski, P., 2006. Transmembrane proton translocation by cytochrome c oxidase. Biochim. Biophys. Acta 1757, 1052–1063. https://doi.org/10.1016/j.bbabio.2006.05.020

Brown, K.A., Guo, Z., Tokmina-Lukaszewska, M., Scott, L.W., Lubner, C.E., Smolinski, S., Mulder, D.W., Bothner, B., King, P.W., 2019. The oxygen reduction reaction catalyzed by Synechocystis sp. PCC 6803 flavodiiron proteins. Sustain. Energy Fuels 3, 3191–3200. https://doi.org/10.1039/C9SE00523D

Büchsenschütz, H.C., Vidimce-Risteski, V., Eggbauer, B., Schmidt, S., Winkler, C.K., Schrittwieser, J.H., Kroutil, W., Kourist, R., 2020. Stereoselective Biotransformations of Cyclic Imines in Recombinant Cells of Synechocystis sp. PCC 6803. ChemCatChem 12, 726–730. https://doi.org/10.1002/cctc.201901592

Calzadilla, P.I., Kirilovsky, D., 2020. Revisiting cyanobacterial state transitions. Photochem. Photobiol. Sci. 19, 585–603. https://doi.org/10.1039/C9PP00451C

Carrasquer-Alvarez, E., Hoffmann, U.A., Geissler, A.S., Knave, A., Gorodkin, J., Seemann, S.E., Hudson, E.P., Frigaard, N.-U., 2025. Photosynthesis in Synechocystis sp. PCC 6803 is not optimally regulated under very high CO2. Appl. Microbiol. Biotechnol. 109, 33. https://doi.org/10.1007/s00253-025-13416-2

Cassier-Chauvat, C., Chauvat, F., 2014. Function and Regulation of Ferredoxins in the Cyanobacterium, Synechocystis PCC6803: Recent Advances. Life 4, 666–680. https://doi.org/10.3390/life4040666

Chánique, A.M., Polidori, N., Sovic, L., Kracher, D., Assil-Companioni, L., Galuska, P., Parra, L.P., Gruber, K., Kourist, R., 2023. A Cold-Active Flavin-Dependent Monooxygenase from Janthinobacterium svalbardensis Unlocks Applications of Baeyer–Villiger Monooxygenases at Low Temperature. ACS Catal. 13, 3549–3562. https://doi.org/10.1021/acscatal.2c05160

Charpy, L., Casareto, B.E., Langlade, M.J., Suzuki, Y., 2012. Cyanobacteria in Coral Reef Ecosystems: A Review. J. Mar. Sci. 2012, 259571. https://doi.org/10.1155/2012/259571

Checchetto, V., Segalla, A., Allorent, G., La Rocca, N., Leanza, L., Giacometti, G.M., Uozumi, N., Finazzi, G., Bergantino, E., Szabò, I., 2012. Thylakoid potassium channel is required for efficient photosynthesis in cyanobacteria. Proc. Natl. Acad. Sci. 109, 11043–11048. https://doi.org/10.1073/pnas.1205960109

Chen, X., Schreiber, K., Appel, J., Makowka, A., Fähnrich, B., Roettger, M., Hajirezaei, M.R., Sönnichsen, F.D., Schönheit, P., Martin, W.F., Gutekunst, K., 2016. The Entner–Doudoroff pathway is an overlooked glycolytic route in cyanobacteria and plants. Proc. Natl. Acad. Sci. 113, 5441–5446. https://doi.org/10.1073/pnas.1521916113

Chen, Y., Taton, A., Go, M., London, R.E., Pieper, L.M., Golden, S.S., Golden, J.W., 2016. Self-replicating shuttle vectors based on pANS, a small endogenous plasmid of the unicellular cyanobacterium Synechococcus elongatus PCC 7942. Microbiology 162, 2029–2041. https://doi.org/10.1099/mic.0.000377

Cheng, J., Zhang, C., Zhang, K., Li, J., Hou, Y., Xin, J., Sun, Y., Xu, C., Xu, W., 2023a. Cyanobacteria-Mediated Light-Driven Biotransformation: The Current Status and Perspectives. ACS Omega 8, 42062–42071. https://doi.org/10.1021/acsomega.3c05407

Cheng, J., Zhang, K., Hou, Y., 2023b. The current situations and limitations of genetic engineering in cyanobacteria: a mini review. Mol. Biol. Rep. 50, 5481–5487. https://doi.org/10.1007/s11033-023-08456-8

Chitnis, P.R., 1996. Photosystem I. Plant Physiol. 111, 661–669. https://doi.org/10.1104/pp.111.3.661

Coleman, J.R., Colman, B., 1981. Inorganic Carbon Accumulation and Photosynthesis in a Blue-green Alga as a Function of External pH 1. Plant Physiol. 67, 917–921. https://doi.org/10.1104/pp.67.5.917

Cooley, J.W., Howitt, C.A., Vermaas, W.F.J., 2000. Succinate:Quinol Oxidoreductases in the Cyanobacterium Synechocystis sp. Strain PCC 6803: Presence and Function in Metabolism and Electron Transport. J. Bacteriol. 182, 714–722. https://doi.org/10.1128/jb.182.3.714-722.2000

Croce, R., Carmo-Silva, E., Cho, Y.B., Ermakova, M., Harbinson, J., Lawson, T., McCormick, A.J., Niyogi, K.K., Ort, D.R., Patel-Tupper, D., Pesaresi, P., Raines, C., Weber, A.P.M., Zhu, X.-G., 2024. Perspectives on improving photosynthesis to increase crop yield. Plant Cell 36, 3944–3973. https://doi.org/10.1093/plcell/koae132

Cruz, J.A., Kanazawa, A., Treff, N., Kramer, D.M., 2005. Storage of light-driven transthylakoid proton motive force as an electric field ($\Delta\psi$) under steady-state conditions in intact cells of Chlamydomonas reinhardtii. Photosynth. Res. 85, 221–233. https://doi.org/10.1007/s11120-005-4731-x

Deprá, M.C., Dias, R.R., Zepka, L.Q., Jacob-Lopes, E., 2025. Tackling Old Challenges in Microalgal Biotechnology: The Role of Photobioreactors to Advance the Technology Readiness Level. Processes 13, 51. https://doi.org/10.3390/pr13010051

Dexter, J., Fu, P., 2009. Metabolic engineering of cyanobacteria for ethanol production. Energy Environ. Sci. 2, 857–864. https://doi.org/10.1039/B811937F

Dienst, D., Wichmann, J., Mantovani, O., Rodrigues, J.S., Lindberg, P., 2020. High density cultivation for efficient sesquiterpenoid biosynthesis in Synechocystis sp. PCC 6803. Sci. Rep. 10, 5932. https://doi.org/10.1038/s41598-020-62681-w

Domínguez-Martín, M.A., Sauer, P.V., Kirst, H., Sutter, M., Bína, D., Greber, B.J., Nogales, E., Polívka, T., Kerfeld, C.A., 2022. Structures of a phycobilisome in light-harvesting and photoprotected states. Nature 609, 835–845. https://doi.org/10.1038/s41586-022-05156-4

Ducat, D.C., Avelar-Rivas, J.A., Way, J.C., Silver, P.A., 2012. Rerouting carbon flux to enhance photosynthetic productivity. Appl. Environ. Microbiol. 78, 2660–2668. https://doi.org/10.1128/AEM.07901-11

Eisenhut, M., Huege, J., Schwarz, D., Bauwe, H., Kopka, J., Hagemann, M., 2008. Metabolome Phenotyping of Inorganic Carbon Limitation in Cells of the Wild Type and Photorespiratory Mutants of the Cyanobacterium Synechocystis sp. Strain PCC 6803. Plant Physiol. 148, 2109–2120. https://doi.org/10.1104/pp.108.129403

Eisenhut, M., Roell, M.-S., Weber, A.P.M., 2019. Mechanistic understanding of photorespiration paves the way to a new green revolution. New Phytol. 223, 1762–1769. https://doi.org/10.1111/nph.15872

Enevoldsen, H.O., Hallegraeff, G.M., Anderson, D.M., Cembella, A.D., 2003. Manual on harmful marine microalgae, 2nd ed, Monographs on oceanographic methodology. UNESCO, Paris.

Erdem, E., Malihan-Yap, L., Assil-Companioni, L., Grimm, H., Barone, G.D., Serveau-Avesque, C., Amouric, A., Duquesne, K., De Berardinis, V., Allahverdiyeva, Y., Alphand, V., Kourist, R., 2022. Photobiocatalytic Oxyfunctionalization with High Reaction Rate using a Baeyer–Villiger

Monooxygenase from *Burkholderia xenovorans* in Metabolically Engineered Cyanobacteria. ACS Catal. 12, 66–72. https://doi.org/10.1021/acscatal.1c04555

Ermakova, M., Huokko, T., Richaud, P., Bersanini, L., Howe, C.J., Lea-Smith, D.J., Peltier, G., Allahverdiyeva, Y., 2016. Distinguishing the Roles of Thylakoid Respiratory Terminal Oxidases in the Cyanobacterium Synechocystis sp. PCC 6803. Plant Physiol. 171, 1307–1319. https://doi.org/10.1104/pp.16.00479

European Commission, Directorate-General for Environment, 2020. A new Circular Economy Action Plan For a cleaner and more competitive Europe, EUR-Lex - 52020DC0098 - EN.

European Commission: European Innovation Council and SMEs Executive Agency, 2024. The future of Solar-to-X: harnessing renewables for a sustainable future. Publications Office of the European Union.

European Commission, Secretariat-General, 2019. The European Green Deal, EUR-Lex - 52019DC0640 - EN.

European Parliament, Council of the European Union, 2025. Directive (EU) 2024/3019 of the European Parliament and of the Council of 27 November 2024 concerning urban wastewater treatment, EUR-Lex - 32024L3019 - EN.

European Parliament, Council of the European Union, 2021. Horizon Europe – the Framework Programme for Research and Innovation, REGULATION (EU) 2021/695.

Evans, S.E., Franks, A.E., Bergman, M.E., Sethna, N.S., Currie, M.A., Phillips, M.A., 2024. Plastid ancestors lacked a complete Entner-Doudoroff pathway, limiting plants to glycolysis and the pentose phosphate pathway. Nat. Commun. 15, 1102. https://doi.org/10.1038/s41467-024-45384-y

Fan, D.-Y., Fitzpatrick, D., Oguchi, R., Ma, W., Kou, J., Chow, W.S., 2016. Obstacles in the quantification of the cyclic electron flux around Photosystem I in leaves of C3 plants. Photosynth. Res. 129, 239–251. https://doi.org/10.1007/s11120-016-0223-4

Fernández, F.G.A., Reis, A., Wijffels, R.H., Barbosa, M., Verdelho, V., Llamas, B., 2021. The role of microalgae in the bioeconomy. New Biotechnol. 61, 99–107. https://doi.org/10.1016/j.nbt.2020.11.011

Findlay, H.S., Feely, R.A., Jiang, L.-Q., Pelletier, G., Bednaršek, N., 2025. Ocean Acidification: Another Planetary Boundary Crossed. Glob. Change Biol. 31, e70238. https://doi.org/10.1111/gcb.70238

Fitzpatrick, T.B., Amrhein, N., Macheroux, P., 2003. Characterization of YqjM, an Old Yellow Enzyme Homolog from Bacillus subtilis Involved in the Oxidative Stress Response. J. Biol. Chem. 278, 19891–19897. https://doi.org/10.1074/jbc.M211778200

Flores, E., Frías, J.E., Rubio, L.M., Herrero, A., 2005. Photosynthetic nitrate assimilation in cyanobacteria. Photosynth. Res. 83, 117–133. https://doi.org/10.1007/s11120-004-5830-9

Flores, E., Schmetterer, G., 1986. Interaction of fructose with the glucose permease of the cyanobacterium Synechocystis sp. strain PCC 6803. J. Bacteriol. 166, 693–696. https://doi.org/10.1128/jb.166.2.693-696.1986

Food and Agriculture Organization of the United Nations, 2023. Caloric supply by food group [WWW Document]. Our World Data. URL https://ourworldindata.org/grapher/calorie-supply-by-food-group (accessed 3.2.25).

Frankenberg, N., Mukougawa, K., Kohchi, T., Lagarias, J.C., 2001. Functional Genomic Analysis of the HY2 Family of Ferredoxin-Dependent Bilin Reductases from Oxygenic Photosynthetic Organisms. Plant Cell 13, 965–978. https://doi.org/10.1105/tpc.13.4.965

Furbank, R., Kelly, S., von Caemmerer, S., 2023. Photosynthesis and food security: the evolving story of C4 rice. Photosynth. Res. 158, 121–130. https://doi.org/10.1007/s11120-023-01014-0

Fürst, M.J.L.J., Gran-Scheuch, A., Aalbers, F.S., Fraaije, M.W., 2019. Baeyer–Villiger Monooxygenases: Tunable Oxidative Biocatalysts. ACS Catal. 9, 11207–11241. https://doi.org/10.1021/acscatal.9b03396

Gibson, D.G., Young, L., Chuang, R.-Y., Venter, J.C., Hutchison, C.A., Smith, H.O., 2009. Enzymatic assembly of DNA molecules up to several hundred kilobases. Nat. Methods 6, 343–345. https://doi.org/10.1038/nmeth.1318

Gisriel, C.J., Wang, J., Liu, J., Flesher, D.A., Reiss, K.M., Huang, H.-L., Yang, K.R., Armstrong, W.H., Gunner, M.R., Batista, V.S., Debus, R.J., Brudvig, G.W., 2022. High-resolution cryo-electron microscopy structure of photosystem II from the mesophilic cyanobacterium, Synechocystis sp. PCC 6803. Proc. Natl. Acad. Sci. 119, e2116765118. https://doi.org/10.1073/pnas.2116765118

Górak, M., Żymańczyk-Duda, E., 2015. Application of cyanobacteria for chiral phosphonate synthesis. Green Chem 17, 4570–4578. https://doi.org/10.1039/C5GC01195G

Grimm, H.C., Erlsbacher, P., Medipally, H., Malihan-Yap, L., Sovic, L., Zöhrer, J., Kosourov, S.N., Allahverdiyeva, Y., Paul, C.E., Kourist, R., 2025. Towards high atom economy in whole-cell redox biocatalysis: up-scaling light-driven cyanobacterial ene-reductions in a flat panel photobioreactor. Green Chem. 27, 2907–2920. https://doi.org/10.1039/D4GC05686H

Gründel, M., Scheunemann, R., Lockau, W., Zilliges, Y., 2012. Impaired glycogen synthesis causes metabolic overflow reactions and affects stress responses in the cyanobacterium Synechocystis sp. PCC 6803. Microbiology 158, 3032–3043. https://doi.org/10.1099/mic.0.062950-0

G. Turrini, N., C. Cioc, R., Niet, D.J.H. van der, Ruijter, E., A. Orru, R.V., Hall, M., Faber, K., 2017. Biocatalytic access to nonracemic γ-oxo esters via stereoselective reduction using ene-reductases. Green Chem. 19, 511–518. https://doi.org/10.1039/C6GC02493A

Guo, J., Nguyen, A.Y., Dai, Z., Su, D., Gaffrey, M.J., Moore, R.J., Jacobs, J.M., Monroe, M.E., Smith, R.D., Koppenaal, D.W., Pakrasi, H.B., Qian, W.-J., 2014. Proteome-wide Light/Dark Modulation of Thiol Oxidation in Cyanobacteria Revealed by Quantitative Site-specific Redox Proteomics. Mol. Cell. Proteomics 13, 3270–3285. https://doi.org/10.1074/mcp.M114.041160

Gutekunst, K., Chen, X., Schreiber, K., Kaspar, U., Makam, S., Appel, J., 2014. The Bidirectional NiFe-hydrogenase in Synechocystis sp. PCC 6803 Is Reduced by Flavodoxin and Ferredoxin and Is Essential under Mixotrophic, Nitrate-limiting Conditions. J. Biol. Chem. 289, 1930–1937. https://doi.org/10.1074/jbc.M113.526376

Hahn, A., Vonck, J., Mills, D.J., Meier, T., Kühlbrandt, W., 2018. Structure, mechanism, and regulation of the chloroplast ATP synthase. Science 360, eaat4318. https://doi.org/10.1126/science.aat4318

Haimovich-Dayan, M., Kahlon, S., Hihara, Y., Hagemann, M., Ogawa, T., Ohad, I., Lieman-Hurwitz, J., Kaplan, A., 2011. Cross-talk between photomixotrophic growth and CO2-concentrating mechanism in Synechocystis sp. strain PCC 6803. Environ. Microbiol. 13, 1767–1777. https://doi.org/10.1111/j.1462-2920.2011.02481.x

Hall, M., Stueckler, C., Ehammer, H., Pointner, E., Oberdorfer, G., Gruber, K., Hauer, B., Stuermer, R., Kroutil, W., Macheroux, P., Faber, K., 2008. Asymmetric Bioreduction of C□C Bonds using Enoate Reductases OPR1, OPR3 and YqjM: Enzyme-Based Stereocontrol. Adv. Synth. Catal. 350, 411–418. https://doi.org/10.1002/adsc.200700458

Hanamghar, S.S., Mellor, S.B., Mikkelsen, L., Crocoll, C., Motawie, M.S., Russo, D.A., Jensen, P.E., Zedler, J.A.Z., 2025. Thylakoid Targeting Improves Stability of a Cytochrome P450 in the Cyanobacterium Synechocystis sp. PCC 6803. ACS Synth. Biol. 14, 867–877. https://doi.org/10.1021/acssynbio.4c00800

Hanke, G.T., Satomi, Y., Shinmura, K., Takao, T., Hase, T., 2011. A screen for potential ferredoxin electron transfer partners uncovers new, redox dependent interactions. Biochim. Biophys. Acta BBA - Proteins Proteomics 1814, 366–374. https://doi.org/10.1016/j.bbapap.2010.09.011

Helman, Y., Barkan, E., Eisenstadt, D., Luz, B., Kaplan, A., 2005. Fractionation of the Three Stable Oxygen Isotopes by Oxygen-Producing and Oxygen-Consuming Reactions in Photosynthetic Organisms. Plant Physiol. 138, 2292–2298. https://doi.org/10.1104/pp.105.063768

Helman, Y., Tchernov, D., Reinhold, L., Shibata, M., Ogawa, T., Schwarz, R., Ohad, I., Kaplan, A., 2003. Genes Encoding A-Type Flavoproteins Are Essential for Photoreduction of O2 in Cyanobacteria. Curr. Biol. 13, 230–235. https://doi.org/10.1016/S0960-9822(03)00046-0

Hill, R., Bendall, F., 1960. Function of the Two Cytochrome Components in Chloroplasts: A Working Hypothesis. Nature 186, 136–137. https://doi.org/10.1038/186136a0

Hisabori, T., 2020. Chapter One - Regulation machineries of ATP synthase from phototroph, in: Hisabori, T. (Ed.), Advances in Botanical Research, ATP Synthase in Photosynthetic Organisms. Academic Press, pp. 1–26. https://doi.org/10.1016/bs.abr.2020.07.003

Hobisch, M., Spasic, J., Malihan-Yap, L., Barone, G.D., Castiglione, K., Tamagnini, P., Kara, S., Kourist, R., 2021. Internal Illumination to Overcome the Cell Density Limitation in the Scale-up of Whole-Cell Photobiocatalysis. ChemSusChem 14, 3219–3225. https://doi.org/10.1002/cssc.202100832

Hoiczyk, E., Hansel, A., 2000. Cyanobacterial Cell Walls: News from an Unusual Prokaryotic Envelope. J. Bacteriol. 182, 1191–1199. https://doi.org/10.1128/jb.182.5.1191-1199.2000

Hölsch, K., Havel, J., Haslbeck, M., Weuster-Botz, D., 2008. Identification, Cloning, and Characterization of a Novel Ketoreductase from the Cyanobacterium Synechococcus sp. Strain PCC 7942. Appl. Environ. Microbiol. 74, 6697–6702. https://doi.org/10.1128/AEM.00925-08

Hölsch, K., Weuster-Botz, D., 2010. New oxidoreductases from cyanobacteria: Exploring nature's diversity. Enzyme Microb. Technol. 47, 228–235. https://doi.org/10.1016/j.enzmictec.2010.06.006

Hoschek, A., Bühler, B., Schmid, A., 2019a. Stabilization and scale-up of photosynthesis-driven ω-hydroxylation of nonanoic acid methyl ester by two-liquid phase whole-cell biocatalysis. Biotechnol. Bioeng. 116, 1887–1900. https://doi.org/10.1002/bit.27006

Hoschek, A., Bühler, B., Schmid, A., 2017. Overcoming the Gas–Liquid Mass Transfer of Oxygen by Coupling Photosynthetic Water Oxidation with Biocatalytic Oxyfunctionalization. Angew. Chem. Int. Ed. 56, 15146–15149. https://doi.org/10.1002/anie.201706886

Hoschek, A., Schmid, A., Bühler, B., 2018. In Situ O2 Generation for Biocatalytic Oxyfunctionalization Reactions. ChemCatChem 10, 5366–5371. https://doi.org/10.1002/cctc.201801262

Hoschek, A., Toepel, J., Hochkeppel, A., Karande, R., Bühler, B., Schmid, A., 2019b. Light-Dependent and Aeration-Independent Gram-Scale Hydroxylation of Cyclohexane to Cyclohexanol by CYP450 Harboring Synechocystis sp. PCC 6803. Biotechnol. J. 14, 1800724. https://doi.org/10.1002/biot.201800724

Ikeuchi, M., Tabata, S., 2001. Synechocystis sp. PCC 6803 — a useful tool in the study of the genetics of cyanobacteria. Photosynth. Res. 70, 73–83. https://doi.org/10.1023/A:1013887908680

Ilhami, S., Rahman, S.N.S.A., Iqhrammullah, M., Hamid, Z., Chai, Y.H., Lam, M.K., 2025. Polyhydroxyalkanoates production from microalgae for sustainable bioplastics: A review. Biotechnol. Adv. 79, 108529. https://doi.org/10.1016/j.biotechadv.2025.108529

Imashimizu, M., Bernát, G., Sunamura, E.-I., Broekmans, M., Konno, H., Isato, K., Rögner, M., Hisabori, T., 2011. Regulation of F0F1-ATPase from Synechocystis sp. PCC 6803 by γ and ∈ Subunits Is Significant for Light/Dark Adaptation *. J. Biol. Chem. 286, 26595–26602. https://doi.org/10.1074/jbc.M111.234138

Intergovernmental Panel on Climate Change, 2023. Urgent climate action can secure a liveable future for all.

ISO 59004:2024, 2024.

Jodlbauer, J., Schmal, M., Waltl, C., Rohr, T., Mach-Aigner, A.R., Mihovilovic, M.D., Rudroff, F., 2024. Unlocking the potential of cyanobacteria: a high-throughput strategy for enhancing biocatalytic performance through genetic optimization. Trends Biotechnol. 42, 1795–1818. https://doi.org/10.1016/j.tibtech.2024.07.011

Johnson, J.E., Cornell, R.B., 1999. Amphitropic proteins: regulation by reversible membrane interactions (Review). Mol. Membr. Biol. 16, 217–235. https://doi.org/10.1080/096876899294544

Junesch, U., Gräber, P., 1987. Influence of the redox state and the activation of the chloroplast ATP synthase on proton-transport-coupled ATP synthesis/hydrolysis. Biochim. Biophys. Acta BBA - Bioenerg. 893, 275–288. https://doi.org/10.1016/0005-2728(87)90049-1

Kämäräinen, J., Huokko, T., Kreula, S., Jones, P.R., Aro, E.-M., Kallio, P., 2017. Pyridine nucleotide transhydrogenase PntAB is essential for optimal growth and photosynthetic integrity under low-light mixotrophic conditions in Synechocystis sp. PCC 6803. New Phytol. 214, 194–204. https://doi.org/10.1111/nph.14353

Kamerbeek, N.M., Fraaije, M.W., Janssen, D.B., 2004. Identifying determinants of NADPH specificity in Baeyer–Villiger monooxygenases. Eur. J. Biochem. 271, 2107–2116. https://doi.org/10.1111/j.1432-1033.2004.04126.x

Kanda, T., Saito, K., Ishikita, H., 2021. Electron Acceptor–Donor Iron Sites in the Iron–Sulfur Cluster of Photosynthetic Electron-Transfer Pathways. J. Phys. Chem. Lett. 12, 7431–7438. https://doi.org/10.1021/acs.jpclett.1c01896

Kaneko, T., Sato, S., Kotani, H., Tanaka, A., Asamizu, E., Nakamura, Y., Miyajima, N., Hirosawa, M., Sugiura, M., Sasamoto, S., Kimura, T., Hosouchi, T., Matsuno, A., Muraki, A., Nakazaki, N., Naruo, K., Okumura, S., Shimpo, S., Takeuchi, C., Wada, T., Watanabe, A., Yamada, M., Yasuda, M., Tabata, S., 1996. Sequence Analysis of the Genome of the Unicellular Cyanobacterium Synechocystis sp. Strain PCC6803. II. Sequence Determination of the Entire Genome and Assignment of Potential Protein-coding Regions. DNA Res. 3, 109–136. https://doi.org/10.1093/dnares/3.3.109

Kannchen, D., Zabret, J., Oworah-Nkruma, R., Dyczmons-Nowaczyk, N., Wiegand, K., Löbbert, P., Frank, A., Nowaczyk, M.M., Rexroth, S., Rögner, M., 2020. Remodeling of photosynthetic electron transport in *Synechocystis* sp. PCC 6803 for future hydrogen production from water. Biochim. Biophys. Acta BBA - Bioenerg. 1861, 148208. https://doi.org/10.1016/j.bbabio.2020.148208

Kaplan, A., 2017. On the cradle of CCM research: discovery, development, and challenges ahead. J. Exp. Bot. 68, 3785–3796. https://doi.org/10.1093/jxb/erx122

Kato, K., Nagao, R., Jiang, T.-Y., Ueno, Y., Yokono, M., Chan, S.K., Watanabe, M., Ikeuchi, M., Shen, J.-R., Akimoto, S., Miyazaki, N., Akita, F., 2019. Structure of a cyanobacterial photosystem I tetramer revealed by cryo-electron microscopy. Nat. Commun. 10, 4929. https://doi.org/10.1038/s41467-019-12942-8

Kauny, J., Sétif, P., 2014. NADPH fluorescence in the cyanobacterium Synechocystis sp. PCC 6803: A versatile probe for in vivo measurements of rates, yields and pools. Biochim. Biophys. Acta BBA - Bioenerg. 1837, 792–801. https://doi.org/10.1016/j.bbabio.2014.01.009

Kerfeld, C.A., Melnicki, M.R., 2016. Assembly, function and evolution of cyanobacterial carboxysomes. Curr. Opin. Plant Biol. 31, 66–75. https://doi.org/10.1016/j.pbi.2016.03.009

Kerfeld, C.A., Melnicki, M.R., Sutter, M., Dominguez-Martin, M.A., 2017. Structure, function and evolution of the cyanobacterial orange carotenoid protein and its homologs. New Phytol. 215, 937–951. https://doi.org/10.1111/nph.14670

Khetkorn, W., Rastogi, R.P., Incharoensakdi, A., Lindblad, P., Madamwar, D., Pandey, A., Larroche, C., 2017. Microalgal hydrogen production – A review. Bioresour. Technol. 243, 1194–1206. https://doi.org/10.1016/j.biortech.2017.07.085

Khorobrykh, S., Havurinne, V., Mattila, H., Tyystjärvi, E., 2020. Oxygen and ROS in Photosynthesis. Plants Basel Switz. 9, 91. https://doi.org/10.3390/plants9010091

Kitzing, K., Fitzpatrick, T.B., Wilken, C., Sawa, J., Bourenkov, G.P., Macheroux, P., Clausen, T., 2005. The 1.3 Å Crystal Structure of the Flavoprotein YqjM Reveals a Novel Class of Old Yellow Enzymes*. J. Biol. Chem. 280, 27904–27913. https://doi.org/10.1074/jbc.M502587200

Kohli, R.M., Massey, V., 1998. The Oxidative Half-reaction of Old Yellow Enzyme: THE ROLE OF TYROSINE 196*. J. Biol. Chem. 273, 32763–32770. https://doi.org/10.1074/jbc.273.49.32763

Kok, B., Forbush, B., McGloin, M., 1970. Cooperation of charges in photosynthetic O2 evolution-I. A linear four step mechanism. Photochem. Photobiol. 11, 457–475. https://doi.org/10.1111/j.1751-1097.1970.tb06017.x

Köninger, K., Gómez Baraibar, Á., Mügge, C., Paul, C.E., Hollmann, F., Nowaczyk, M.M., Kourist, R., 2016. Recombinant Cyanobacteria for the Asymmetric Reduction of C=C Bonds Fueled by the

Biocatalytic Oxidation of Water. Angew. Chem. Int. Ed. 55, 5582–5585. https://doi.org/10.1002/anie.201601200

Korhonen, J., Koskivaara, A., Toppinen, A., 2020. Riding a Trojan horse? Future pathways of the fiber-based packaging industry in the bioeconomy. For. Policy Econ., Forest-based circular bioeconomy: matching sustainability challenges and new business opportunities 110, 101799. https://doi.org/10.1016/j.forpol.2018.08.010

Koskinen, S., Kurkela, J., Linhartová, M., Tyystjärvi, T., 2023. The genome sequence of Synechocystis sp. PCC 6803 substrain GT-T and its implications for the evolution of PCC 6803 substrains. FEBS Open Bio 13, 701–712. https://doi.org/10.1002/2211-5463.13576

Kosourov, S., Böhm, M., Senger, M., Berggren, G., Stensjö, K., Mamedov, F., Lindblad, P., Allahverdiyeva, Y., 2021. Photosynthetic hydrogen production: Novel protocols, promising engineering approaches and application of semi-synthetic hydrogenases. Physiol. Plant. 173, 555–567. https://doi.org/10.1111/ppl.13428

Kosourov, S., Nagy, V., Shevela, D., Jokel, M., Messinger, J., Allahverdiyeva, Y., 2020. Water oxidation by photosystem II is the primary source of electrons for sustained H2 photoproduction in nutrient-replete green algae. Proc. Natl. Acad. Sci. U. S. A. 117, 29629–29636. https://doi.org/10.1073/pnas.2009210117

Kosourov, S., Tammelin, T., Allahverdiyeva, Y., 2025. Engineered biocatalytic architecture for enhanced light utilisation in algal H2 production. Energy Environ. Sci. 18, 937–947. https://doi.org/10.1039/D4EE03075C

Kossalbayev, B.D., Tomo, T., Zayadan, B.K., Sadvakasova, A.K., Bolatkhan, K., Alwasel, S., Allakhverdiev, S.I., 2020. Determination of the potential of cyanobacterial strains for hydrogen production. Int. J. Hydrog. Energy 45, 2627–2639. https://doi.org/10.1016/j.ijhydene.2019.11.164

Kozuleva, M., Petrova, A., Milrad, Y., Semenov, A., Ivanov, B., Redding, K.E., Yacoby, I., 2021. Phylloquinone is the principal Mehler reaction site within photosystem I in high light. Plant Physiol. 186, 1848. https://doi.org/10.1093/plphys/kiab221

Kramer, D.M., Avenson, T.J., Edwards, G.E., 2004. Dynamic flexibility in the light reactions of photosynthesis governed by both electron and proton transfer reactions. Trends Plant Sci. 9, 349–357. https://doi.org/10.1016/j.tplants.2004.05.001

Kramer, D.M., Cruz, J.A., Kanazawa, A., 2003. Balancing the central roles of the thylakoid proton gradient. Trends Plant Sci. 8, 27–32. https://doi.org/10.1016/S1360-1385(02)00010-9

Kramer, D.M., Evans, J.R., 2011. The Importance of Energy Balance in Improving Photosynthetic Productivity. Plant Physiol. 155, 70–78. https://doi.org/10.1104/pp.110.166652

Kubota-Kawai, H., Mutoh, R., Shinmura, K., Sétif, P., Nowaczyk, M.M., Rögner, M., Ikegami, T., Tanaka, H., Kurisu, G., 2018. X-ray structure of an asymmetrical trimeric ferredoxin–photosystem I complex. Nat. Plants 4, 218–224. https://doi.org/10.1038/s41477-018-0130-0

Kugler, A., Stensjö, K., 2023. Optimal energy and redox metabolism in the cyanobacterium Synechocystis sp. PCC 6803. Npj Syst. Biol. Appl. 9, 1–13. https://doi.org/10.1038/s41540-023-00307-3

Kurkela, J., Tyystjärvi, T., 2024. Inorganic carbon sensing and signalling in cyanobacteria. Physiol. Plant. 176, e14140. https://doi.org/10.1111/ppl.14140

Lan, X., Tans, P., Thoning, K.W., 2025. Trends in globally-averaged CO2 determined from NOAA Global Monitoring Laboratory measurements. Version Friday, 14-Mar-2025 11:33:44 MDT. https://doi.org/10.15138/9N0H-ZH07

Lassen, L.M., Nielsen, A.Z., Olsen, C.E., Bialek, W., Jensen, K., Møller, B.L., Jensen, P.E., 2014. Anchoring a Plant Cytochrome P450 via PsaM to the Thylakoids in Synechococcus sp. PCC 7002: Evidence for Light-Driven Biosynthesis. PLOS ONE 9, e102184. https://doi.org/10.1371/journal.pone.0102184

Laughlin, T.G., Bayne, A.N., Trempe, J.-F., Savage, D.F., Davies, K.M., 2019. Structure of the complex I-like molecule NDH of oxygenic photosynthesis. Nature 566, 411–414. https://doi.org/10.1038/s41586-019-0921-0

Lea-Smith, D.J., Bombelli, P., Vasudevan, R., Howe, C.J., 2016. Photosynthetic, respiratory and extracellular electron transport pathways in cyanobacteria. Biochim. Biophys. Acta BBA - Bioenerg., Organization and dynamics of bioenergetic systems in bacteria 1857, 247–255. https://doi.org/10.1016/j.bbabio.2015.10.007

Lea-Smith, D.J., Ross, N., Zori, M., Bendall, D.S., Dennis, J.S., Scott, S.A., Smith, A.G., Howe, C.J., 2013. Thylakoid Terminal Oxidases Are Essential for the Cyanobacterium Synechocystis sp. PCC 6803 to Survive Rapidly Changing Light Intensities. Plant Physiol. 162, 484. https://doi.org/10.1104/pp.112.210260

Lee, S., Ryu, J.-Y., Kim, S.Y., Jeon, J.-H., Song, J.Y., Cho, H.-T., Choi, S.-B., Choi, D., Marsac, N.T. de, Park, Y.-I., 2007. Transcriptional Regulation of the Respiratory Genes in the Cyanobacterium Synechocystis sp. PCC 6803 during the Early Response to Glucose Feeding. Plant Physiol. 145, 1018. https://doi.org/10.1104/pp.107.105023

Lettau, E., Lorent, C., Appel, J., Boehm, M., Cordero, P.R.F., Lauterbach, L., 2025. Insights into electron transfer and bifurcation of the *Synechocystis* sp. PCC6803 hydrogenase reductase module. Biochim. Biophys. Acta BBA - Bioenerg. 1866, 149508. https://doi.org/10.1016/j.bbabio.2024.149508

Li, H., Nakajima, Y., Nango, E., Owada, S., Yamada, D., Hashimoto, K., Luo, F., Tanaka, R., Akita, F., Kato, K., Kang, J., Saitoh, Y., Kishi, S., Yu, H., Matsubara, N., Fujii, H., Sugahara, M., Suzuki, M., Masuda, T., Kimura, T., Thao, T.N., Yonekura, S., Yu, L.-J., Tosha, T., Tono, K., Joti, Y., Hatsui, T., Yabashi, M., Kubo, M., Iwata, S., Isobe, H., Yamaguchi, K., Suga, M., Shen, J.-R., 2024. Oxygen-evolving photosystem II structures during S1–S2–S3 transitions. Nature 626, 670–677. https://doi.org/10.1038/s41586-023-06987-5

Li, J., Hamaoka, N., Makino, F., Kawamoto, A., Lin, Y., Rögner, M., Nowaczyk, M.M., Lee, Y.-H., Namba, K., Gerle, C., Kurisu, G., 2022. Structure of cyanobacterial photosystem I complexed with ferredoxin at 1.97 Å resolution. Commun. Biol. 5, 1–13. https://doi.org/10.1038/s42003-022-03926-4

Li, M., Calteau, A., Semchonok, D.A., Witt, T.A., Nguyen, J.T., Sassoon, N., Boekema, E.J., Whitelegge, J., Gugger, M., Bruce, B.D., 2019. Physiological and evolutionary implications of tetrameric photosystem I in cyanobacteria. Nat. Plants 5, 1309–1319. https://doi.org/10.1038/s41477-019-0566-x

Li, M., Semchonok, D.A., Boekema, E.J., Bruce, B.D., 2014. Characterization and Evolution of Tetrameric Photosystem I from the Thermophilic Cyanobacterium Chroococcidiopsis sp TS-821. Plant Cell 26, 1230–1245. https://doi.org/10.1105/tpc.113.120782

Ligrone, R., 2019. The Great Oxygenation Event, in: Ligrone, R. (Ed.), Biological Innovations That Built the World: A Four-Billion-Year Journey through Life and Earth History. Springer International Publishing, Cham, pp. 129–154. https://doi.org/10.1007/978-3-030-16057-9_5

Liguori, N., van Stokkum, I.H.M., Muzzopappa, F., Kennis, J.T.M., Kirilovsky, D., Croce, R., 2024. The Orange Carotenoid Protein Triggers Cyanobacterial Photoprotection by Quenching Bilins via a Structural Switch of Its Carotenoid. J. Am. Chem. Soc. 146, 21913–21921. https://doi.org/10.1021/jacs.4c06695

Liu, X., Xie, H., Roussou, S., Lindblad, P., 2022. Current advances in engineering cyanobacteria and their applications for photosynthetic butanol production. Curr. Opin. Biotechnol. 73, 143–150. https://doi.org/10.1016/j.copbio.2021.07.014

Lo, C., Wijffels, R.H., Boboescu, I., Kazbar, A., Eppink, M.H.M., 2023. Multimethod and multiproduct microalgae biorefineries: Industrial scale feasibility: Eutectic solvents as a novel extraction system for microalgae biorefinery, in: Microalgae-Based Systems: Process Integration and Process Intensification Approaches. pp. 67–80. https://doi.org/10.1515/9783110781267-005

Lo, C., Wijffels, R.H., Eppink, M.H.M., 2024. Lipid recovery from deep eutectic solvents by polar antisolvents. Food Bioprod. Process. 143, 21–27. https://doi.org/10.1016/j.fbp.2023.10.003

Lonardi, G., Parolin, R., Licini, G., Orlandi, M., 2023. Catalytic Asymmetric Conjugate Reduction. Angew. Chem. Int. Ed. 62, e202216649. https://doi.org/10.1002/anie.202216649

Lucius, S., Hagemann, M., 2024. The primary carbon metabolism in cyanobacteria and its regulation. Front. Plant Sci. 15. https://doi.org/10.3389/fpls.2024.1417680

Lucius, S., Theune, M., Arrivault, S., Hildebrandt, S., Mullineaux, C.W., Gutekunst, K., Hagemann, M., 2022. CP12 fine-tunes the Calvin-Benson cycle and carbohydrate metabolism in cyanobacteria. Front. Plant Sci. 13. https://doi.org/10.3389/fpls.2022.1028794

Luimstra, V.M., Schuurmans, J.M., Hellingwerf, K.J., Matthijs, H.C.P., Huisman, J., 2020. Blue light induces major changes in the gene expression profile of the cyanobacterium Synechocystis sp. PCC 6803. Physiol. Plant. 170, 10. https://doi.org/10.1111/ppl.13086

Lupacchini, S., Appel, J., Stauder, R., Bolay, P., Klähn, S., Lettau, E., Adrian, L., Lauterbach, L., Bühler, B., Schmid, A., Toepel, J., 2021. Rewiring cyanobacterial photosynthesis by the implementation of an oxygen-tolerant hydrogenase. Metab. Eng. 68, 199–209. https://doi.org/10.1016/j.ymben.2021.10.006

Mackinder, L.C.M., 2018. The Chlamydomonas CO2-concentrating mechanism and its potential for engineering photosynthesis in plants. New Phytol. 217, 54–61. https://doi.org/10.1111/nph.14749

Madavi, T.B., Chauhan, S., Keshri, A., Alavilli, H., Choi, K.-Y., Pamidimarri, S.D.V.N., 2022. Whole-cell biocatalysis: Advancements toward the biosynthesis of fuels. Biofuels Bioprod. Biorefining 16, 859–876. https://doi.org/10.1002/bbb.2331

Magnuson, A., Cardona, T., 2016. Thylakoid membrane function in heterocysts. Biochim. Biophys. Acta BBA - Bioenerg., Organization and dynamics of bioenergetic systems in bacteria 1857, 309–319. https://doi.org/10.1016/j.bbabio.2015.10.016

Majhi, B.K., 2024. Cyanobacteria: Photosynthetic cell factories for biofuel production. J. Bioresour. Bioprod. https://doi.org/10.1016/j.jobab.2024.10.001

Makowka, A., Nichelmann, L., Schulze, D., Spengler, K., Wittmann, C., Forchhammer, K., Gutekunst, K., 2020. Glycolytic Shunts Replenish the Calvin–Benson–Bassham Cycle as Anaplerotic Reactions in Cyanobacteria. Mol. Plant, Photobiology 13, 471–482. https://doi.org/10.1016/j.molp.2020.02.002

Malavath, T., Caspy, I., Netzer-El, S.Y., Klaiman, D., Nelson, N., 2018. Structure and function of wild-type and subunit-depleted photosystem I in *Synechocystis*. Biochim. Biophys. Acta BBA - Bioenerg., 20th European Bioenergetics Conference 1859, 645–654. https://doi.org/10.1016/j.bbabio.2018.02.002

Malihan-Yap, L., Liang, Q., Valotta, A., Alphand, V., Gruber-Woelfler, H., Kourist, R., 2025. Light-Driven Photobiocatalytic Oxyfunctionalization in a Continuous Reactor System without External Oxygen Supply. ACS Sustain. Chem. Eng. 13, 3939–3950. https://doi.org/10.1021/acssuschemeng.4c08560

Malito, E., Alfieri, A., Fraaije, M.W., Mattevi, A., 2004. Crystal structure of a Baeyer–Villiger monooxygenase. Proc. Natl. Acad. Sci. 101, 13157–13162. https://doi.org/10.1073/pnas.0404538101

Mallén-Ponce, M.J., Huertas, M.J., Florencio, F.J., 2022. Exploring the Diversity of the Thioredoxin Systems in Cyanobacteria. Antioxidants 11, 654. https://doi.org/10.3390/antiox11040654

Malone, L.A., Proctor, M.S., Hitchcock, A., Hunter, C.N., Johnson, M.P., 2021. Cytochrome *b6f* – Orchestrator of photosynthetic electron transfer. Biochim. Biophys. Acta BBA - Bioenerg. 1862, 148380. https://doi.org/10.1016/j.bbabio.2021.148380

Mangan, N.M., Flamholz, A., Hood, R.D., Milo, R., Savage, D.F., 2016. pH determines the energetic efficiency of the cyanobacterial CO2 concentrating mechanism. Proc. Natl. Acad. Sci. U. S. A. 113, E5354. https://doi.org/10.1073/pnas.1525145113

Mascia, F., Pereira, S.B., Pacheco, C.C., Oliveira, P., Solarczek, J., Schallmey, A., Kourist, R., Alphand, V., Tamagnini, P., 2022. Light-driven hydroxylation of testosterone by Synechocystis sp. PCC 6803 expressing the heterologous CYP450 monooxygenase CYP110D1. Green Chem. 24, 6156–6167. https://doi.org/10.1039/D1GC04714K

Matson, M.M., Atsumi, S., 2018. Photomixotrophic chemical production in cyanobacteria. Curr. Opin. Biotechnol., Energy biotechnology • Environmental biotechnology 50, 65–71. https://doi.org/10.1016/j.copbio.2017.11.008

McFadden, G.I., 2001. Primary and Secondary Endosymbiosis and the Origin of Plastids. J. Phycol. 37, 951–959. https://doi.org/10.1046/j.1529-8817.2001.01126.x

Meah, Y., Massey, V., 2000. Old Yellow Enzyme: Stepwise reduction of nitro-olefins and catalysis of aci-nitro tautomerization. Proc. Natl. Acad. Sci. U. S. A. 97, 10733. https://doi.org/10.1073/pnas.190345597

Medipally, H., Mann, M., Kötting, C., van Berkel, W.J.H., Nowaczyk, M.M., 2023. A Clickable Photosystem I, Ferredoxin, and Ferredoxin NADP+ Reductase Fusion System for Light-Driven NADPH Regeneration. ChemBioChem 24, e202300025. https://doi.org/10.1002/cbic.202300025

Mehler, A.H., 1951. Studies on reactions of illuminated chloroplasts: I. Mechanism of the reduction of oxygen and other hill reagents. Arch. Biochem. Biophys. 33, 65–77. https://doi.org/10.1016/0003-9861(51)90082-3

Mellor, S.B., Nielsen, A.Z., Burow, M., Motawia, M.S., Jakubauskas, D., Møller, B.L., Jensen, P.E., 2016. Fusion of Ferredoxin and Cytochrome P450 Enables Direct Light-Driven Biosynthesis. ACS Chem. Biol. 11, 1862–1869. https://doi.org/10.1021/acschembio.6b00190

Miller, N.T., Ajlani, G., Burnap, R.L., 2022. Cyclic Electron Flow-Coupled Proton Pumping in Synechocystis sp. PCC6803 Is Dependent upon NADPH Oxidation by the Soluble Isoform of Ferredoxin:NADP-Oxidoreductase. Microorganisms 10, 855. https://doi.org/10.3390/microorganisms10050855

Miller, N.T., Vaughn, M.D., Burnap, R.L., 2021. Electron flow through NDH-1 complexes is the major driver of cyclic electron flow-dependent proton pumping in cyanobacteria. Biochim. Biophys. Acta BBA - Bioenerg. 1862, 148354. https://doi.org/10.1016/j.bbabio.2020.148354

Moroney, J.V., Jungnick, N., DiMario, R.J., Longstreth, D.J., 2013. Photorespiration and carbon concentrating mechanisms: two adaptations to high O2, low CO2 conditions. Photosynth. Res. 117, 121–131. https://doi.org/10.1007/s11120-013-9865-7

Mulgrew-Nesbitt, A., Diraviyam, K., Wang, J., Singh, S., Murray, P., Li, Z., Rogers, L., Mirkovic, N., Murray, D., 2006. The role of electrostatics in protein–membrane interactions. Biochim. Biophys. Acta BBA - Mol. Cell Biol. Lipids, Lipid-Binding Domains 1761, 812–826. https://doi.org/10.1016/j.bbalip.2006.07.002

Mullineaux, C.W., 2014. Co-existence of photosynthetic and respiratory activities in cyanobacterial thylakoid membranes. Biochim. Biophys. Acta BBA - Bioenerg., Dynamic and ultrastructure of bioenergetic membranes and their components 1837, 503–511. https://doi.org/10.1016/j.bbabio.2013.11.017

Muscat, A., De Olde, E.M., Ripoll-Bosch, R., Van Zanten, H.H.E., Metze, T.A.P., Termeer, C.J.A.M., Van Ittersum, M.K., De Boer, I.J.M., 2021. Principles, drivers and opportunities of a circular bioeconomy. Nat. Food 2, 561–566. https://doi.org/10.1038/s43016-021-00340-7

Mustila, H., Allahverdiyeva, Y., Isojärvi, J., Aro, E.M., Eisenhut, M., 2014. The bacterial-type [4Fe–4S] ferredoxin 7 has a regulatory function under photooxidative stress conditions in the cyanobacterium *Synechocystis* sp. PCC 6803. Biochim. Biophys. Acta BBA - Bioenerg. 1837, 1293–1304. https://doi.org/10.1016/j.bbabio.2014.04.006

Mustila, H., Paananen, P., Battchikova, N., Santana-Sánchez, A., Muth-Pawlak, D., Hagemann, M., Aro, E.-M., Allahverdiyeva, Y., 2016. The Flavodiiron Protein Flv3 Functions as a Homo-Oligomer During Stress Acclimation and is Distinct from the Flv1/Flv3 Hetero-Oligomer Specific to the O 2 Photoreduction Pathway. Plant Cell Physiol. 57, 1468–1483. https://doi.org/10.1093/pcp/pcw047

Muth-Pawlak, D., Kreula, S., Gollan, P.J., Huokko, T., Allahverdiyeva, Y., Aro, E.-M., 2022. Patterning of the Autotrophic, Mixotrophic, and Heterotrophic Proteomes of Oxygen-Evolving Cyanobacterium Synechocystis sp. PCC 6803. Front. Microbiol. 13, 891895. https://doi.org/10.3389/fmicb.2022.891895

Nakajima, T., Kajihata, S., Yoshikawa, K., Matsuda, F., Furusawa, C., Hirasawa, T., Shimizu, H., 2014. Integrated Metabolic Flux and Omics Analysis of Synechocystis sp. PCC 6803 under Mixotrophic and Photoheterotrophic Conditions. Plant Cell Physiol. 55, 1605–1612. https://doi.org/10.1093/pcp/pcu091

Nakamura, K., Yamanaka, R., 2002. Light mediated cofactor recycling system in biocatalytic asymmetric reduction of ketone. Chem. Commun. 1782–1783. https://doi.org/10.1039/B203844G

Navarro, F., Martín-Figueroa, E., Candau, P., Florencio, F.J., 2000. Ferredoxin-Dependent Iron–Sulfur Flavoprotein Glutamate Synthase (GlsF) from the Cyanobacterium Synechocystis sp. PCC 6803: Expression and Assembly in Escherichia coli. Arch. Biochem. Biophys. 379, 267–276. https://doi.org/10.1006/abbi.2000.1894

Nelson, D.R., 2018. Cytochrome P450 diversity in the tree of life. Biochim. Biophys. Acta BBA - Proteins Proteomics, Cytochrome P450 biodiversity and biotechnology 1866, 141–154. https://doi.org/10.1016/j.bbapap.2017.05.003

Nickelsen, J., Rengstl, B., 2013. Photosystem II Assembly: From Cyanobacteria to Plants. Annu. Rev. Plant Biol. 64, 609–635. https://doi.org/10.1146/annurev-arplant-050312-120124

Niederholtmeyer, H., Wolfstädter, B.T., Savage, D.F., Silver, P.A., Way, J.C., 2010. Engineering Cyanobacteria To Synthesize and Export Hydrophilic Products. Appl. Environ. Microbiol. 76, 3462. https://doi.org/10.1128/AEM.00202-10

Niino, Y.S., Chakraborty, S., Brown, B.J., Massey, V., 1995. A New Old Yellow Enzyme of *Saccharomyces cerevisiae*(∗). J. Biol. Chem. 270, 1983–1991. https://doi.org/10.1074/jbc.270.5.1983

Nikkanen, L., Santana Sánchez, A., Ermakova, M., Rögner, M., Cournac, L., Allahverdiyeva, Y., 2020. Functional redundancy between flavodiiron proteins and NDH-1 in *Synechocystis* sp. PCC 6803. Plant J. 103, 1460–1476. https://doi.org/10.1111/tpj.14812

Nikkanen, L., Solymosi, D., Jokel, M., Allahverdiyeva, Y., 2021. Regulatory electron transport pathways of photosynthesis in cyanobacteria and microalgae: Recent advances and biotechnological prospects. Physiol. Plant. 173, 514–525. https://doi.org/10.1111/ppl.13404

Nilsson, A., Shabestary, K., Brandão, M., Hudson, E.P., 2020. Environmental impacts and limitations of third-generation biobutanol: Life cycle assessment of n-butanol produced by genetically engineered cyanobacteria. J. Ind. Ecol. 24, 205–216. https://doi.org/10.1111/jiec.12843

Nobre, G.C., Tavares, E., 2021. The quest for a circular economy final definition: A scientific perspective. J. Clean. Prod. 314, 127973. https://doi.org/10.1016/j.jclepro.2021.127973

Noreña-Caro, D., Benton, M.G., 2018. Cyanobacteria as photoautotrophic biofactories of high-value chemicals. J. CO2 Util. 28, 335–366. https://doi.org/10.1016/j.jcou.2018.10.008

Olejarz, J., Iwasa, Y., Knoll, A.H., Nowak, M.A., 2021. The Great Oxygenation Event as a consequence of ecological dynamics modulated by planetary change. Nat. Commun. 12, 3985. https://doi.org/10.1038/s41467-021-23286-7

Oliver, J.W.K., Atsumi, S., 2015. A carbon sink pathway increases carbon productivity in cyanobacteria. Metab. Eng. 29, 106–112. https://doi.org/10.1016/j.ymben.2015.03.006

Origin, 2024.

Origin, 2016.

Ortega-Martínez, P., Nikkanen, L., Wey, L.T., Florencio, F.J., Allahverdiyeva, Y., Díaz-Troya, S., 2024. Glycogen synthesis prevents metabolic imbalance and disruption of photosynthetic electron transport from photosystem II during transition to photomixotrophy in Synechocystis sp. PCC 6803. New Phytol. 243, 162–179. https://doi.org/10.1111/nph.19793

Ossa Ossa, F., Spangenberg, J.E., Bekker, A., König, S., Stüeken, E.E., Hofmann, A., Poulton, S.W., Yierpan, A., Varas-Reus, M.I., Eickmann, B., Andersen, M.B., Schoenberg, R., 2022. Moderate levels of oxygenation during the late stage of Earth's Great Oxidation Event. Earth Planet. Sci. Lett. 594, 117716. https://doi.org/10.1016/j.epsl.2022.117716

Pan, X., Cao, D., Xie, F., Xu, F., Su, X., Mi, H., Zhang, X., Li, M., 2020. Structural basis for electron transport mechanism of complex I-like photosynthetic NAD(P)H dehydrogenase. Nat. Commun. 11, 610. https://doi.org/10.1038/s41467-020-14456-0

Passow, U., Carlson, C.A., 2012. The biological pump in a high CO2 world. Mar. Ecol. Prog. Ser. 470, 249–271. https://doi.org/10.3354/meps09985

Patel, A.K., Singhania, R.R., Sim, S.J., Dong, C.D., 2021. Recent advancements in mixotrophic bioprocessing for production of high value microalgal products. Bioresour. Technol. 320, 124421. https://doi.org/10.1016/j.biortech.2020.124421

Peltier, G., Aro, E.-M., Shikanai, T., 2016. NDH-1 and NDH-2 Plastoquinone Reductases in Oxygenic Photosynthesis. Annu. Rev. Plant Biol. 67, 55–80. https://doi.org/10.1146/annurev-arplant-043014-114752

Pesic, M., Fernández-Fueyo, E., Hollmann, F., 2017. Characterization of the Old Yellow Enzyme Homolog from Bacillus subtilis (YqjM). ChemistrySelect 2, 3866–3871. https://doi.org/10.1002/slct.201700724

Pogoryelov, D., Reichen, C., Klyszejko, A.L., Brunisholz, R., Muller, D.J., Dimroth, P., Meier, T., 2007. The Oligomeric State of c Rings from Cyanobacterial F-ATP Synthases Varies from 13 to 15. J. Bacteriol. 189, 5895–5902. https://doi.org/10.1128/jb.00581-07

Porto, R.S., Porto, V.A., 2023. Morita–Baylis–Hillman Adducts and Their Derivatives: A Patent-Based Exploration of Diverse Biological Activities. Pharm. Pat. Anal. 12, 127–141. https://doi.org/10.4155/ppa-2023-0021

Price, G.D., 2011. Inorganic carbon transporters of the cyanobacterial CO2 concentrating mechanism. Photosynth. Res. 109, 47–57. https://doi.org/10.1007/s11120-010-9608-y

R Core Team, 2020. R: A language and environment for statistical computing.

Ranade, S., Zhang, Y., Kaplan, M., Majeed, W., He, Q., 2015. Metabolic Engineering and Comparative Performance Studies of Synechocystis sp. PCC 6803 Strains for Effective Utilization of Xylose. Front. Microbiol. 6. https://doi.org/10.3389/fmicb.2015.01484

Redding, K.E., Appel, J., Boehm, M., Schuhmann, W., Nowaczyk, M.M., Yacoby, I., Gutekunst, K., 2022. Advances and challenges in photosynthetic hydrogen production. Trends Biotechnol. 40, 1313–1325. https://doi.org/10.1016/j.tibtech.2022.04.007

Reimer, A., Wedde, S., Staudt, S., Schmidt, S., Höffer, D., Hummel, W., Kragl, U., Bornscheuer, U.T., Gröger, H., 2017. Process Development through Solvent Engineering in the Biocatalytic Synthesis of the Heterocyclic Bulk Chemical ε-Caprolactone. J. Heterocycl. Chem. 54, 391–396. https://doi.org/10.1002/jhet.2595

Rexroth, S., Nowaczyk, M.M., Rögner, M., 2017. Cyanobacterial Photosynthesis: The Light Reactions, in: Hallenbeck, P.C. (Ed.), Modern Topics in the Phototrophic Prokaryotes: Metabolism, Bioenergetics, and Omics. Springer International Publishing, Cham, pp. 163–191. https://doi.org/10.1007/978-3-319-51365-2_5

Richardson, K., Steffen, W., Lucht, W., Bendtsen, J., Cornell, S.E., Donges, J.F., Drüke, M., Fetzer, I., Bala, G., von Bloh, W., Feulner, G., Fiedler, S., Gerten, D., Gleeson, T., Hofmann, M., Huiskamp, W., Kummu, M., Mohan, C., Nogués-Bravo, D., Petri, S., Porkka, M., Rahmstorf, S., Schaphoff, S., Thonicke, K., Tobian, A., Virkki, V., Wang-Erlandsson, L., Weber, L., Rockström, J., 2023. Earth beyond six of nine planetary boundaries. Sci. Adv. 9, eadh2458. https://doi.org/10.1126/sciadv.adh2458

Rippka, R., 1972. Photoheterotrophy and chemoheterotrophy among unicellular blue-green algae. Arch. Für Mikrobiol. 87, 93–98. https://doi.org/10.1007/BF00424781

Rippka, R., Deruelles, J., Waterbury, J.B., Herdman, M., Stanier, R.Y., 1979. Generic Assignments, Strain Histories and Properties of Pure Cultures of Cyanobacteria. Microbiology 111, 1–61. https://doi.org/10.1099/00221287-111-1-1

Robescu, M.S., Cendron, L., Bacchin, A., Wagner, K., Reiter, T., Janicki, I., Merusic, K., Illek, M., Aleotti, M., Bergantino, E., Hall, M., 2022. Asymmetric Proton Transfer Catalysis by

Stereocomplementary Old Yellow Enzymes for C═C Bond Isomerization Reaction. ACS Catal. 12, 7396–7405. https://doi.org/10.1021/acscatal.2c01110

Robescu, M.S., Niero, M., Hall, M., Cendron, L., Bergantino, E., 2020. Two new ene-reductases from photosynthetic extremophiles enlarge the panel of old yellow enzymes: CtOYE and GsOYE. Appl. Microbiol. Biotechnol. 104, 2051–2066. https://doi.org/10.1007/s00253-019-10287-2

Rockström, J., Steffen, W., Noone, K., Persson, Å., Chapin, F.S., Lambin, E.F., Lenton, T.M., Scheffer, M., Folke, C., Schellnhuber, H.J., Nykvist, B., de Wit, C.A., Hughes, T., van der Leeuw, S., Rodhe, H., Sörlin, S., Snyder, P.K., Costanza, R., Svedin, U., Falkenmark, M., Karlberg, L., Corell, R.W., Fabry, V.J., Hansen, J., Walker, B., Liverman, D., Richardson, K., Crutzen, P., Foley, J.A., 2009. A safe operating space for humanity. Nature 461, 472–475. https://doi.org/10.1038/461472a

Rodrigues, J.S., Lindberg, P., 2021a. Engineering Cyanobacteria as Host Organisms for Production of Terpenes and Terpenoids, in: Cyanobacteria Biotechnology. John Wiley & Sons, Ltd, pp. 267–300. https://doi.org/10.1002/9783527824908.ch9

Rodrigues, J.S., Lindberg, P., 2021b. Metabolic engineering of *Synechocystis* sp. PCC 6803 for improved bisabolene production. Metab. Eng. Commun. 12, e00159. https://doi.org/10.1016/j.mec.2020.e00159

Roussou, S., Pan, M., Krömer, J., Lindblad, P., 2025. Exploring and increased acetate biosynthesis in Synechocystis PCC 6803 through insertion of a heterologous phosphoketolase and overexpressing phosphotransacetylase. Metab. Eng. S1096717625000084. https://doi.org/10.1016/j.ymben.2025.01.008

Salazar, J., Santana-Sánchez, A., Näkkilä, J., Sirin, S., Allahverdiyeva, Y., 2023. Complete N and P removal from hydroponic greenhouse wastewater by *Tetradesmus obliquus*: A strategy for algal bioremediation and cultivation in Nordic countries. Algal Res. 70, 102988. https://doi.org/10.1016/j.algal.2023.102988

Santana-Sánchez, A., Nikkanen, L., Werner, E., Tóth, G., Ermakova, M., Kosourov, S., Walter, J., He, M., Aro, E.-M., Allahverdiyeva, Y., 2023. Flv3A facilitates O2 photoreduction and affects H2 photoproduction independently of Flv1A in diazotrophic Anabaena filaments. New Phytol. 237, 126–139. https://doi.org/10.1111/nph.18506

Santana-Sanchez, A., Solymosi, D., Mustila, H., Bersanini, L., Aro, E.-M., Allahverdiyeva, Y., 2019. Flavodiiron proteins 1–to-4 function in versatile combinations in O2 photoreduction in cyanobacteria. eLife 8, e45766. https://doi.org/10.7554/eLife.45766

Santos-Merino, M., Torrado, A., Davis, G.A., Röttig, A., Bibby, T.S., Kramer, D.M., Ducat, D.C., 2021. Improved photosynthetic capacity and photosystem I oxidation via heterologous metabolism engineering in cyanobacteria. Proc. Natl. Acad. Sci. 118, e2021523118. https://doi.org/10.1073/pnas.2021523118

Santos-Merino, M., Yun, L., Ducat, D.C., 2023. Cyanobacteria as cell factories for the photosynthetic production of sucrose. Front. Microbiol. 14, 1126032. https://doi.org/10.3389/fmicb.2023.1126032

Schirrmeister, B.E., Gugger, M., Donoghue, P.C.J., 2015. Cyanobacteria and the Great Oxidation Event: evidence from genes and fossils. Palaeontology 58, 769–785. https://doi.org/10.1111/pala.12178

Schmermund, L., Jurkaš, V., Özgen, F.F., Barone, G.D., Büchsenschütz, H.C., Winkler, C.K., Schmidt, S., Kourist, R., Kroutil, W., 2019. Photo-Biocatalysis: Biotransformations in the Presence of Light. ACS Catal. 9, 4115–4144. https://doi.org/10.1021/acscatal.9b00656

Schorsch, M., Kramer, M., Goss, T., Eisenhut, M., Robinson, N., Osman, D., Wilde, A., Sadaf, S., Brückler, H., Walder, L., Scheibe, R., Hase, T., Hanke, G.T., 2018. A unique ferredoxin acts as a player in the low-iron response of photosynthetic organisms. Proc. Natl. Acad. Sci. U. S. A. 115, E12111–E12120. https://doi.org/10.1073/pnas.1810379115

Schreiber, U., Klughammer, C., 2009. New NADPH/9-AA module for the DUAL-PAM-100: Description, operation and examples of application.

Schuller, J.M., Birrell, J.A., Tanaka, H., Konuma, T., Wulfhorst, H., Cox, N., Schuller, S.K., Thiemann, J., Lubitz, W., Sétif, P., Ikegami, T., Engel, B.D., Kurisu, G., Nowaczyk, M.M., 2019. Structural adaptations of photosynthetic complex I enable ferredoxin-dependent electron transfer. Science 363, 257–260. https://doi.org/10.1126/science.aau3613

Schuller, J.M., Saura, P., Thiemann, J., Schuller, S.K., Gamiz-Hernandez, A.P., Kurisu, G., Nowaczyk, M.M., Kaila, V.R.I., 2020. Redox-coupled proton pumping drives carbon concentration in the photosynthetic complex I. Nat. Commun. 11, 494. https://doi.org/10.1038/s41467-020-14347-4

Schulze, D., Kohlstedt, M., Becker, J., Cahoreau, E., Peyriga, L., Makowka, A., Hildebrandt, S., Gutekunst, K., Portais, J.-C., Wittmann, C., 2022. GC/MS-based 13C metabolic flux analysis resolves the parallel and cyclic photomixotrophic metabolism of Synechocystis sp. PCC 6803 and selected deletion mutants including the Entner-Doudoroff and phosphoketolase pathways. Microb. Cell Factories 21, 69. https://doi.org/10.1186/s12934-022-01790-9

Sétif, P., Boussac, A., Krieger-Liszkay, A., 2019. Near-infrared in vitro measurements of photosystem I cofactors and electron-transfer partners with a recently developed spectrophotometer. Photosynth. Res. 142, 307–319. https://doi.org/10.1007/s11120-019-00665-2

Sétif, P., Shimakawa, G., Krieger-Liszkay, A., Miyake, C., 2020. Identification of the electron donor to flavodiiron proteins in Synechocystis sp. PCC 6803 by in vivo spectroscopy. Biochim. Biophys. Acta BBA - Bioenerg. 1861, 148256. https://doi.org/10.1016/j.bbabio.2020.148256

Sever, R.R., Root, T.W., 2003. Computational Study of Tin-Catalyzed Baeyer−Villiger Reaction Pathways Using Hydrogen Peroxide as Oxidant. J. Phys. Chem. B 107, 10848–10862. https://doi.org/10.1021/jp034332c

Shimakawa, G., Shaku, K., Nishi, A., Hayashi, R., Yamamoto, H., Sakamoto, K., Makino, A., Miyake, C., 2015. FLAVODIIRON2 and FLAVODIIRON4 Proteins Mediate an Oxygen-Dependent Alternative Electron Flow in Synechocystis sp. PCC 6803 under CO2-Limited Conditions. Plant Physiol. 167, 472–480. https://doi.org/10.1104/pp.114.249987

Siitonen, V., Probst, A., Tóth, G., Kourist, R., Schroda, M., Kosourov, S., Allahverdiyeva, Y., 2023. Engineered green alga Chlamydomonas reinhardtii as a whole-cell photosynthetic biocatalyst for stepwise photoproduction of H 2 and ε-caprolactone. Green Chem. 25, 5945–5955. https://doi.org/10.1039/D3GC01400B

Singh, A.K., Santos-Merino, M., Sakkos, J.K., Walker, B.J., Ducat, D.C., 2022. Rubisco regulation in response to altered carbon status in the cyanobacterium Synechococcus elongatus PCC 7942. Plant Physiol. 189, 874–888. https://doi.org/10.1093/plphys/kiac065

Smith, E.N., van Aalst, M., Tosens, T., Niinemets, Ü., Stich, B., Morosinotto, T., Alboresi, A., Erb, T.J., Gómez-Coronado, P.A., Tolleter, D., Finazzi, G., Curien, G., Heinemann, M., Ebenhöh, O., Hibberd, J.M., Schlüter, U., Sun, T., Weber, A.P.M., 2023. Improving photosynthetic efficiency toward food security: Strategies, advances, and perspectives. Mol. Plant, Special Issue on Climate Change and Food Security: Plant Science Roles 16, 1547–1563. https://doi.org/10.1016/j.molp.2023.08.017

Solymosi, D., Nikkanen, L., Muth-Pawlak, D., Fitzpatrick, D., Vasudevan, R., Howe, C.J., Lea-Smith, D.J., Allahverdiyeva, Y., 2020. Cytochrome cM Decreases Photosynthesis under Photomixotrophy in Synechocystis sp. PCC 68031 [CC-BY]. Plant Physiol. 183, 700–716. https://doi.org/10.1104/pp.20.00284

Spasic, J., Oliveira, P., Pacheco, C., Kourist, R., Tamagnini, P., 2022. Engineering cyanobacterial chassis for improved electron supply toward a heterologous ene-reductase. J. Biotechnol. 360, 152–159. https://doi.org/10.1016/j.jbiotec.2022.11.005

Stanier, R.Y., Kunisawa, R., Mandel, M., Cohen-Bazire, G., 1971. Purification and properties of unicellular blue-green algae (order Chroococcales). Bacteriol. Rev. 35, 171. https://doi.org/10.1128/br.35.2.171-205.1971

Stauffer, W., Sheng, H., Lim, H.N., 2018. EzColocalization: An ImageJ plugin for visualizing and measuring colocalization in cells and organisms. Sci. Rep. 8, 15764. https://doi.org/10.1038/s41598-018-33592-8

Stebegg, R., Schmetterer, G., Rompel, A., 2023. Heterotrophy among Cyanobacteria. ACS Omega 8, 33098–33114. https://doi.org/10.1021/acsomega.3c02205

Stensjö, K., Vavitsas, K., Tyystjärvi, T., 2018. Harnessing transcription for bioproduction in cyanobacteria. Physiol. Plant. 162, 148–155. https://doi.org/10.1111/ppl.12606

Stiles, W.A.V., Styles, D., Chapman, S.P., Esteves, S., Bywater, A., Melville, L., Silkina, A., Lupatsch, I., Fuentes Grünewald, C., Lovitt, R., Chaloner, T., Bull, A., Morris, C., Llewellyn, C.A., 2018. Using microalgae in the circular economy to valorise anaerobic digestate: challenges and opportunities. Bioresour. Technol. 267, 732–742. https://doi.org/10.1016/j.biortech.2018.07.100

Storti, M., Puggioni, M.P., Segalla, A., Morosinotto, T., Alboresi, A., 2020. The chloroplast NADH dehydrogenase-like complex influences the photosynthetic activity of the moss Physcomitrella patens. J. Exp. Bot. 71, 5538–5548. https://doi.org/10.1093/jxb/eraa274

Strand, D.D., Fisher, N., Kramer, D.M., 2017. The higher plant plastid NAD(P)H dehydrogenase-like complex (NDH) is a high efficiency proton pump that increases ATP production by cyclic electron flow. J. Biol. Chem. 292, 11850–11860. https://doi.org/10.1074/jbc.M116.770792

Sun, J., Xu, W., Hervás, M., Navarro, J.A., Rosa, M.A.D.L., Chitnis, P.R., 1999. Oxidizing Side of the Cyanobacterial Photosystem I: EVIDENCE FOR INTERACTION BETWEEN THE ELECTRON DONOR PROTEINS AND A LUMINAL SURFACE HELIX OF THE PsaB SUBUNIT*. J. Biol. Chem. 274, 19048–19054. https://doi.org/10.1074/jbc.274.27.19048

Sutardja, L., Mellor, S.B., Dodge, N., Matthes, A., Burow, M., Nielsen, A.Z., Jensen, P.E., 2024. Expression of Redox Partner Fusions for Light Driven Cytochrome P450s in the Cyanobacterium Synechocystis sp. PCC. 6803. Synth. Biol. Eng. 2, 10008. https://doi.org/10.35534/sbe.2024.10008

Sweetman, A.K., Smith, A.J., de Jonge, D.S.W., Hahn, T., Schroedl, P., Silverstein, M., Andrade, C., Edwards, R.L., Lough, A.J.M., Woulds, C., Homoky, W.B., Koschinsky, A., Fuchs, S., Kuhn, T., Geiger, F., Marlow, J.J., 2024. Evidence of dark oxygen production at the abyssal seafloor. Nat. Geosci. 17, 737–739. https://doi.org/10.1038/s41561-024-01480-8

Takahashi, H., Uchimiya, H., Hihara, Y., 2008. Difference in metabolite levels between photoautotrophic and photomixotrophic cultures of Synechocystis sp. PCC 6803 examined by capillary electrophoresis electrospray ionization mass spectrometry. J. Exp. Bot. 59, 3009. https://doi.org/10.1093/jxb/ern157

Takahashi, T., Inoue-Kashino, N., Ozawa, S., Takahashi, Y., Kashino, Y., Satoh, K., 2009. Photosystem II Complex in Vivo Is a Monomer *. J. Biol. Chem. 284, 15598–15606. https://doi.org/10.1074/jbc.M109.000372

Talukder, P., Sinha, B., Biswas, S., Ghosh, A., Banerjee, A., Paul, S., 2024. A study on the prospect of converting C3 plants into C4 plants. Biocatal. Agric. Biotechnol. 58, 103191. https://doi.org/10.1016/j.bcab.2024.103191

Tanaka, K., Shimakawa, G., Tabata, H., Kusama, S., Miyake, C., Nakanishi, S., 2021. Quantification of NAD(P)H in cyanobacterial cells by a phenol extraction method. Photosynth. Res. 148, 57. https://doi.org/10.1007/s11120-021-00835-1

Teuber, M., Rögner, M., Berry, S., 2001. Fluorescent probes for non-invasive bioenergetic studies of whole cyanobacterial cells. Biochim. Biophys. Acta BBA - Bioenerg. 1506, 31–46. https://doi.org/10.1016/S0005-2728(01)00178-5

Theune, M.L., Hildebrandt, S., Steffen-Heins, A., Bilger, W., Gutekunst, K., Appel, J., 2021. In-vivo quantification of electron flow through photosystem I – Cyclic electron transport makes up about 35% in a cyanobacterium. Biochim. Biophys. Acta BBA - Bioenerg. 1862, 148353. https://doi.org/10.1016/j.bbabio.2020.148353

Thiel, K., Mulaku, E., Dandapani, H., Nagy, C., Aro, E.-M., Kallio, P., 2018. Translation efficiency of heterologous proteins is significantly affected by the genetic context of RBS sequences in engineered cyanobacterium Synechocystis sp. PCC 6803. Microb. Cell Factories 17, 34. https://doi.org/10.1186/s12934-018-0882-2

Thomas, J.-C., Ughy, B., Lagoutte, B., Ajlani, G., 2006. A second isoform of the ferredoxin:NADP oxidoreductase generated by an in-frame initiation of translation. Proc. Natl. Acad. Sci. U. S. A. 103, 18368. https://doi.org/10.1073/pnas.0607718103

Toogood, H.S., Scrutton, N.S., 2014. New developments in 'ene'-reductase catalysed biological hydrogenations. Curr. Opin. Chem. Biol. 19, 107–115. https://doi.org/10.1016/j.cbpa.2014.01.019

Torrado, A., Connabeer, H.M., Röttig, A., Pratt, N., Baylay, A.J., Terry, M.J., Moore, C.M., Bibby, T.S., 2022. Directing cyanobacterial photosynthesis in a cytochrome c oxidase mutant using a heterologous electron sink. Plant Physiol. 189, 2554–2566. https://doi.org/10.1093/plphys/kiac203

Tóth, G.S., Backman, O., Siivola, T., Xu, W., Kosourov, S., Siitonen, V., Xu, C., Allahverdiyeva, Y., 2024. Employing photocurable biopolymers to engineer photosynthetic 3D-printed living materials for production of chemicals. Green Chem. 26, 4032–4042. https://doi.org/10.1039/D3GC04264B

Transforming our world: the 2030 Agenda for Sustainable Development, 2015. , A/RES/70/1.

Tüllinghoff, A., Djaya-Mbissam, H., Toepel, J., Bühler, B., 2023. Light-driven redox biocatalysis on gram-scale in Synechocystis sp. PCC 6803 via an in vivo cascade. Plant Biotechnol. J. 21, 2074–2083. https://doi.org/10.1111/pbi.14113

Tüllinghoff, A., Toepel, J., Bühler, B., 2024. Enlighting Electron Routes In Oxyfunctionalizing Synechocystis sp. PCC 6803. ChemBioChem 25, e202300475. https://doi.org/10.1002/cbic.202300475

Tüllinghoff, A., Uhl, M.B., Nintzel, F.E.H., Schmid, A., Bühler, B., Toepel, J., 2022. Maximizing Photosynthesis-Driven Baeyer–Villiger Oxidation Efficiency in Recombinant Synechocystis sp. PCC6803. Front. Catal. 1, 780474. https://doi.org/10.3389/fctls.2021.780474

Umena, Y., Kawakami, K., Shen, J.-R., Kamiya, N., 2011. Crystal structure of oxygen-evolving photosystem II at a resolution of 1.9 Å. Nature 473, 55–60. https://doi.org/10.1038/nature09913

UNFCCC, 2015. Paris Agreement, 3156 U.N.T.S. 54113.

Usher, K.M., Bergman, B., Raven, J.A., 2007. Exploring Cyanobacterial Mutualisms. Annu. Rev. Ecol. Evol. Syst. 38, 255–273. https://doi.org/10.1146/annurev.ecolsys.38.091206.095641

Vajravel, S., Sirin, S., Kosourov, S., Allahverdiyeva, Y., 2020. Towards sustainable ethylene production with cyanobacterial artificial biofilms. Green Chem. 22, 6404–6414. https://doi.org/10.1039/D0GC01830A

Velikogne, S., Resch, V., Dertnig, C., Schrittwieser, J.H., Kroutil, W., 2018. Sequence-Based In-silico Discovery, Characterisation, and Biocatalytic Application of a Set of Imine Reductases. ChemCatChem 10, 3236–3246. https://doi.org/10.1002/cctc.201800607

Vicente, J.B., Gomes, C.M., Wasserfallen, A., Teixeira, M., 2002. Module fusion in an A-type flavoprotein from the cyanobacterium *Synechocystis* condenses a multiple-component pathway in a single polypeptide chain. Biochem. Biophys. Res. Commun. 294, 82–87. https://doi.org/10.1016/S0006-291X(02)00434-5

Viola, S., Sellés, J., Bailleul, B., Joliot, P., Wollman, F.-A., 2021. *In vivo* electron donation from plastocyanin and cytochrome *c*6 to PSI in *Synechocystis* sp. PCC6803. Biochim. Biophys. Acta BBA - Bioenerg. 1862, 148449. https://doi.org/10.1016/j.bbabio.2021.148449

Vogt, E.T.C., Weckhuysen, B.M., 2024. The refinery of the future. Nature 629, 295–306. https://doi.org/10.1038/s41586-024-07322-2

Walker, J.E., 2013. The ATP synthase: the understood, the uncertain and the unknown. Biochem. Soc. Trans. 41, 1–16. https://doi.org/10.1042/BST20110773

Wan, N., DeLorenzo, D.M., He, L., You, L., Immethun, C.M., Wang, G., Baidoo, E.E.K., Hollinshead, W., Keasling, J.D., Moon, T.S., Tang, Y.J., 2017. Cyanobacterial carbon metabolism: Fluxome plasticity and oxygen dependence. Biotechnol. Bioeng. 114, 1593–1602. https://doi.org/10.1002/bit.26287

Wang, L., Wu, Y., Hu, J., Yin, D., Wei, W., Wen, J., Chen, X., Gao, C., Zhou, Y., Liu, J., Hu, G., Li, X., Wu, J., Zhou, Z., Liu, L., Song, W., 2024. Unlocking the function promiscuity of old yellow

enzyme to catalyze asymmetric Morita-Baylis-Hillman reaction. Nat. Commun. 15, 5737. https://doi.org/10.1038/s41467-024-50141-2

Wang, Y., Chen, X., Spengler, K., Terberger, K., Boehm, M., Appel, J., Barske, T., Timm, S., Battchikova, N., Hagemann, M., Gutekunst, K., 2022. Pyruvate:ferredoxin oxidoreductase and low abundant ferredoxins support aerobic photomixotrophic growth in cyanobacteria. eLife 11, e71339. https://doi.org/10.7554/eLife.71339

Watanabe, M., Ikeuchi, M., 2013. Phycobilisome: architecture of a light-harvesting supercomplex. Photosynth. Res. 116, 265–276. https://doi.org/10.1007/s11120-013-9905-3

Webb, B., Sali, A., 2016. Comparative Protein Structure Modeling Using MODELLER. Curr. Protoc. Bioinforma. Ed. Board Andreas Baxevanis Al 54, 5.6.1. https://doi.org/10.1002/cpbi.3

Williams, J.G.K., 1988. [85] Construction of specific mutations in photosystem II photosynthetic reaction center by genetic engineering methods in *Synechocystis* 6803, in: Methods in Enzymology, Cyanobacteria. Academic Press, pp. 766–778. https://doi.org/10.1016/0076-6879(88)67088-1

Wlodarczyk, A., Gnanasekaran, T., Nielsen, A.Z., Zulu, N.N., Mellor, S.B., Luckner, M., Thøfner, J.F.B., Olsen, C.E., Mottawie, M.S., Burow, M., Pribil, M., Feussner, I., Møller, B.L., Jensen, P.E., 2016. Metabolic engineering of light-driven cytochrome P450 dependent pathways into Synechocystis sp. PCC 6803. Metab. Eng. 33, 1–11. https://doi.org/10.1016/j.ymben.2015.10.009

WMO confirms 2024 as warmest year on record at about 1.55°C above pre-industrial level [WWW Document], 2025. . World Meteorol. Organ. URL https://wmo.int/news/media-centre/wmo-confirms-2024-warmest-year-record-about-155degc-above-pre-industrial-level (accessed 2.28.25).

Xie, N., Sharma, C., Rusche, K., Wang, X., 2025. Phosphoketolase and KDPG aldolase metabolisms modulate photosynthetic carbon yield in cyanobacteria. Plant Cell 37, koae291. https://doi.org/10.1093/plcell/koae291

Xue, Y., Zhang, Y., Grace, S., He, Q., 2014. Functional expression of an Arabidopsis p450 enzyme, p-coumarate-3-hydroxylase, in the cyanobacterium Synechocystis PCC 6803 for the biosynthesis of caffeic acid. J. Appl. Phycol. 26, 219–226. https://doi.org/10.1007/s10811-013-0113-5

Yamanaka, R., Nakamura, K., Murakami, M., Murakami, A., 2015. Selective synthesis of cinnamyl alcohol by cyanobacterial photobiocatalysts. Tetrahedron Lett. 56, 1089–1091. https://doi.org/10.1016/j.tetlet.2015.01.092

Yang, C., Hua, Q., Shimizu, K., 2002. Metabolic Flux Analysis in *Synechocystis* Using Isotope Distribution from 13C-Labeled Glucose. Metab. Eng. 4, 202–216. https://doi.org/10.1006/mben.2002.0226

Yashavanth, P.R., Meenakshi, D., Soumen K., M., 2021. Recent progress and challenges in cyanobacterial autotrophic production of polyhydroxybutyrate (PHB), a bioplastic. J. Environ. Chem. Eng. 9, 105379. https://doi.org/10.1016/j.jece.2021.105379

Yehezkeli, O., Tel-Vered, R., Michaeli, D., Nechushtai, R., Willner, I., 2013. Photosystem I (PSI)/Photosystem II (PSII)-Based Photo-Bioelectrochemical Cells Revealing Directional Generation of Photocurrents. Small 9, 2970–2978. https://doi.org/10.1002/smll.201300051

Yeong, T.K., Jiao, K., Zeng, X., Lin, L., Pan, S., Danquah, M.K., 2018. Microalgae for biobutanol production – Technology evaluation and value proposition. Algal Res. 31, 367–376. https://doi.org/10.1016/j.algal.2018.02.029

Yoon, H.S., Hackett, J.D., Ciniglia, C., Pinto, G., Bhattacharya, D., 2004. A molecular timeline for the origin of photosynthetic eukaryotes. Mol. Biol. Evol. 21, 809–818. https://doi.org/10.1093/molbev/msh075

Yu, H., Hamaguchi, T., Nakajima, Y., Kato, K., Kawakami, K., Akita, F., Yonekura, K., Shen, J.-R., 2021. Cryo-EM structure of monomeric photosystem II at 2.78 Å resolution reveals factors important for the formation of dimer. Biochim. Biophys. Acta BBA - Bioenerg. 1862, 148471. https://doi.org/10.1016/j.bbabio.2021.148471

Yuan, B., Yang, D., Qu, G., Turner, N.J., Sun, Z., 2024. Biocatalytic reductive aminations with NAD(P)H-dependent enzymes: enzyme discovery, engineering and synthetic applications. Chem. Soc. Rev. 53, 227–262. https://doi.org/10.1039/D3CS00391D

Yuan, X., Xiao, S., Taylor, T.N., 2005. Lichen-Like Symbiosis 600 Million Years Ago. Science 308, 1017–1020. https://doi.org/10.1126/science.1111347

Zavřel, T., Knoop, H., Steuer, R., Jones, P.R., Červený, J., Trtílek, M., 2016. A quantitative evaluation of ethylene production in the recombinant cyanobacterium Synechocystis sp. PCC 6803 harboring the ethylene-forming enzyme by membrane inlet mass spectrometry. Bioresour. Technol. 202, 142–151. https://doi.org/10.1016/j.biortech.2015.11.062

Zavřel, T., Segečová, A., Kovács, L., Lukeš, M., Novák, Z., Pohland, A.-C., Szabó, M., Somogyi, B., Prášil, O., Červený, J., Bernát, G., 2024. A Comprehensive Study of Light Quality Acclimation in Synechocystis Sp. PCC 6803. Plant Cell Physiol. 65, 1285–1297. https://doi.org/10.1093/pcp/pcae062

Zhang, C., Shuai, J., Ran, Z., Zhao, J., Wu, Z., Liao, R., Wu, J., Ma, W., Lei, M., 2020. Structural insights into NDH-1 mediated cyclic electron transfer. Nat. Commun. 11, 888. https://doi.org/10.1038/s41467-020-14732-z

Zhang, L., McSpadden, B., Pakrasi, H.B., Whitmarsh, J., 1992. Copper-mediated regulation of cytochrome c553 and plastocyanin in the cyanobacterium Synechocystis 6803. J. Biol. Chem. 267, 19054–19059. https://doi.org/10.1016/S0021-9258(18)41739-5

Zhang, P., Allahverdiyeva, Y., Eisenhut, M., Aro, E.-M., 2009. Flavodiiron Proteins in Oxygenic Photosynthetic Organisms: Photoprotection of Photosystem II by Flv2 and Flv4 in Synechocystis sp. PCC 6803. PLOS ONE 4, e5331. https://doi.org/10.1371/journal.pone.0005331

Zhang, P., Eisenhut, M., Brandt, A.-M., Carmel, D., Silén, H.M., Vass, I., Allahverdiyeva, Y., Salminen, T.A., Aro, E.-M., 2012. Operon *flv4-flv2* Provides Cyanobacterial Photosystem II with Flexibility of Electron Transfer. Plant Cell 24, 1952–1971. https://doi.org/10.1105/tpc.111.094417

Zhang, S., Zou, B., Cao, P., Su, X., Xie, F., Pan, X., Li, M., 2023. Structural insights into photosynthetic cyclic electron transport. Mol. Plant, "Celebrating 15 Years of Publication" Special Issue 16, 187–205. https://doi.org/10.1016/j.molp.2022.12.014

Zhang, X., Ward, B.B., Sigman, D.M., 2020. Global Nitrogen Cycle: Critical Enzymes, Organisms, and Processes for Nitrogen Budgets and Dynamics. Chem. Rev. 120, 5308–5351. https://doi.org/10.1021/acs.chemrev.9b00613

TURUN
YLIOPISTO
UNIVERSITY
OF TURKU

Painosalama, Turku, Finland 2025

ISBN 978-952-02-0261-3 (PRINT)
ISBN 978-952-02-0262-0 (PDF)
ISSN 0082-7002 (Print)
ISSN 2343-3175 (Online)